Electrolytic determination of phthalates organic pollutants with nanostructured titanium and iron oxides sensors

BY

Nolubabalo Matinise

A full thesis submitted in fulfillment of the requirements thesis for a degree of

MAGISTER SCIENTIAE

in the Department of Chemistry,

University of the Western Cape

Supervisors

Professor Emmanuel I. Iwuoha

and

Professor Priscilla G.L. Baker

November 2010

KEYWORDS

Electrochemical sensor

Titanium dioxide nanoparticles

Iron oxide nanoparticles

Polymer nanocomposites

Phthalates

Dibutyl phthalates

Dioctyl phthalates

Diethylhexyl phthalates

Endocrine disruptors

Organic pollutants

Glassy Carbon Electrode

Voltammetry

Impedance

ABSTRACT

Some phthalates such as dibutyl, diethylhexyl and dioctyl phthalates are endocrine disruptors and therefore their determination is of utmost importance. This work reports the chemical synthesis, characterisation and electrochemical application of titanium dioxide (TiO_2) and iron oxide (Fe_2O_3) nanoparticles in the determination of phthalates. The other part of this work involved electrochemical polymerization of aniline doped with titanium and iron oxide nanoparticles for the sensor platform in the electrolytic determination of phthalates. The TiO_2 and Fe_2O_3 nanoparticles were prepared by sol gel and hydrothermal methods respectively. Particle sizes of 20 nm (TiO_2) and 50 nm (Fe_2O_3) were estimated from transmission electron microscopy (TEM) The other technical methods used in this study for the characterization of the TiO_2 and iron oxide Fe_2O_3 NPs were SEM, XRD and UV- visible spectroscopy. Cyclic voltammetry, square wave voltammetry and electrochemical impedance spectroscopy (EIS) were used to study the electrochemical properties of the nanoparticles. These electrochemical studies of the nanoparticles were performed with a Fe_2O_3 or TiO_2/nafion/glassy carbon membrane electrode in 0.1 M phosphate buffer (pH 7.0) and 0.1 M lithium perchlorate (pH 6.8) under an aerobic condition. The results found show that the nanoparticles are catalytic effective and semi-conductivity. The polymer nanocomposites had a higher catalytic activity and conductivity as compared to the PANI alone in 0.1 M H_2SO_4. The composite membrane electrode successfully used in the electrolytic determination of dibutyl , dioctyl and diethylhexyl phthalates in 0.1 M lithium perchlorate, 0.1 M phosphate buffer (pH 7.0) as well as in 0.1 M H_2SO_4.

DECLARATION

I declare that ñElectrolytic determination of phthalates organic pollutants with nanostructured titanium and iron oxides sensorò is my own work, that it has not been submitted before for any degree or assessment in any other university, and that all the sources I have used or quoted have been indicated by means of complete references.

Signature _____

Nolubabalo Matinise

Date: 15 November 2010

DEDICATION

I dedicate this thesis to

My mother

Nolusapho Matinise,

My Daughter

Anita Matinise and

My Uncle

Mthetho Batala

ACKNOWLEDGEMENTS

I acknowledge God as the one behind all my successes and thank him for enabling me to complete the research project written in this thesis. I thank my mother (Nolusapho) for the support and get me to where I am today. My daughter (Anita), thank you for coming to my life. I want to express my appreciation to Mthetho Batala for his understanding, courage and his bless to see me in a great future. Big thanks to my sisters and brother Siziwe, Nolusindiso, Nobuhle and Mhlanganiseli who believed in my ability to succeed. I am grateful thank to my supervisors Professor Emmanuel Iwuoha and Prof. Priscilla Baker for their academic guidance, as well as my co- supervisor Omotayo Ademola Arotiba. I wish to also express my appreciation for the advice and encouragement I received from my SensorLab colleagues Dr. Nazeem, Evelyn, Nicolette, Busiswa, Fanelwa, Sibusiso, Lundi, Combs, Masikini, Stephen, Noluthando, Sibongile, Abdo, Zelo, Natasha, Njomo, Chinwe, Takalani, Wale and Peter. Thank you guys! My heart-felt thanks goes to the Chemistry Department staff especially Prof. Farouk Ameer, the Chairperson, and also technical staff (Andile, Ben, Timmy, and Bongani) and administrative staff (Wilma and Chyril) for always providing assistance and motivation. I very much appreciate the moral support given to me by my friends Bonelwa Mabovu, Linda Mazwi, Nomvano Mketho, Yolanda Tancu, Nomso Hintsho, Xolelwa Ralam, Okounathi Gcilitshane and Bulelwa which sustained me throughout the program. I would also like to thank NRF and DST for their financial support, in helping me to finish my postgraduate study.

TABLE OF CONTENTS

LIST OF FIGURES

determination of DEHP illustrating linear of PANI/Fe_2O_3 NPs sensor, potential vs concentration

LIST OF TABLES

LIST OF ABBREVIATIONS

Ag/AgCl	Silver/silver Chloride
GCE	Glassy Carbon Electrode
°C	Degrees Celsius
cm^2	Cubic centimetre
CV	Cyclic Voltammetry
SWV	Square Wave Voltammetry
$E_{p,a}$	Anodic peak potential
$E_{p,c}$	Cathodic peak potential
H_2O	Water
H_2SO_4	Sulphuric acid
DBP	Dibutyl phthalates
DOP	Dioctyl phthalates
DEHP	Dibutylhexyl phthalates
DMP	Dimethyl phthalates
DBBzP	Dibutylbenzyl phthalates
DEP	Diethyl phthalates
PANI	Polyaniline
PANI/TiO_2	Polyaniline/titanium dioxide
PANI/Fe_2O_3	Polyaniline/iron oxide
NPs	Nanoparticles
TiO_2	Titanium dioxide
Fe_2O_3	Iron oxide

HRTEM	High resolution transmission electron microscopy
SEM	Scanning electron microscopy
XRD	X-ray diffraction
UV-vis	Ultra violet ï visible spectroscopy
EIS	Electrochemical impedance spectroscopy

CHAPTER ONE

BACKGROUND

1. BACKGROUND

1.1 INTRODUCTION

Nanoparticles refer to particles with a diameter smaller than 100 nm. These minute molecules have been studied due to their unique properties such as their specificity, quantum effects and better quality in decomposing organic and inorganic material in gaseous or liquid phase. There are various types of nanoparticles are reviewed on the literature for example metal oxide (TiO_2, Tin (11) oxide and iron oxide), polymers (polythiophene, polyaniline), alloys nanoparticles (Nikel-Cobalt and Nikel Copper), etc.

The synthesis of titanium dioxide nanoparticles has been intensively researched because of its unique, optical (Allen, Edge et al. 2002), dielectric, and electrochemical properties. Titanium dioxide has been found to be suitable for a variety of application due to its long- term stability, high photo activity (Alonso, Montequi et al. 2009), strong oxidizing agent, low cost and non-toxicity. In the past years the titanium dioxide was only predominantly used in paints, enamels and vanishes to impart a white colour and brightness as a result of its high refractive index. Nowadays titanium oxide has wide applications in manufacturing of cosmetics (Brezová, Vrecková et al. 2009), coating materials, solar cell components (Zeng, Lo et al. 2009) catalyst in the removal of wastewater organic and inorganic compounds (Mazille, Schoettl et al. 2009). Titanium dioxide is also used in pain relievers (Pardeike, Hommoss et al. 2009), such as Tylenol and rite aid brand aspirin. Titanium dioxide offers great potential for application in industrial technology for detoxification or remediation of wastewater due to several factors.

The synthesized iron oxide has a great potential in the application such as magnetic storage (for example in the magnetic layer of floppy disks) (Noginov, Noginova et al. 2008), in the production of pure iron in a blast furnace, in an extremely exothermic reaction , as a pigment (Stengl, Subrt et al. 2003) , in cosmetic (Pardeike, Hommoss et al. 2009), in biomedical application (Gupta and Gupta 2005), as contrast agents in magnetic resonance imaging (Morales, Bomati-Miguel et al. 2003), Ferro fluids (Ghasemi, Mirhabibi et al. 2008) and biosensor. The iron oxide nanoparticles have been shown to be extremely efficient at de-contamination of organic pollutants in wastewater (Parham and Rahbar 2009). The particles act as catalyst on the reduction of very toxic organic pollutants to less harmful compounds (Xu, Wang et al.). Phthalates are examples of these dangerous chemical in human health. Phthalates are usually used in industries as plasticizers for polyvinyl chlorine resins and cellulose film coating; they are also used in cosmetics, insect repellents and propellants. Phthalates such as diethylhexyl phthalates (DEHP), butylbenzyl phthalates (BBzP), diethyl phthalates (DEP), dibutyl phthalates (DBP) and dioctyl phthalates (DOB) are suspected as endocrine disruptors and carcinogens. Endocrine disruptors are the chemical compounds that can disrupt the normal function of the body by mimicking or blocking natural hormones reaction. These compounds can be introduced in the human body system by ingestion of contaminated food, water or air like other environmental pollutants such as pesticides. There are three major endocrine disruptions: Endpoints are estrogenic ï the compounds that mimic or block natural estrogens, androgenic - the compounds that mimic or block natural testosterone, and thyroidal - the compounds with direct and/or indirect impacts on the thyroid. There are many different kinds of endocrine disruptors but those are usually found in industrial wastewater are classified into three classes namely bisphenols, alkylphenols and phthalates. This study involved firstly the chemical

synthesis of titanium dioxide and iron oxide nanoparticles, secondly, the characterization of the iron oxide and titanium dioxide nanoparticles by electrochemical and technical methods and thirdly, the development of a membrane by the deposition of the nanomaterial on platinum and glassy carbon electrodes support and support for the electrolytic determination and of organic pollutants principally the phthalates i.e. dibutyl and dioctyl phthalates in wastewater and lastly , the electrochemical development of polymer nanocomposite for the determination of phthalates.

1.2 RATIONALE AND MOTIVATION

Many industries produce wastewater containing organic pollutants such as phthalates that pollutes the environment owing to their toxicity. Some phthalates such as diethylhexyl phthalates and dibutyl phthalates are endocrine disruptors and carcinogenic. Phthalate esters (ethylhexyl phthalate and di-n-butyl phthalate) are used as plasticizers in many industrial processes and materials. Plasticizers are additives that increase the plasticity or fluidity of the material to which they are added, these include plastics, cement, concrete, wallboard and clay bodies. Phthalates are therefore introduced into the environment through leaching from these products and industrial discharges (Brown and E Thompson 1982; Eveillard, Mselli-Lakhal et al. 2009). Phthalates are well known organic pollutants especially in wastewater. Untreated wastewater potentially contains a variety of chemical constituents hazardous to human health and the environment. The ultimate goal of waste-water treatment is the protection of the environment in a manner commensurate with public health and socio-economic concerns. Therefore, the detection of these pollutants especially the ones mentioned are of utmost importance. Existing methods of detecting phthalates are based on classical techniques such as high performance liquid chromatography (HPLC) which are expensive, laboratory borne and need a lot of expertise

to operate (Heudorf, Mersch-Sundermann et al. 2007). There is a need to develop, a simple, clean and relatively cheaper method for the detection of an endocrine disrupting chemical pollutants especially phthalates in wastewater.

1.3 AIMS AND OBJECTIVE OF THE STUDY

The aim of the study involved the chemical synthesis and characterization of the titanium dioxide and iron oxide nanoparticles. The application of these oxide nanoparticles as electrochemical sensor membrane for determination of phthalates in wastewater was evaluated. The detailed objectives of the study are tabled below

Objectives

- To synthesized the titanium dioxide and iron oxide nanoparticles by chemical method i.e. sol-gel and hydrothermal respectively.
- To characterized the metal oxides using technical method such as TEM, SEM, XRD and UV-vis spectroscopy
- To determined the electrochemical behavior of the metal oxide nanoparticles by CV, SWV and EIS
- To developed the sensor membrane by drop-coating the nanoparticles on the surface area of a GCE
- To used the sensor membrane in the determination of phthalates organic pollutants i.e. dioctyl, dibutyl and diethylhexyl phthalates
- To fabricated polyaniline nanocomposites of the iron oxide and titanium dioxide platforms and thus enhancing the conductivity of the nanoparticles in the determination of phthalates.

1.4. REFERENCES

- Allen, N.S., Edge M., Ortega A., Liauw C.M., Stratton J., McIntyre R.B. (2002) Behaviour of nanoparticle (ultrafine) titanium dioxide pigments and stabilisers on the photooxidative stability of water based acrylic and isocyanate based acrylic coatings. Polymer Degradation and Stability 78:467-478.
- Alonso, E., Montequi I., Cocero M.J. (2009) Effect of synthesis conditions on photocatalytic activity of TiO_2 powders synthesized in supercritical CO_2. The Journal of Supercritical Fluids 49:233-238.
- Brezová, V., Vrecková Z., Billik P., Caplovicová M., Plesch G. (2009) Photoactivity of mechanochemically prepared nanoparticulate titanium dioxide investigated by EPR spectroscopy. Journal of Photochemistry and Photobiology A: Chemistry 206:177-187.
- Ghasemi, E., Mirhabibi A., Edrissi M. (2008) Synthesis and rheological properties of an iron oxide ferrofluid. Journal of Magnetism and Magnetic Materials 320:2635-2639.
- Gupta, A.K., Gupta M. (2005) Synthesis and surface engineering of iron oxide nanoparticles for biomedical applications. Biomaterials 26:3995-4021.
- Mazille, F., Schoettl T., Pulgarin C. (2009) Synergistic effect of TiO_2 and iron oxide supported on fluorocarbon films. Part 1: Effect of preparation parameters on photocatalytic degradation of organic pollutant at neutral pH. Applied Catalysis B: Environmental 89:635-644.
- Morales, M.P., Bomati-Miguel O., Pérez de Alejo R., Ruiz-Cabello J., Veintemillas-Verdaguer S., O'Grady K. (2003) Contrast agents for MRI based on iron oxide nanoparticles prepared by laser pyrolysis. Journal of Magnetism and Magnetic Materials 266:102-109.

- Noginov, M.M., N. Noginova, O. Amponsah, R. Bah, R. Rakhimov and V.A. Atsarkin (2008) Magnetic resonance in iron oxide nanoparticles: Quantum features and effect of size. Journal of Magnetism and Magnetic Materials 320:2228-2232.
- Pardeike, J., A. Hommoss and R.H. Müller (2009) Lipid nanoparticles (SLN, NLC) in cosmetic and pharmaceutical dermal products. International Journal of Pharmaceutics 366:170-184.
- Parham, H. and N. Rahbar (2009) Solid phase extraction-spectrophotometric determination of fluoride in water samples using magnetic iron oxide nanoparticles. Talanta 80:664-669.
- Stengl, V., J. Subrt, S. Bakardjieva, A. Kalendova and P.Kalenda (2003) The preparation and characteristics of pigments based on mica coated with metal oxides. Dyes and Pigments 58:239-244.
- Xu, X., Q. Wang, H.C. Choi and Kim Y.H. Encapsulation of iron nanoparticles with PVP nanofibrous membranes to maintain their catalytic activity. Journal of Membrane Science In Press, Accepted Manuscript.
- Zeng, T.-W., H.-H. Lo, C.-H. Y.-Y. Chang, Lin, C.-W. Chen and W.-F. Su (2009) Hybrid poly (3-hexylthiophene)/titanium dioxide nanorods material for solar cell applications. Solar Energy Materials and Solar Cells 93:952-957.

CHAPTER TWO

LITERATURE REVIEW

2. LITERATURE REVIEW

2.1. What are Nanoparticles

Nanoparticles are very fine particles that are less than 100 nm in diameter. Since nanoparticles are very small many of them are free pass through skin and enter cells where they interfere with cellular processes by binding to micro molecule. Nanoparticles have become extremely popular in electrochemical sensing research due to their electrical conductivity, unique structural and catalytically properties, high loading biocatalysts, good stability and excellent penetrability (Haley and Frenkel ; Haddad, Martins et al. 2008; Kang, Wang et al. 2008). In the past 20 years, there has been a marked increase in synthesis and application of nanotechnology to many industrial processes. At a diameter of 1-5 nm, quantum dots effects begin to dominate affecting optical, conductive and semi conductive properties. These drastic changes in properties due to particle size have been successfully utilized in manufacturing of electronic devices such as faster computers, flat screens, LCD television and digital cameras.

Nanoparticles made of transition metals, semiconductors or oxides due to their special function have made them an interesting hot research topic in the recent decades. Metal oxide nanoparticles have much attracted intense attention due to their optical, magnetic and electronic properties. These properties make nanostructured metal oxide more importantly useful for a wide range of application such as catalysts, bactericidal agents, sensor, optical materials (Seirafianpour, Badilescu et al. 2008), electrical materials (Kruis, Fissan et al. 1998), magnetic storages, fillers, semiconductors, cosmetics (Pardeike, Hommoss et al. 2009), microelectronics, drug delivery vehicles, imaging, biosensor (Kang, Wang et al. 2008) and environmental remediation.

In the environmental remediation application, nanoparticles are utilized to transform toxic metals like chromium, lead, mercury, arsenic and cadmium in lakes, rivers and in groundwater for easier cleanup (Shen, Tang et al. 2009). Researchers have utilized this nanoparticles in the reduction of a toxic chromium VI from hexavalent to trivalent which is insoluble in water therefore is much easier to cleanup. The metal oxide nanoparticles with high magnetic properties have been off great interest in the treatment of cancer, the magnetic nanoparticles can attach to the cancer cells in the blood stream allowing the cancer to be removed before they establish new tumours (Yezhelyev, Gao et al. 2006). Some nanoparticles have photo-catalytic properties such as TiO_2 and Zinc oxide provide high sun protection factors in clear sun scream due to a high surface area to mass ratio. Other applications of metal oxide nanoparticles are metallic paints and thin films, self cleaning window and solar panel technology, car tyres, hydrogen fuel storage and now as antimicrobial additives in laundry. They have been used as pigments to enhance the appearance and improve the durability of polymeric product as well as used to enhance the stiffness, toughness and service life of polymeric material. Nanoparticles used in bioremediation and disinfection, in water application are divided into three categories (i) treatment and remediation (ii) sensing and detection (iii) pollution prevention. Within the category of treatment and remediation, nanotechnology has the potential to contribute to long term water quality, availability and viability of water resources. Metal oxide nanoparticles have also been extensively used in treatment and the determination of organic and inorganic pollutants in wastewater with titanium dioxide and iron oxide nanoparticles being the most popular because of their properties and catalytic effect.

2.1.1. Synthesis of the metal oxide nanoparticles

The metal oxide are often prepared by chemical and electrochemical synthesis, according to the literature there are several methods employed for the chemical synthesis such as sol-gel, solvorthermal, hydrothermal, thermal decomposition and chemical reduction etc. In thermal decomposition the preparation of iron oxide nanoparticles is usually accomplished by dissolving $Fe(CO)_5$ in an organic solvent such as octyl which make the nanoparticles unsuitable for biological applications. The use of sol-gel method for the preparation of metal oxide nanoparticles has attracted a lot of attention for its advantageous in obtaining the meta-stable material and achieving superior purity product at moderated temperature with simple laboratory equipment. Other advantages of the sol-gel method are;

- The possibility to obtain material with a predetermined structure according to experimental conditions,
- The possibility to obtain a pure amorphous phase, monodispersity and good control of particle size.
- The control of the microstructure and the homogeneity of the reaction product.
- The possibility to embed molecules, which maintain their stability and properties within the so-gel matrix.

Sol-gel derived materials have many applications in optics, electronics, energy, space, sensors, biosensors, medicines and separation techniques. For a while the main objective in chemistry has been synthesis of controlled particles size, shape and crystalline structured compounds, this has only been realized in nanotechnology. This process is based on the hydroxylation and condensation of precursors in solution. There are the main parameters such as solvents, temperature, nature, concentration of the precursors employed, pH and agitation that influence

the kinetics, growth reactions, hydrolysis, condensation reactions, the structure and the properties of the gel.

In hydrothermal method, is a promising method of preparation of iron oxide nanoparticles and give high quality iron oxide nanocrystals. The metal oxide nanoparticles prepared by hydrothermal are usually useful in the biomedical applications especial in the treatment of cancer by Hyperthermia and as contrast agents for MRI

2.1.2. Iron oxide nanoparticles

The synthesized iron oxide has a great potential in the application such as magnetic storage (for example in the magnetic layer of floppy disks) (Kim, Ahn et al. 2007; Noginov, Noginova et al. 2008), in the production of pure iron in a blast furnace, as a pigment in paint (Stengl, Subrt et al. 2003) , in cosmetic (Pardeike, Hommoss et al. 2009), in biomedical applications (Gupta and Gupta 2005), magnetic stability and low toxicity level in biological system, as medical application such as drug delivery, contrast agents in magnetic resonance imaging and magnetic ink for jet printing (Morales, Bomati-Miguel et al. 2003), Ferro fluids (Ghasemi, Mirhabibi et al. 2008), sensors and biosensors(Kang, Wang et al. 2008). The iron oxide nanoparticles have been shown to be extremely efficient at de-contamination of organic pollutants and arsenic in groundwater (Parham and Rahbar 2009). They also act as a catalyst (Xu, Wang et al.) and ground water remediation (Shen, Tang et al. 2009). The iron oxide nanoparticles also reduced the very toxic gases to less harmful products such as methane, hydrogen gas and carbon monoxide. Super paramagnetic iron oxide nanoparticles with appropriate surface chemistry can be used in MRI contrast enhancement, tissue repair, immunoassay, detoxification of biological fluids, hyperthermia, drug delivery and cell separation (Kim, Ahn et al. 2007). All these applications required the iron oxide to have high magnetic properties so that the magnetic can bind to drugs,

proteins, enzymes, antibodies or nucleotides and can be directed to an organ, tissue or tumour using an external magnetic field. The papers have been reported the iron oxide nanoparticles prepared by hydrothermal method for the removal of ethylene glycol organic pollutants in wastewater. The method was based on the chemical oxidation of organic pollutant by advanced oxidation processes for the purification of drinking water and cleaning of industrial wastewater using Fenton and Fenton- like reagents ($Fe^{2+}/Fe^{3+}/H_2O$) for the generation of very reactive free radicals ($OH^{\cdot}$) to complete the degradation and mineralization to CO_2, H_2O and mineral acids. The researchers shown in the literature that the iron oxide have special photochemical and catalytic properties are strongly depend on particle size, surface properties and different methodology. Another method of organic pollutant removal such as naphthalene and antraquinone- sulphonic acids in the literature was indirect electrolysis using Fe electrogenerated Fentonôs reagents. The iron oxide nanoparticles is a more suitable and stable material to use in the laboratory. The iron oxide is stable in water and phosphate buffer saline at pH 7. The iron oxide nanoparticles show safety profile to human use; human tissues contain certain amount of iron carried by haemosiderin, ferritin and transferrerric.

2.1.3. Titanium dioxide nanoparticles

The synthesized titanium dioxide nanoparticles have much attention because of its electrochemical, optical (Seirafianpour, Badilescu et al. 2008), dielectric, and electrical properties. TiO_2 NPs is advantageous and promising material because of their properties in many applications such as sensing, UV protection, high photo activity (Li, Ma et al. 2008), photo catalyst decomposition of various pollutant (Doong, Hsieh et al. 2010), photovoltaicôs,

photochromics, environmental remediation including water/air purification (Nabi, Aslam et al. 2009), solar conversion through photelectrolytic water splitting to yield oxygen and hydrogen and strong oxidizing agent. TiO_2 NPs are very stable, low cast and non-toxicity material (Li, Zhu et al. 2008). Their optical, electrical and biological properties make them suitable for UV protection, a as sensor of various gas and humidity. Titanium dioxide is used in pain relievers, such as Tylenol and rite aid brand aspirin and also used in pigments for paints because of its brightness (Allen, Edge et al. 2002) and very high refractive index, vanishes, enamels, and lacquers to impart white, optical. Titanium dioxide offers great potential as an industrial technology for detoxification or remediation of wastewater due to several factors (Han, Kambala et al. 2009). The titanium dioxide nanoparticles are also used as a catalyst in the oxidation of hydrazine (Dong, He et al. 2008). Chac.et.al. studied about the photo-catalytic activities of TiO_2 NPs on the decomposition of 2-propanol at a different particle size and conclude that the smaller particle size showed a better photo catalytic activity (from 7 nm ï 100 nm). The researchers also shown that TiO_2 NPs can be used to kill bacteria and tumour cells in cancer treatment (Thevenot, Cho et al. 2008). Zulkarnainôs work showed TiO_2 NPs-chitoson has a great potential in the degradation of organic pollutants (methyl orange) in wastewater to non- toxic end products such as CO_2, H_2O and mineral acids (Zulkarnain et. al) . Dianlu and Jiangôs work was involve the photo electrochemical oxidation of phthalic acid on the TiO_2 film electrode (Dianlu Jiang et. al). The literature shown the photo catalyst of TiO_2 NPs involves light leading to the generation of electron-hole on TiO_2 which make them a very powerful oxidising agent for the oxidation of adsorbed organic material. Titanium dioxide nanoparticles can exist in two forms i.e. amorphous and crystalline forms. There are three main crystalline phases which are brookite, anatase (Liu, Hong et al. 2005)and rutile. Brookite exists in orthorhombic crystal structure where as anatase

and rutile their crystal structures are similar, tetragonal but the crystal structure of anatase is longer. Anatase and rutile are physically in density, hardness, luster and refractive index. Anatase has a lower physical density and hardness than rutile and optical negative while rutile is optical positive. The rutile crystal form is thermodynamically stable and existing as an off white powder, whereas brookite and anatase are metastable and existing as a white powder. As the temperature increases, anatase and brookite will transform to rutile. Rutile is applied in the production of pigments, cosmetics, paints, papers and foods (Bian and Xue 2007). Anatase is found to be kinetically favoured at low temperature. The low temperature explains higher surface area and higher surface density of active sites for adsorption and for catalysis. Anatase has high photo catalytic with wider gap (3.2eV) and is often used as photo catalyst under visible and ultraviolet light than other phase.

2.2 Polymer nanocomposite

A nanocomposite is a multiple phase material where one of the phases has one, two or three dimension of less than 100 nm and they are microscopic and also usually found in nature (Gurunathan and Trivedi 2000). There are several types of conductive polymer nanocomposites reported in the literature such as clay/polymer nanocomposite, carbon nanotube/polymer nanocomposite and metal oxide/polymer nanocomposite (Li, Wang et al. 2008). The nanocomposites can be synthesized chemically and electrochemically polymerization, but the most preferred method is electrochemically polymerization because of their simplicity, reliability, selectivity, sensitivity, compatibility as well as inexpensiveness (Li, Wang et al. 2004). During electrochemically polymerization some monomers such as aniline or pyrrole undergo electrochemical oxidation at a high positive electrode potential, leads to the formation of cation radicals or other reactive species and spontaneous polymerization process which in turn

leads to formation of oligomers and or polymers. The conducting polymers are polypyrrole, polythiophene and polyaniline. Although all of them are conducting polymers, polyaniline has received a lot of research attention in the past due to the presence of reactive ï NH- group and unique properties such as good redox reversibility, special doping material, environmental stability and high electric conductivity properties, which makes the conducting polymers are so attractive in many applications such as batteries, electro-chemical display devices, molecular electronics, electrical magnetic shield and microwave absorbing materials (Li, Wang et al. 2004; Li, Wang et al. 2008; Li, Zhang et al. 2010). During the electro polymerization of aniline, the voltammogram appears into three redox peaks i.e. emeraldine, leucoemeraldine and pernigraniline states. The nanocomposite of metal oxide/conducting polymer have been offered a great interest in electrical, optical or catalytic properties, due to these properties the nanocomposite of metal oxide/conducting polymers are the promising material in many applications such as catalysis, optics, electronics, batteries, memory devices, biosensor and sensor (Li, Zhang et al. 2010). Polymer that contain transition metal complex either attached or directly in a ´ ï conjugated backbone are an exciting and a promising class modern materials. The introduction of inorganic nanoparticles (TiO_2 & Fe_2O_3) in the polymerization of PANI is to improve their conductivity and dispersibility (Zhang, Yang et al. 2009). In the literature shown that the introduction of Fe_2O_3 NPs in the polymerization of aniline was concerned with their conductivity, magnetic and electrical properties (Sathiyanarayanan, Azim et al. 2007; Zhang, Yang et al. 2009). Karuppamy Gurunathanôs work reported the nanocomposite polyaniline in the presence of TiO_2 to enhance the photo catalytic effect of TiO_2, because the TiO_2 is one of the n-type semiconductor whereas PANI is consider as p-type conductive polymers (Gurunathan and Trivedi 2000). It was reported that TiO_2 consists of the two band i.e. valence and conduction

band which has the energy difference between these two band known as band gap. The Authors shown the band gap of PANI/TiO_2 nanocomposite is smaller than that of TiO_2 and allows PANI/TiO_2 to absorb more photons under sunlight and this will enhance the photo catalytic efficiently of TiO_2 NPs (Li, Wang et al. 2004; Liu, Zhou et al. 2006; Li, Zhang et al. 2010). The work of C. Lai was dealing with PANI/TiO_2 as anode material for lithium-ion batteries. The polymerization of PANI exists in three different forms; the oxidation state of polyaniline (PANI) can be varied from the fully reduced leucoemeraldine base (LEB, #1) to the half oxidized emeraldine base (EB) and to the fully oxidized form pernigraniline base (PNB).

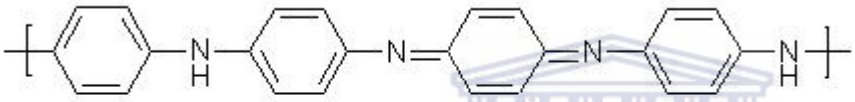

Emeraldine

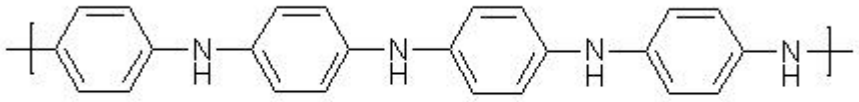

Leucoemeraldine

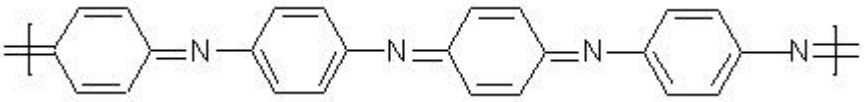

Pernigraniline.

Figure 2.1. The different forms of aniline: emeraldine; leucoemeraldine and pernigraniline (Zengin, Spencer et al. 2007).

2. 3. PHTHALATES

2.3.1. What are the phthalates

A family of chemicals, produced from phthalic anhydride and alcohols, frequently used as plasticisers to give flexibility, durability, longevity and low cost to poly vinyl chloride (PVC) (Heudorf, Mersch-Sundermann et al. 2007; Peijnenburg 2008). Phthalates are esters of phthalic acid and are colorless liquid with a faint odor. They are insoluble in water but are miscible in mineral oil, hexane and the most organic solvents. Phthalates are hormone disrupting chemicals and commonly detected in groundwater, rivers, lakes, pharmaceuticals, food, childrenôs toys, air pollutions, drinking water and industrial wastewater (Sánchez-Avila, Bonet et al. 2009). Phthalates are classified to be a major source of environmental pollution. Although phthalates has a low solubility in water, the amount present in water may be higher due to adsorption onto organic and interaction with dissolved organic matter. They are non-covalently bonded to plastics and allow required degree of flexibility, so they can easily be released from consumer products into the environment during manufacturing, disposal and leaching from plastic material. Phthalates are mostly used as plasticizers in the production of PVC and plastic medical devices such as blood transfusion sets, blood storage bag and syringes (Heudorf, Mersch-Sundermann et al. 2007; Peijnenburg 2008). These medical plastics devices are more advantageous other than the glass medical devices because of their lightweight, non-breakable and are easily shipped. Without the use of plasticizers in certain plastic formulation, the product will remain nonflexible. There many publications in the determination of the phthalates especial in wastewater using the different methods namely: advanced oxidation process, gas chromatography method, safonification and gravimetric methods (Sánchez-Avila, Bonet et al. 2009). The gas chromatography method was based on the alkaline hydrolysis of phthalates to phthalic acid by

Ivan Ostrorsky et.al. but are very expensive, complicated and time- consuming (Ostrovský, Cabala et al. 2011). The public is concern about phthalates because of widespread use and occurrence in the environment , they have undergone extensive testing for possible human health problem (Ostrovský, Cabala et al. 2011). The new method was developed based on the electrolytic determination of phthalates in wastewater by using nanocomposite as a sensor membrane. This method is less expensive, simple, environmental friendly and is able to treat very toxic metals. The different phthalates are mostly used in industries, which each have specific properties, uses and health effects namely : di-*n*-octyl phthalate (DnOP), di-isodecyl phthalate (DIDP), di-isononyl phthalate (DINP), butylbenzyl phthalate (BBP), dibutyl phthalate (DBP), and diethylhexyl phthalate (DEHP) , dimetyl phthalates (DMP) etc.(Asai, Tahara et al. 2000; Bagó, MartIn et al. 2005; Huang, Tien et al. 2008; Eveillard, Mselli-Lakhal et al. 2009). Phthalates structure containing benzene ring, two carbonyl groups and two alcohol group to generate a diester structure, common branched of phthalates such as DEHP, DBP etc feature branched chain of 6 to 13 carbons. Figure 2.2 shows the structure of phthalates whereas figure 2.3 shows the different sources of phthalates

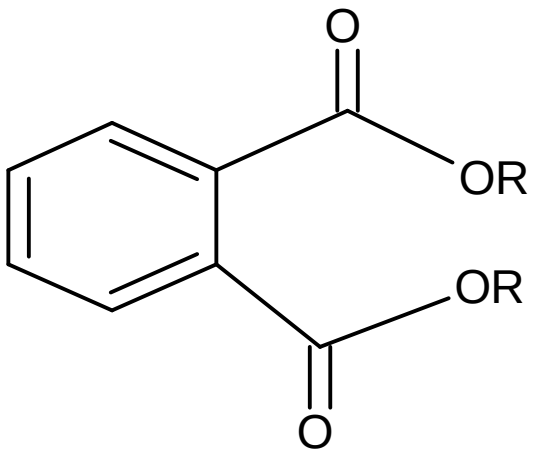

Figure 2.2: Phthalates structures (Zhao, Chu et al. 2010)

Figure 2. 3: Sources of phthalates

Drinking water

Sewage

Lakes

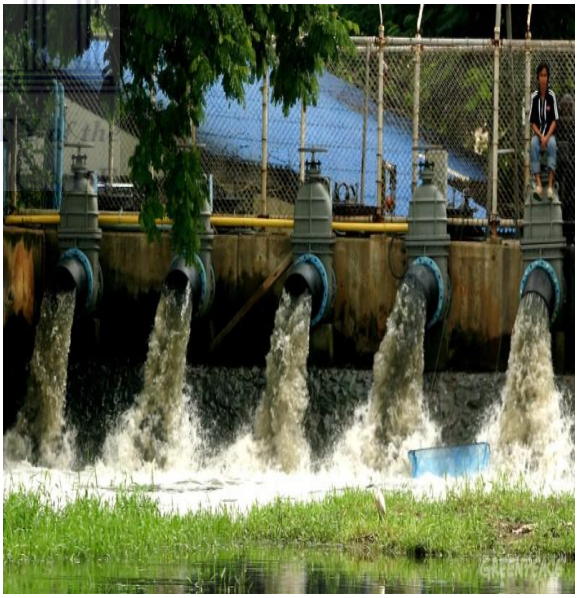

industrial discharge

Images adopted from www.filtersfast.com//2010/10/dirty-water.jpg
www.waterrecycling.blogspot.com
www.pubs.usgs.gov/fs/2006/3131/images/figure1.png
www.greenpeace.org/international/Global/inter

Table 2.1 the most common types of phthalates

Name	**Acronym**	**Structural formula**	**CAS No.**
Dimethyl phthalate	DMP	$C_6H_4(COOCH_3)_2$	131-11-3
Diethyl phthalate	DEP	$C_6H_4(COOC_2H_5)_2$	84-66-9
Diallyl phthalate	DAP	$C_6H_4(COOCH_2CH=CH_2)_2$	131-17-9
Di-n-butyl phthalates	DBP	$C_6H_4(COO(CH_2)_3CH_3)_2$	84-74-2
Di-n-propyl phthalates	DPP	$C_6H_4(COO(CH_2)_3CH_3)_2$	84-74-2
Diisobutyl phthalates	DIBP	$C_6H_4(COOCH_2CH(CH_3)_2)_2$	84-69-5
Di-n-pentyl phthalates	DNPP	$C_6H_4(COO(CH_2)_4CH_3)_2$	131-18-0
Dicyclohexyl phthalates	DCP	$C_6H_4(COOC_6H_{11})$	84-69-5
Di-n-hexyl phthalates	DNHP	$C_6H_4(COO(CH_2)_5CH_3)_2$	84-68-7
Di(2-ethylhexyl) phthalates	DEHP	$C_6H_4[COOCH_2CH(C_2H_5)(CH_2)_3CH_3]_2$	117-81-7
Dioctyl phthalate	DOP	$C_6H_4[COO(CH_2)_7CH_3]_2$	117-84-0

Reference: (Heudorf, Mersch-Sundermann et al. 2007; Benson 2009; Amiridou and Voutsa 2011)

2.3.1. Types of phthalates

The phthalates of concern are those which are usually found in industrial wastewater and they are classified as endocrine disrupt.

1. Di-*n*-octyl phthalate (DOP)

DOP is the most used plasticizer in PVC and low cost, flooring materials, carpet tile, canvas tarps, notebook covers. DOP used to be utilized in the production of medical blood bags. DOP is classified as endocrine disrupting chemical to human; it may effects on embryo or fetus, skin eye and respiratory irritant. It is biodegradable in water with a half life of 2-3 weeks, thus leading to the risk in aquatic animals. It is also classified as carcinogenic.

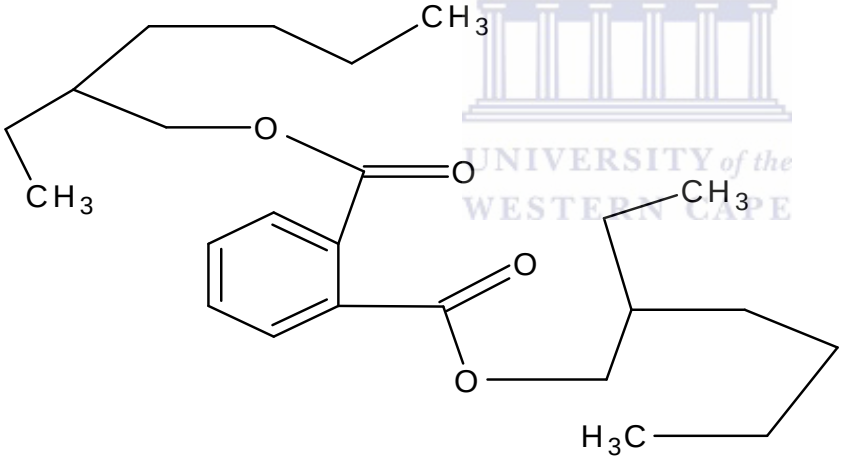

Figure 2. 4: Structure of di-*n*-octyl phthalate (DOP) (Shende and Lombardo 2002)

2. Di-isononyl phthalate (DINP) and di-isodecyl phthalate (DIDP)

They have common core structure with long chain of molecules; in the case of DINP the long chain contain 9 carbon atoms whereas in the case of DIDP it contains 10 carbon atoms. They are sticky, oily liquids and they are soluble in fat and not very soluble in water. They are used as plasticisers in PVC that is used to make film, sheeting, coated products, flooring, roofing, wall coverings, hoses, tubing, wires, cables, injection moulded shoe soles, car undercoating, sealants, vinyl resins, cellulose, adhesives, pool-liners, paints and printing inks.

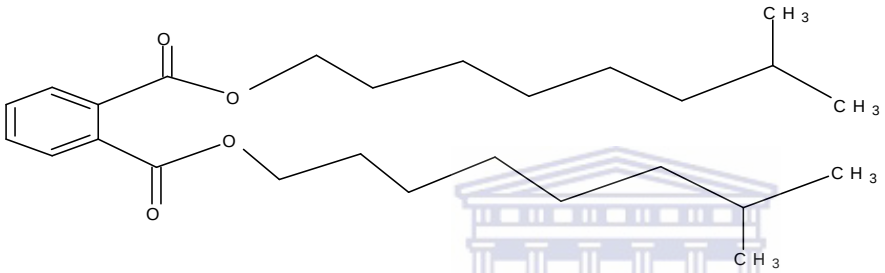

Figure 2. 5: Structure of di-isononyl phthalate (DINP) (Amiridou and Voutsa 2011)

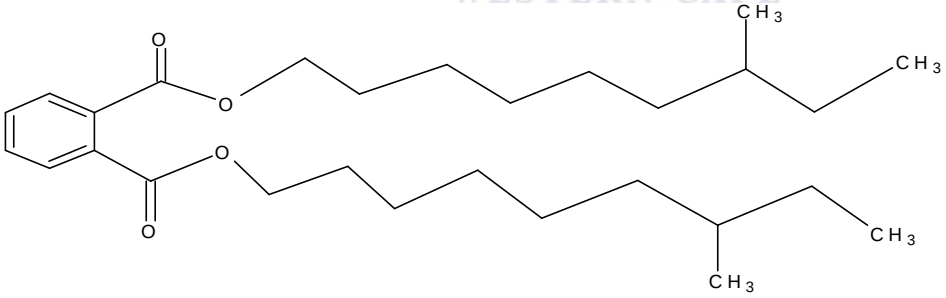

Figure 2. 6: Structure of di-isodecyl phthalate (DIDP) (Amiridou and Voutsa 2011)

3. Butylbenzyl phthalate (BBP)

BBP is used in car care products and in a range of soft PVC products such as flooring, packing and artificial leather. Other uses are in vinyl tile, food, conveyer belts and traffic cones. BBP is added to make PVC flexible, expanded and provides particular good processing and end product performance. BBP is very toxic in aquatic organism; it may cause long ï term adverse effect in the aquatic environment and is dangerous for the environment. BBP may be released into the environment during disposal and its production. The most expected route of BBP into the environmental exposure is air and water.

Figure 2. 7: Structure of butylbenzyl phthalate (BBP) (Benson 2009)

4. Dibutyl phthalate (DBP)

They used DBP in cellulose plastics, solvents for dyes, food wrap, adhesives, perfumes, cosmetics, skin emollients, hair spray, nail polish and insects repellents (Norwitz 1958). DBP is also used in glosses, enamels and hardeners in order to give the coating flexibility. It is also used in shampoos and sunscreens. Publications on animal exposure indicate that the high levels of DBP can cause defects in the male sex organs. The reports also show that women are more exposed to DBP than men especially in the women age group 20 and 45 due to their frequent use of cosmetics. The literature suggests the photo catalytic degradation of DBP endocrine disruptor in wastewater by ZnO or TiO_2 under sunlight using an artificial light such as a Hg-Xe lamp but the lamp is very expensive.

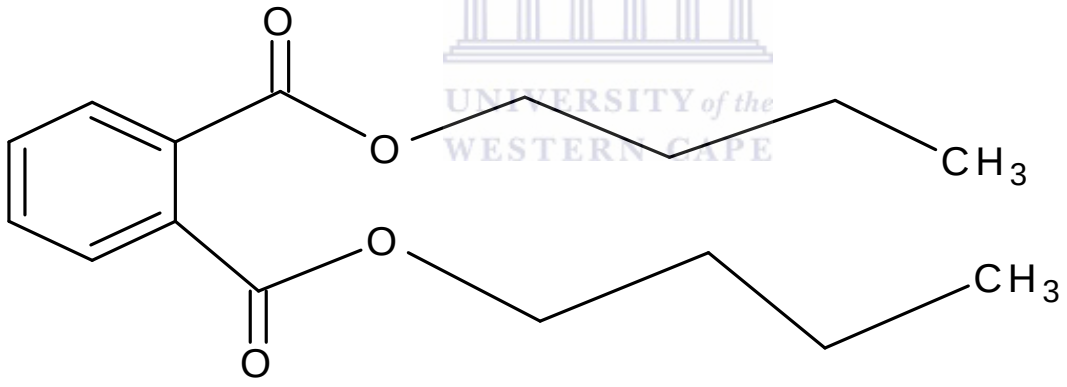

Figure 2. 8: Structure of dibutyl phthalate (DBP) (Hoang, Li et al. 2008)

5. Diethylhexyl phthalate (DEHP)

DEHP are used as a plasticiser PVC for building material, food packaging, children toys and medical devices (Bagó, MartIn et al. 2005; Eveillard, Mselli-Lakhal et al. 2009). It has been found in various types of food such as cheese, shellfish, fish and eggs. The researchers found high level of DEHP in the wrapped cheeses because the plasticisers are more likely to leach into fatty foods (Eveillard, Mselli-Lakhal et al. 2009). Therefore people who eat wrapped cheeses everyday could get a very high level of DEHP that could cause health problem. The reports show that patients are sometimes victims of DEHP from the medical devices such as blood bags and intravenous (IV) and IV bags (Eveillard, Mselli-Lakhal et al. 2009). These bags are used to store blood and DEHP can leach out from the plastic bags into the blood. There are some studies showing that young children may be ingesting small amount of DEHP when they are chewing or sucking on the flexible toys. The animal exposure of DEHP can cause damage to the kidneys, liver, reproductive system, lungs, heart and developing fetus.

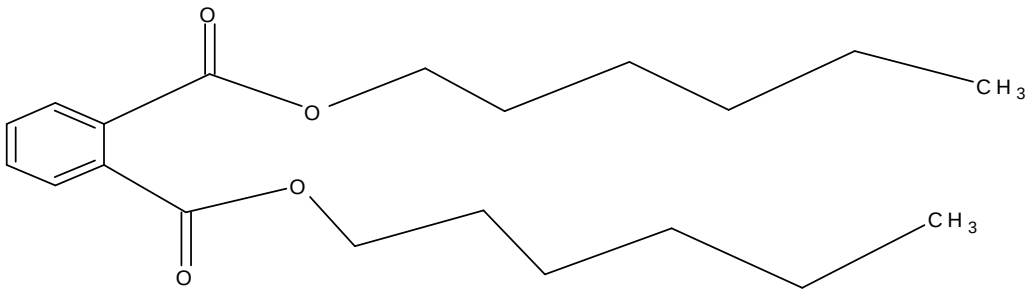

Figure 2. 9: Structure of diethylhexyl phthalate (DEHP) (Koch, Rossbach et al. 2003)

2.3.3. Human exposure to phthalates

There are various sources and routes of exposure to phthalates, some of them can occur in work places. Human beings can be easily exposed to phthalates through direct contact and use of products containing phthalates, through leaching phthalates into other products or through general contamination like discharge of untreated sewage into streams, rivers, lakes and oceans (Latini, Del Vecchio et al. 2006). Phthalates also reach the environment through pesticides and industrial lubricants (Peijnenburg 2008). The major source of human exposure is food contaminated during growth, production, processing, or packaging. Phthalates are not covalently bounded to the polymer, they are easily released to air, water, saliva, nutritional formulas and other extracting materials (Peijnenburg 2008). Human are exposed to phthalates because of they use it in plastics and other common consumer products most commonly used in plasticizer for polyvinyl chloride (PVC). Another source of human exposure by ingestion, inhalation and dermal contact, may occur in workers involved in the manufacture and use of phthalates (Norwitz 1958; Sánchez-Avila, Bonet et al. 2009). Inhalation exposure to 1000 mg/ms of phthalates has been reported to produce lacrimination and cough in humans. Health effects resulting from exposure to phthalates depend on the timing and the dose. Young, developing children are more vulnerable to phthalates exposure than adults because of the frequent use of phthalates in the making of sexy toys. Human exposure to DEHP from PVC medical devices and woman are more vulnerable exposure to DBP than men because DBP is used in variety of cosmetic and personal care like hair spray, fragrances, deodorants and nail polish. Phthalates present in the blood stream of pregnant women can cross through the placenta to the unborn child. Breastfeeding is another mode of mother to child transmission, if the breast milk is contaminated.

2.3.4. Variety of health problem cause by phthalates

Phthalates can cause so many problems in the human body namely:

Fertility especially among men

Cancer e.g. liver breast, prostate, testicular, colon

Autoimmune disease

Fertility problems like low sperm count, poor mobility of sperm, DNA damage in sperm lower testosterone level and ovarian dysfunction

Obesity, resistance to insulin and diabetes in men

Smaller testes and smaller genitals on average among male babies exposed to phthalates in mothers wombs

Asthma

Feminization of male fish, frogs and other amphibians living in rivers which is contaminated with phthalates

2.3.5. Human protection from exposure to phthalates

- Do not use the plastics shelves, rather use solid wood shelves

- Never use plastic bags use cloth bags for your groceries

- Use glass container with lids, stainless steel or ceramic food bowls

- Do not heat up food in the microwave in a containers such as margarine tubs, cottage cheese cartons or deli container

- Do not heat up or defrost food in the microwave in their packing material

- Avoid plastics with the # 3 recycling code that indicates PVC

2.4. ENDOCRINE DISRUPTORS COMPOUND (EDC's)

EDCôs can occur when some chemicals mimic or block the effects of natural hormones and disrupt the normal function of the body due to the recognition that the environment is contaminated with numerous endocrine disrupting compounds. Another definition of EDCôs is an estrogeneous agent that interferes with the synthesis, secretion, transport, binding, action or elimination of natural hormones in the body that are responsible for the maintenance of homeostasis, reproduction, development and behaviour (Rudel and Perovich 2009). The function of EDCôs can occur by different mechanisms namely

(i) By mimicking the sex steroid hormones estrogens and andogrogen by binding to their natural receptors either agonists or agonistics.

(ii) By altering the synthesis and breakdown of natural hormone.

(iii)By modifying the production and functioning of hormone receptors.

The pathway of EDCôs involve estrogenic, androgenic and thyroid

Estrogenic: are the subclasses of EDCôs that are mimic or block natural estrogens. Estrogenic consists of natural compound such as phytoestrogens, bioflavonoid and mycoestrogen and synthetic compound such as pesticides, herbicides, plastics and also include the synthetic hormone such as contraceptives (Matsui 2008).

Androgen: compounds that are mimic or block natural testosterone

Thyroid: compounds with direct and indirect impacts on the thyroid

The compounds that mimic a natural hormone named as estrogens, whereas compounds that block the effects of a natural hormone named as anti-estrogens. or anti-androgens. These EDCôs are usually found in industrial wastewater and are classify into three classes namely bisphenols,

alkyl phenols and phthalates (vom Saal, Guillette Jr et al. 2008). The classes of EDC are useful in industries in the production of many products like organ chlorinated, pesticides, plasticizers, fuels, plastics, polycarbonate, and unsaturated polyester-styrene resin, fungicides and antioxidants (vom Saal, Guillette Jr et al. 2008). According to the Scientific statement of endocrine safety, they presented the evidence that endocrine disruptors have effects on male and female production, breast development and cancer, prostate cancer, neuro endocrinology, thyroid, metabolism and obesity and cardiovascular endocrinology (Rudel and Perovich 2009).

Health effects caused by the endocrine disrupting compounds in humans, namely:

Alligator reproductive effects / birth defects

Breast cancer

Testicular and prostate cancer in men

Low sperm count / sexual dysfunction

Heart disease

Cognitive disorder and behavioural impairment in children

Premative puberty

Altered immune function

Hypospadia in infants

(Brouwers, Besselink et al. ; Eertmans, Dhooge et al. ; Jimènez ; Safe 2004; Porte, Janer et al. 2006; Safe, Jutooru et al. 2010)

Effects attribute to EDCôs in animals include the demasculation, feminization, alteration of immune functions and decrease fertility in birds, fish and mammals (Izzotti, Kanitz et al. ; Ishido, Morita et al. 2005; vom Saal, Guillette Jr et al. 2008)

2.4.1. Sources of EDCs

Table 2.2 Sources of EDCs

Source	Example
Natural environment	Air, water, soil
Food products	Soybeans, legumes, flax, yams and clover
Natural products	Phyto estrogens, Bioflavonoid, Myco estrogens
Phyto estrogens	Plants
Household products	Detergents
Additives	Parabenes
Pesticides	DDT, endosulfon, atrazine, nitrofen and tributyl tin
phthalates	Plastics, paint
Bisphenol A	Polymer production
Pharmaceuticals	Drug estrogens ï birth control pills, DES, cimedine Ethynylestradiol, Flutamide
Industrial chemicals	Polychlorinated bisphenol (PCBs), dioxin, benzo(a)pyrene
Products of incineration	
Paper production	
Fuel combustion	
Heavy metals	Cadmium, lead, mercury

Ref.: (Brouwers, Besselink et al. ; Gültekin and Ince 2007; Snyder, Adham et al. 2007; Broséus, Vincent et al. 2009; Kasprzyk-Hordern, Dinsdale et al. 2009; Loffredo, Eliana Gattullo et al. 2010)

2.4.2. Human exposure to EDC's

The human can be exposed to these EDCôs through inhalation, digestion , absorption through the skin and ingestion of drinking water, contaminated food, air , environmental pollutant and consumer products , that interfere with hormone biosynthesis metabolism, or any action resulting in a deviation from natural homeostatic control or reproduction (Rudel and Perovich 2009).

2.5 SENSOR

Electrochemical sensors have improved the performance of the conventional analytical tools, by eliminating slow sample preparation steps and use of expensive reagents. Therefore, they provide low cost analytical tools. Electro-analytical methods are used to obtain the quantities of an electro active analyte such as oxidation and reduction potentials, diffusion coefficients, electron transfer rates and electron transfer numbers (Wang and Lee 1997). Electro analytical methods such as cyclic voltammetry (CV), stripping voltammetry (SV), differential pulse polarography (DPP) and chronoamperometry are the most sensitive and informative analytical techniques. These techniques are capable of assaying trace concentrations of an electro active analyte and supply the useful information concerning its physical and chemical properties. Electrochemical sensor was developed over the past years because of the attractive the interest of clinical chemistry, it offer reliable, fast, portable, compact, sensitive and selective analytical results. Electrochemical sensor is advantageous as compared to other methods due to high sensitivity, accurate method, and rapid response time, simple to operate, able to determine various substances with different properties and provide high pollutant degradation. Many researchers have employed the electro-catalytic technique to treat and determine a variety of organic

pollutant in wastewater such as phenol, dye, phthalates etc. This method of electrochemistry is useful to study the behavior of ionic solution, monitoring the electron transfer process and the thermodynamic qualities. There are different types of electrochemical sensors based upon Voltammetric; amperometric or impedimetric measurements.

2.5.1 Voltammetric measurements

Voltammetry is an analytical technique involves the measurements of the current flowing through an electrode dipped solution containing electro-active compounds, while a potential scanning is imposed upon it over a period of time (Abo El-Maali 2004; Veiga, Dordio et al. 2010). Voltammetric techniques is based on the qualitative determination of organic and inorganic compounds in aqueous and non-aqueous solution, the measurement of kinetic rates and constant and also the determination electron transfer and reaction mechanism (Zanoni, Sousa et al. 2006). One of the most important applications of voltammetry is the qualitative analysis of trace of metals at εg/L levels or less (Choi, Seo et al. 2001; Buffle and Tercier-Waeber 2005). The other applications of voltammetry are the determination of redox potential, determination number of electrons in redox reaction and kinetics studies of reaction (Ibrahim 2000; Etienne, Bessiere et al. 2001; González-García, Ariño et al. 2005; Mohadesi and Taher 2007; Gong, Wang et al. 2010). Voltammetric techniques offer a great interest in excellent sensitivity with a very large useful linear concentration, a wide range of temperature, rapid analysis times and simultaneous determination of several analyses a large number of solvents and electrolytes (Ni, Qiu et al. 2004; Süslü and AltInöz 2005). Voltammetric techniques are used for a variety of purpose, including fundamental studies of oxidation and reduction processes in various media. Voltammetric measurements is carried out on the electrochemical cell, which consists of a

working electrode (where the reaction of interest is taking place), a reference electrode (constant potential (Ag/AgCl or SCE)) and a counter electrode (plays no part in redox but completes circuit (Hg or Pt)). In voltammetry, the effects of the applied potential and the behavior of the redox current for a reversible electrochemical reaction can be described by Nernst and Butler-Volmer equations (García-Hernández, Castilla et al. 1997; Shimizu, Hutcheson et al. 2007; Hamelers, ter Heijne et al. 2011).

$$E = E° - \frac{RT}{nF} \ln \frac{c_R^0}{c_O^0}$$ --- *Equation 1* (Nernst equation)

Where R is the molar gas constant (8.314J $mol^{-1}K^{-1}$), T is the absolute temperature (K), n is the number of electrons transferred, F is the Faradays constant (96.485 C/ equiv), c^0_R / c^0_O concentration of oxidation and reduction and E^0 is the standard reduction potential for the redox couple.

$$\frac{1}{nFA} = k^0\{c_O^0 \exp[-\alpha\theta] - c_R^0 \exp[(1-\alpha)]\}$$ -- *Equation 2* (Butler ï Volmer equation)

Where ɗ = nF ($E-E^0$)/RT, k^0 is the heterogeneous rate constant, Ŭis the transfer coefficient and A is the area of the electrode.

2.5.2 Amperometric

Amperometric is the method that is used to measure the current of the electrochemical cell, which produced in the redox action of analyte, in which the current signal is linearly dependent upon the concentration of the analyte captured on the electrode surface. The current is monitoring as a function of time, which is related to the concentration of the analyte by Faraday law and the law of mass transport. Amperometric sensor is more advantageous other than

potentiometric sensor because of its high selectivity, combines small size, low power, portable toxic, explosive gas and inexpensive,

2.5.3 Impedimetric

Electrochemical impedance spectroscopy (EIS) is an effective tool to validate the capacitance behavior and readily available technique for obtaining important electrochemical information, such as electrolyte resistance, charge transfer resistance, and Faradaic capacitance using Nyquist and Bode plot (Dubois, Froyer et al. 2004). EIS is a very powerful tool for the analysis of interfacial properties related to biorecognition events occurring at the modified surfaces to monitoring the time resolved capacitance (McIntyre and Pham). EIS is a tool for identifying and separation of different contribution to the electric and dielectric response of material. EIS sensor or biosensors, which are based on the change of electron transfer resistance using a redox probe couple such as $[Fe(CN)_6]^{3\bar{1}/4\bar{1}}$, have received much attention due to high sensitivity, potential advantages, reduced assay time, multiplexing sensing and simple operation. EIS is a sensitive method for identifying and separation of different contribution to the electric and dielectric response of material and also gives a possibility to study the process of immobilization and characterize electric features (Freger and Bason 2007). The impedance data usually simulated using Randles equivalent circuit in fig 1.10 consisting of a combination of the capacitance (C) and charge transfer resistance by redox reaction (R_{ct}) in series with the supporting electrolyte resistance (R_{sol}). Figure 2.10 is an example of Randles circuit (a) and Nyquist plot (b)

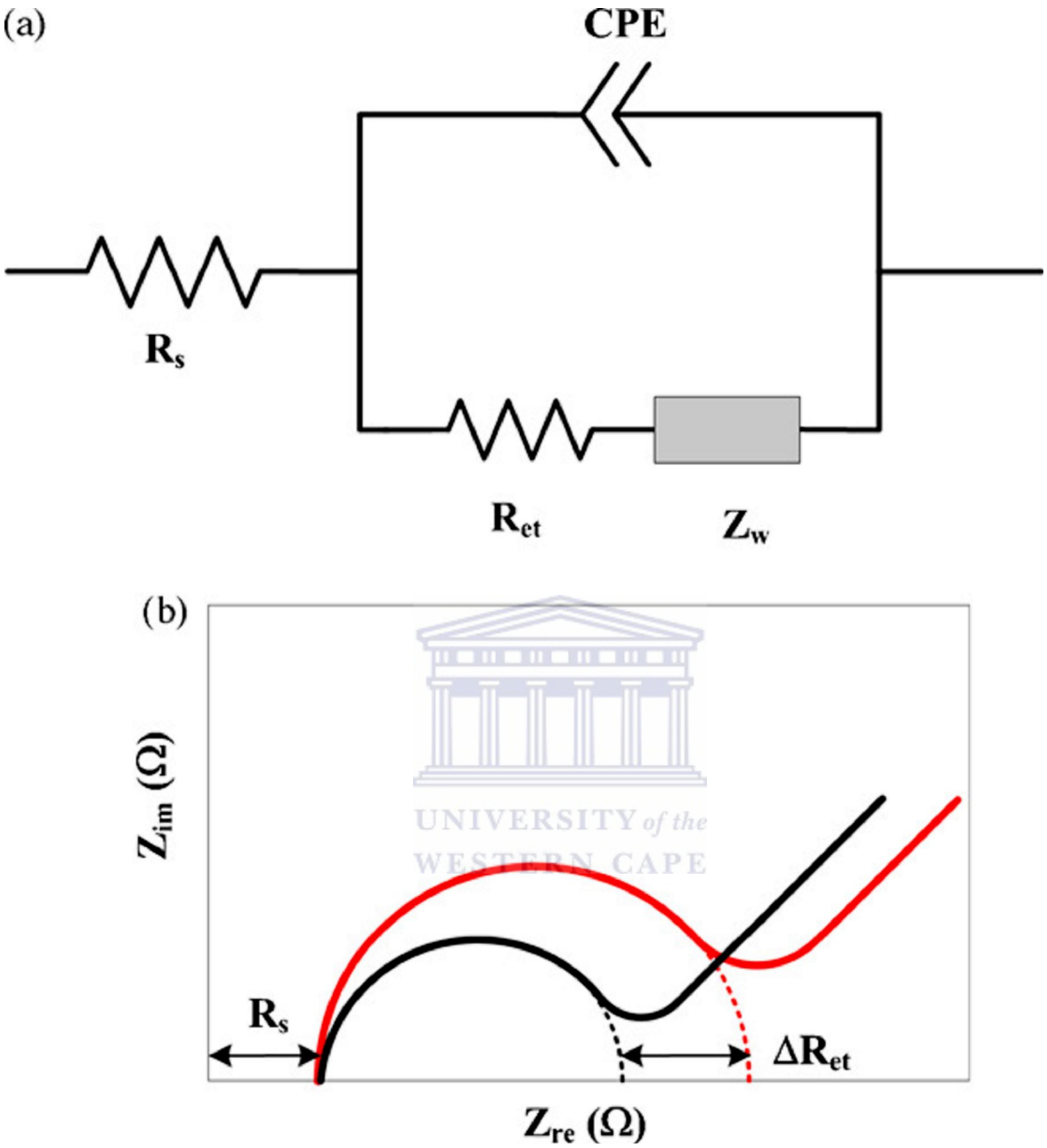

Figure 2.10: (a) Randles circuit and (b) Nyquist plot (www.consultrsr.com)

2.6 REFERENCES

Abo El-Maali, N. (2004). "Voltammetric analysis of drugs." Bioelectrochemistry **64**(1): 99-107.

Allen, N. S., M. Edge, A. Ortega, C. M. Liauw, J. Stratton and R. B. McIntyre (2002). "Behaviour of nanoparticle (ultrafine) titanium dioxide pigments and stabilisers on the photooxidative stability of water based acrylic and isocyanate based acrylic coatings." Polymer Degradation and Stability **78**(3): 467-478.

Alonso, E., I. Montequi and M. J. Cocero (2009). "Effect of synthesis conditions on photocatalytic activity of TiO_2 powders synthesized in supercritical CO_2." The Journal of Supercritical Fluids **49**(2): 233-238.

Amiridou, D. and D. Voutsa (2011). "Alkylphenols and phthalates in bottled waters." Journal of Hazardous Materials **185**(1): 281-286.

Asai, D., Y. Tahara, M. Nakai, Y. Yakabe, M. Takatsuki, T. Nose, T. Shinmyozu and Y. Shimohigashi (2000). "Structural essentials of xenoestrogen dialkyl phthalates to bind to the estrogen receptors." Toxicology Letters **118**(1-2): 1-8.

Bagó, B., Y. MartIn, G. MejIa, F. Broto-Puig, J. Diaz-Ferrero, M. Agut and L. Comellas (2005). "Di-(2-ethylhexyl)phthalate in sewage sludge and post-treated sludge: Quantitative determination by HRGC-MS and mass spectral characterization." Chemosphere **59**(8): 1191-1195.

Benson, R. (2009). "Hazard to the developing male reproductive system from cumulative exposure to phthalate esters--dibutyl phthalate, diisobutyl phthalate, butylbenzyl phthalate, diethylhexyl phthalate, dipentyl phthalate, and diisononyl phthalate." Regulatory Toxicology and Pharmacology **53**(2): 90-101.

Bian, C. and G. Xue (2007). "Nanocomposites based on rutile-TiO_2 and polyaniline." Materials Letters **61**(6): 1299-1302.

Brezová, V., Z. Vrecková, P. Billik, M. Caplovicová and G. Plesch (2009). "Photoactivity of mechanochemically prepared nanoparticulate titanium dioxide investigated by EPR spectroscopy." Journal of Photochemistry and Photobiology A: Chemistry **206**(2-3): 177-187.

Broséus, R., S. Vincent, K. Aboulfadl, A. Daneshvar, S. Sauvé, B. Barbeau and M. Prévost (2009). "Ozone oxidation of pharmaceuticals, endocrine disruptors and pesticides during drinking water treatment." Water Research **43**(18): 4707-4717.

Brouwers, M. M., H. Besselink, R. W. Bretveld, R. Anzion, P. T. J. Scheepers, A. Brouwer and N. Roeleveld "Estrogenic and androgenic activities in total plasma measured with reporter-gene bioassays: Relevant exposure measures for endocrine disruptors in epidemiologic studies?" Environment International

Brown, D. and S. E Thompson (1982). "Phthalates and the aquatic environment: Part I The effect of di-2-ethylhexyl phthalate (DEHP) and di-isodecyl phthalate (DIDP) on the

reproduction of and observations on their bioconcentration." Chemosphere **11**(4): 417-426.

Buffle, J. and M. L. Tercier-Waeber (2005). "Voltammetric environmental trace-metal analysis and speciation: from laboratory to in situ measurements." TrAC Trends in Analytical Chemistry **24**(3): 172-191.

Choi, J.-Y., K. Seo, S.-R. Cho, J.-R. Oh, S.-H. Kahng and J. Park (2001). "Screen-printed anodic stripping voltammetric sensor containing HgO for heavy metal analysis." Analytica Chimica Acta **443**(2): 241-247.

Dong, B., B.-L. He, J. Huang, G.-Y. Gao, Z. Yang and H.-L. Li (2008). "High dispersion and electrocatalytic activity of Pd/titanium dioxide nanotubes catalysts for hydrazine oxidation." Journal of Power Sources **175**(1): 266-271.

Doong, R.-A., T.-C. Hsieh and C.-P. Huang (2010). "Photoassisted reduction of metal ions and organic dye by titanium dioxide nanoparticles in aqueous solution under anoxic conditions." Science of The Total Environment **408**(16): 3334-3341.

Dubois, M., G. Froyer and D. Billaud (2004). "Electrochemical impedance spectroscopy and electron spin resonance characterization of the conductive state of parasexiphenylene electrochemically intercalated with sodium." Spectrochimica Acta Part A: Molecular and Biomolecular Spectroscopy **60**(8-9): 1831-1838.

Eertmans, F., W. Dhooge, S. Stuyvaert and F. Comhaire "Endocrine disruptors: effects on male fertility and screening tools for their assessment." Toxicology in Vitro **17**(5-6): 515-524.

Etienne, M., J. Bessiere and A. Walcarius (2001). "Voltammetric detection of copper(II) at a carbon paste electrode containing an organically modified silica." Sensors and Actuators B: Chemical **76**(1-3): 531-538.

Eveillard, A., L. Mselli-Lakhal, A. Mogha, F. Lasserre, A. Polizzi, J.-M. Pascussi, H. Guillou, P. G. P. Martin and T. Pineau (2009). "Di-(2-ethylhexyl)-phthalate (DEHP) activates the constitutive androstane receptor (CAR): A novel signalling pathway sensitive to phthalates." Biochemical Pharmacology **77**(11): 1735-1746.

Fernandes, D. M., A. A. W. Hechenleitner, M. F. Silva, M. K. Lima, P. R. S. Bittencourt, R. Silva, M. A. C. Melo and E. A. G. Pineda (2009). "Preparation and characterization of NiO, Fe_2O_3, $Ni_{0.04}Zn_{0.96}O$ and $Fe_{0.03}Zn_{0.97}O$ nanoparticles." Materials Chemistry and Physics **118**(2-3): 447-452.

Freger, V. and S. Bason (2007). "Characterization of ion transport in thin films using electrochemical impedance spectroscopy: I. Principles and theory." Journal of Membrane Science **302**(1-2): 1-9.

García-Hernández, M. T., J. Castilla, C. F. González-Fernández and J. Horno (1997). "Application of the network method to simulation of a square scheme with Butler-Volmer charge transfer." Journal of Electroanalytical Chemistry **424**(1-2): 207-212.

Ghasemi, E., A. Mirhabibi and M. Edrissi (2008). "Synthesis and rheological properties of an iron oxide ferrofluid." Journal of Magnetism and Magnetic Materials **320**(21): 2635-2639.

Gong, J., L. Wang, X. Miao and L. Zhang (2010). "Efficient stripping voltammetric detection of organophosphate pesticides using NanoPt intercalated Ni/Al layered double hydroxides as solid-phase extraction." Electrochemistry Communications **12**(11): 1658-1661.

González-García, O., C. Ariño, J. M. Díaz-Cruz and M. Esteban (2005). "Comparison of voltammetric detection assisted by multivariate curve resolution with amperometric detection in liquid chromatographic analysis of cysteine-containing compounds." Journal of Chromatography A **1062**(1): 95-101.

Gültekin, I. and N. H. Ince (2007). "Synthetic endocrine disruptors in the environment and water remediation by advanced oxidation processes." Journal of Environmental Management **85**(4): 816-832.

Gupta, A. K. and M. Gupta (2005). "Synthesis and surface engineering of iron oxide nanoparticles for biomedical applications." Biomaterials **26**(18): 3995-4021.

Gurunathan, K. and D. C. Trivedi (2000). "Studies on polyaniline and colloidal TiO_2 composites." Materials Letters **45**(5): 262-268.

Haddad, P. S., T. M. Martins, L. D'Souza-Li, L. M. Li, K. Metze, R. L. Adam, M. Knobel and D. Zanchet (2008). "Structural and morphological investigation of magnetic nanoparticles based on iron oxides for biomedical applications." Materials Science and Engineering: C **28**(4): 489-494.

Haley, B. and E. Frenkel "Nanoparticles for drug delivery in cancer treatment." Urologic Oncology: Seminars and Original Investigations **26**(1): 57-64.

Hamelers, H. V. M., A. ter Heijne, N. Stein, R. A. Rozendal and C. J. N. Buisman (2011). "Butler-Volmer-Monod model for describing bio-anode polarization curves." Bioresource Technology **102**(1): 381-387.

Han, F., V. S. R. Kambala, M. Srinivasan, D. Rajarathnam and R. Naidu (2009). "Tailored titanium dioxide photocatalysts for the degradation of organic dyes in wastewater treatment: A review." Applied Catalysis A: General **359**(1-2): 25-40.

Heudorf, U., V. Mersch-Sundermann and J. Angerer (2007). "Phthalates: Toxicology and exposure." International Journal of Hygiene and Environmental Health **210**(5): 623-634.

Hoang, V. L. T., Y. Li and S.-K. Kim (2008). "Cathepsin B inhibitory activities of phthalates isolated from a marine Pseudomonas strain." Bioorganic & Medicinal Chemistry Letters **18**(6): 2083-2088.

Huang, P.-C., C.-J. Tien, Y.-M. Sun, C.-Y. Hsieh and C.-C. Lee (2008). "Occurrence of phthalates in sediment and biota: Relationship to aquatic factors and the biota-sediment accumulation factor." Chemosphere **73**(4): 539-544.

Ibrahim, M. S. (2000). "Voltammetric behaviour and determination of the anthracycline antitumor drug nogalamycin." Analytica Chimica Acta **409**(1-2): 105-112.

Im, J. S., S. K. Lee and Y.-S. Lee "Cocktail effect of Fe_2O_3 and TiO_2 semiconductors for a high performance dye-sensitized solar cell." Applied Surface Science.

Ishido, M., M. Morita, S. Oka and Y. Masuo (2005). "Alteration of gene expression of G protein-coupled receptors in endocrine disruptors-caused hyperactive rats." Regulatory Peptides **126**(1-2): 145-153.

Izzotti, A., S. Kanitz, F. D'Agostini, A. Camoirano and S. De Flora "Formation of adducts by bisphenol A, an endocrine disruptor, in DNA in vitro and in liver and mammary tissue of mice." Mutation Research/Genetic Toxicology and Environmental Mutagenesis **679**(1-2): 28-32.

Jimènez, B. "Environmental effects of endocrine disruptors and current methodologies for assessing wildlife health effects." TrAC Trends in Analytical Chemistry **16**(10): 596-606.

Kang, H., L. Wang, M. O'Donoghue, Y. C. Cao, W. Tan, S. L. Frances and T. Chris Rowe (2008). Nanoparticles for biosensors. Optical Biosensors (Second Edition). Amsterdam, Elsevier**:** 583-621.

Kasprzyk-Hordern, B., R. M. Dinsdale and A. J. Guwy (2009). "The removal of pharmaceuticals, personal care products, endocrine disruptors and illicit drugs during wastewater treatment and its impact on the quality of receiving waters." Water Research **43**(2): 363-380.

Kim, E. H., Y. Ahn and H. S. Lee (2007). "Biomedical applications of superparamagnetic iron oxide nanoparticles encapsulated within chitosan." Journal of Alloys and Compounds **434-435**: 633-636.

Koch, H. M., B. Rossbach, H. Drexler and J. Angerer (2003). "Internal exposure of the general population to DEHP and other phthalates--determination of secondary and primary phthalate monoester metabolites in urine." Environmental Research **93**(2): 177-185.

Kruis, F. E., H. Fissan and A. Peled (1998). "Synthesis of nanoparticles in the gas phase for electronic, optical and magnetic applications--a review." Journal of Aerosol Science **29**(5-6): 511-535.

Latini, G., A. Del Vecchio, M. Massaro, A. Verrotti and C. De Felice (2006). "Phthalate exposure and male infertility." Toxicology **226**(2-3): 90-98.

Li, K., Y. Y. Ding, J. Guo and D. Wang (2008). "Surface electron structures and mechanism of nonradiative transitions on crystalline TiO_2 nanoparticles." Materials Chemistry and Physics **112**(3): 1001-1007.

Li, Q., C. Zhang and J. Li (2010). "Photocatalysis and wave-absorbing properties of polyaniline/TiO_2 microbelts composite by in situ polymerization method." Applied Surface Science **257**(3): 944-948.

Li, S.-Q., R.-R. Zhu, H. Zhu, M. Xue, X.-Y. Sun, S.-D. Yao and S.-L. Wang (2008). "Nanotoxicity of TiO2 nanoparticles to erythrocyte in vitro." Food and Chemical Toxicology **46**(12): 3626-3631.

Li, X., D. Wang, G. Cheng, Q. Luo, J. An and Y. Wang (2008). "Preparation of polyaniline-modified TiO_2 nanoparticles and their photocatalytic activity under visible light illumination." Applied Catalysis B: Environmental **81**(3-4): 267-273.

Li, X., G. Wang, X. Li and D. Lu (2004). "Surface properties of polyaniline/nano-TiO_2 composites." Applied Surface Science **229**(1-4): 395-401.

Li, Y., M. Ma, S. Sun, W. Yan and Y. Ouyang (2008). "Preparation of TiO_2-carbon surface composites with high photoactivity by supercritical pretreatment and sol-gel processing." Applied Surface Science **254**(13): 4154-4158.

Liu, Z., L. Hong and B. Guo (2005). "Physicochemical and electrochemical characterization of anatase titanium dioxide nanoparticles." Journal of Power Sources **143**(1-2): 231-235.

Liu, Z., J. Zhou, H. Xue, L. Shen, H. Zang and W. Chen (2006). "Polyaniline/TiO_2 solar cells." Synthetic Metals **156**(9-10): 721-723.

Loffredo, E., C. Eliana Gattullo, A. Traversa and N. Senesi (2010). "Potential of various herbaceous species to remove the endocrine disruptor bisphenol A from aqueous media." Chemosphere **80**(11): 1274-1280.

Matsui, S. (2008). Endocrine Disruptors. Encyclopedia of Ecology. J. Sven Erik and F. Brian. Oxford, Academic Press**:** 1259-1260.

Mazille, F., T. Schoettl and C. Pulgarin (2009). "Synergistic effect of TiO_2 and iron oxide supported on fluorocarbon films. Part 1: Effect of preparation parameters on photocatalytic degradation of organic pollutant at neutral pH." Applied Catalysis B: Environmental **89**(3-4): 635-644.

McIntyre, J. M. and H. Q. Pham "Electrochemical impedance spectroscopy; a tool for organic coatings optimizations." Progress in Organic Coatings **27**(1-4): 201-207.

Mohadesi, A. and M. A. Taher (2007). "Voltammetric determination of Cu(II) in natural waters and human hair at a meso-2,3-dimercaptosuccinic acid self-assembled gold electrode." Talanta **72**(1): 95-100.

Morales, M. P., O. Bomati-Miguel, R. Pérez de Alejo, J. Ruiz-Cabello, S. Veintemillas-Verdaguer and K. O'Grady (2003). "Contrast agents for MRI based on iron oxide nanoparticles prepared by laser pyrolysis." Journal of Magnetism and Magnetic Materials **266**(1-2): 102-109.

Nabi, D., I. Aslam and I. A. Qazi (2009). "Evaluation of the adsorption potential of titanium dioxide nanoparticles for arsenic removal." Journal of Environmental Sciences **21**(3): 402-408.

Ni, Y., P. Qiu and S. Kokot (2004). "Study of the voltammetric behaviour of maleic hydrazide and its determination at a hanging mercury drop electrode." Talanta **63**(3): 561-565.

Nishio, K., M. Ikeda, N. Gokon, S. Tsubouchi, H. Narimatsu, Y. Mochizuki, S. Sakamoto, A. Sandhu, M. Abe and H. Handa (2007). "Preparation of size-controlled (30-100 nm) magnetite nanoparticles for biomedical applications." Journal of Magnetism and Magnetic Materials **310**(2, Part 3): 2408-2410.

Noginov, M. M., N. Noginova, O. Amponsah, R. Bah, R. Rakhimov and V. A. Atsarkin (2008). "Magnetic resonance in iron oxide nanoparticles: Quantum features and effect of size." Journal of Magnetism and Magnetic Materials **320**(18): 2228-2232.

Norwitz, G. (1958). "Determination of diethyl and dibutyl phthalates in propellants." Analytica Chimica Acta **19**: 216-223.

Ostrovský, I., R. Cabala, R. Kubinec, R. Górová, J. Blasko, J. Kubincová, L. Rimnácová and W. Lorenz (2011). "Determination of phthalate sum in fatty food by gas chromatography." Food Chemistry **124**(1): 392-395.

Pardeike, J., A. Hommoss and R. H. Müller (2009). "Lipid nanoparticles (SLN, NLC) in cosmetic and pharmaceutical dermal products." International Journal of Pharmaceutics **366**(1-2): 170-184.

Parham, H. and N. Rahbar (2009). "Solid phase extraction-spectrophotometric determination of fluoride in water samples using magnetic iron oxide nanoparticles." Talanta **80**(2): 664-669.

Peijnenburg, W. J. G. M. (2008). Phthalates. Encyclopedia of Ecology. J. Sven Erik and F. Brian. Oxford, Academic Press**:** 2733-2738.

Porte, C., G. Janer, L. C. Lorusso, M. Ortiz-Zarragoitia, M. P. Cajaraville, M. C. Fossi and L. Canesi (2006). "Endocrine disruptors in marine organisms: Approaches and perspectives." Comparative Biochemistry and Physiology Part C: Toxicology & Pharmacology **143**(3): 303-315.

Quintin, M., O. Devos, M. H. Delville and G. Campet (2006). "Study of the lithium insertion-deinsertion mechanism in nanocrystalline [gamma]-Fe_2O_3 electrodes by means of electrochemical impedance spectroscopy." Electrochimica Acta **51**(28): 6426-6434.

Rudel, R. A. and L. J. Perovich (2009). "Endocrine disrupting chemicals in indoor and outdoor air." Atmospheric Environment **43**(1): 170-181.

Safe, S. (2004). "Endocrine disruptors and human health: is there a problem." Toxicology **205**(1-2): 3-10.

Safe, S., I. Jutooru and G. Chadalapaka (2010). Estrogenic Endocrine Disruptors: Molecular Characteristics and Human Impacts. Comprehensive Toxicology. A. M. Charlene. Oxford, Elsevier**:** 609-621.

Sánchez-Avila, J., J. Bonet, G. Velasco and S. Lacorte (2009). "Determination and occurrence of phthalates, alkylphenols, bisphenol A, PBDEs, PCBs and PAHs in an industrial sewage grid discharging to a Municipal Wastewater Treatment Plant." Science of The Total Environment **407**(13): 4157-4167.

Sathiyanarayanan, S., S. S. Azim and G. Venkatachari (2007). "Preparation of polyaniline-Fe_2O_3 composite and its anticorrosion performance." Synthetic Metals **157**(18-20): 751-757.

Seirafianpour, N., S. Badilescu, Y. Djaoued, R. Brüning, S. Balaji, M. Kahrizi and V.-V. Truong (2008). "Optical properties of low temperature prepared granular titanium dioxide on a silver substrate." Thin Solid Films **516**(18): 6359-6364.

Shen, Y. F., J. Tang, Z. H. Nie, Y. D. Wang, Y. Ren and L. Zuo (2009). "Preparation and application of magnetic Fe_3O_4 nanoparticles for wastewater purification." Separation and Purification Technology **68**(3): 312-319.

Shende, R. V. and S. J. Lombardo (2002). "Supercritical extraction with carbon dioxide and ethylene of poly(vinyl butyral) and dioctyl phthalate from multilayer ceramic capacitors." The Journal of Supercritical Fluids **23**(2): 153-162.

Shimizu, K., R. Hutcheson, M. D. Engelmann and I. Francis Cheng (2007). "Cyclic voltammetric and aqueous equilibria model study of the pH dependant iron(II/III)ethylenediamminetetraacetate complex reduction potential." Journal of Electroanalytical Chemistry **603**(1): 44-50.

Singh, K., A. Ohlan, R. K. Kotnala, A. K. Bakhshi and S. K. Dhawan (2008). "Dielectric and magnetic properties of conducting ferromagnetic composite of polyaniline with [gamma]-Fe_2O_3 nanoparticles." Materials Chemistry and Physics **112**(2): 651-658.

Snyder, S. A., S. Adham, A. M. Redding, F. S. Cannon, J. DeCarolis, J. Oppenheimer, E. C. Wert and Y. Yoon (2007). "Role of membranes and activated carbon in the removal of endocrine disruptors and pharmaceuticals." Desalination **202**(1-3): 156-181.

Stengl, V., J. Subrt, S. Bakardjieva, A. Kalendova and P. Kalenda (2003). "The preparation and characteristics of pigments based on mica coated with metal oxides." Dyes and Pigments **58**(3): 239-244.

Süslü, I. and S. AltInöz (2005). "Electrochemical characteristics of zafirlukast and its determination in pharmaceutical formulations by voltammetric methods." Journal of Pharmaceutical and Biomedical Analysis **39**(3-4): 535-542.

Thevenot, P., J. Cho, D. Wavhal, R. B. Timmons and L. Tang (2008). "Surface chemistry influences cancer killing effect of TiO_2 nanoparticles." Nanomedicine: Nanotechnology, Biology and Medicine **4**(3): 226-236.

Veiga, A., A. Dordio, A. J. P. Carvalho, D. M. Teixeira and J. G. Teixeira (2010). "Ultra-sensitive voltammetric sensor for trace analysis of carbamazepine." Analytica Chimica Acta **674**(2): 182-189.

vom Saal, F. S., L. J. Guillette Jr, J. P. Myers and S. H. Swan (2008). Endocrine Disruptors: Effect in Wildlife and Laboratory Animals. Encyclopedia of Ecology. J. Sven Erik and F. Brian. Oxford, Academic Press**:** 1261-1264.

Wang, S. S. and H.-S. Lee (1997). "An electrochemical sensor for distinguishing two-stroke-engine oils." Sensors and Actuators B: Chemical **40**(2-3): 199-203.

Wang, X., L. Gao, H. Zheng, M. Ji, T. Shen and Z. Zhang (2004). "Fabrication and electrochemical properties of α-Fe_2O_3 nanoparticles." Journal of Crystal Growth **269**(2-4): 489-492.

Xu, X., Q. Wang, H. C. Choi and Y. H. Kim "Encapsulation of iron nanoparticles with PVP nanofibrous membranes to maintain their catalytic activity." Journal of Membrane Science.

Yezhelyev, M. V., X. Gao, Y. Xing, A. Al-Hajj, S. Nie and R. M. O'Regan (2006). "Emerging use of nanoparticles in diagnosis and treatment of breast cancer." The Lancet Oncology **7**(8): 657-667.

Zanoni, M. V. B., W. R. Sousa, J. P. de Lima, P. A. Carneiro and A. G. Fogg (2006). "Application of voltammetric technique to the analysis of indanthrene dye in alkaline solution." Dyes and Pigments **68**(1): 19-25.

Zeng, T.-W., H.-H. Lo, C.-H. Chang, Y.-Y. Lin, C.-W. Chen and W.-F. Su (2009). "Hybrid poly (3-hexylthiophene)/titanium dioxide nanorods material for solar cell applications." Solar Energy Materials and Solar Cells **93**(6-7): 952-957.

Zengin, H., H. G. Spencer, G. Zengin and R. V. Gregory (2007). "Studies of solution properties of polyaniline by membrane osmometry." Synthetic Metals **157**(2-3): 147-154.

Zhang, W., T. Yang, X. Li, D. Wang and K. Jiao (2009). "Conductive architecture of Fe_2O_3 microspheres/self-doped polyaniline nanofibers on carbon ionic liquid electrode for impedance sensing of DNA hybridization." Biosensors and Bioelectronics **25**(2): 428-434.

Zhao, B., Y. Chu, Y. Huang, D. O. Hardy, S. Lin and R.-S. Ge (2010). "Structure-dependent inhibition of human and rat 11[beta]-hydroxysteroid dehydrogenase 2 activities by phthalates." Chemico-Biological Interactions **183**(1): 79-84.

CHAPTER THREE

EXPERIMENTAL PROCEDURE

3. Experimental procedure

3.1. Materials

Dibutyl, Diethylhexyl and Dioctyl phthalates (99%), Acetonitrile, Titanium isopropoxide (97%), isopropanol, chitoson, starch, iron sulphate, acetic acid, ethanol, lithium perchlorate, nitric acid, aniline. All chemicals were purchased from Sigma Aldrich.

3.1.1. Chemical synthesis of titanium dioxide nanoparticles using sol-gel method

The preparation method of metal oxide nanoparticles follow procedures similar to earlier reported (S.Mahshid[a] et.al., 2009) such as sol-gel method was carried out by mixing two different solutions, a precursor and a hydrolysis solution. A precursor solution was a mixture of 5 ml Titanium isopropoxide and 15 ml isopropanol. Hydrolysis solution was a mixture of 25 ml distilled water and 75 ml 2 ï propanol. Nitric acid was used to adjust the pH of the hydrolysis solution. The gel was started by mixing the two solutions together under vigorous stirring at room temperature for 30 minutes at the mixing rate of 1125 rp/minutes. The white precipitation was observed after mixing the two solutions. After stirring the solution for 30 minutes the stirring rate was reduced to 500 rp/minutes to minimize the coagulation of the titanium oxide particle during sol- gel reaction. The product was washed with ethanol and dried for 3 hrs at 100 °C, then annealed for 3 hrs at 550 °C.

3.1.2. Chemical synthesis of iron oxide nanoparticles on polysaccharide template

An accurately weighed 0.5 g starch was dissolved in 20 ml of distilled water and about 2.49 g $FeSO_4$.$7H_2O$ was added to the solution. The solution was stirred for 30 minutes using the magnetic stirrer at 1250 rp/minutes and heated the solution at 800 °C (heating rate of 5 °C/min) and maintained the temperature for 120 minutes. The use of template could prevent aggregation of particles and indicating the stability of the nanoparticles against agglomeration

3.2. Solutions

Saline PBS of pH 7.0 containing 10 mM of Na_2HPO_4, KH_2PO_4 and 0.3 mM KCl was prepared. 5 mM solution of dibutyl, dioctyl and diethylhexyl phthalates were prepared separately in 5 ml of ethanol. 100 mM solution of lithium per chlorate was prepared in 100 ml of water.

3.3. Electrochemical measurements

A BASi 100 system was used to perform all electrochemical experiments using three electrodes cell. Glassy carbon electrode (GCE) with diameter 0.3 cm was used as the working electrode, platinum wire as the counter electrode, and Ag/AgCl as the reference electrode. For square wave voltammetry (SWV) measurements, amplitude of 25 mV and frequency of 15 Hz were applied. All solutions were de-oxygenated by bubbling argon through it for 15 min.

3.4. Preparation of sensor membrane electrode (Fe_2O_3 or TiO_2 NPs*)*

The amount of 2 mg of Fe_2O_3 or TiO_2 NPs was weighed, then 1000 ul water/ethanol (50%) was added and 12 ul of 5 % nafion was also added to the solution. The nafion in the solution was used as a binder of nanoparticles on the surface area of the glassy carbon electrode. The solution was ultrasonicated using water bath for 10 minutes. Glassy carbon electrode (GCE) was first

polished with 1, 0.3 and 0.05 micron alumina powder rinsed with water and then ultrasonicated in ethanol for 5 minutes followed by ultrasonicated in water for another 5 minutes. The experiment was performed in a three electrochemical cell under nitrogen bubbling in a solution of PBS for 15 minutes, with scanning rate of 50 mV/s. The cleaned GCE was dried with nitrogen. 2 ul of iron oxide nanoparticles was drop coating on the surface area of the glassy carbon, dried it in the oven at 35 °C for 5 minutes. Then, the metal oxide-loaded GCE was immersed into 0.1 M PBS or 0.1 M $LiClO_4$ as a working electrode. Pt wire was used as a counter electrode and Ag/AgCl as a reference. 0.1 M PBS or 0.1 M $LiClO_4$ was chosen as electrolyte due to its stability and the superior performance in proton transport. The blank glassy carbon before modification shows no electrochemistry (redox peaks) in the saline PBS was determined using cyclic voltammetry (CV) and square wave voltammetry (SWV).

3.5 Preparation of polymer nanocomposites (PANI/Fe_2O_3 or TiO_2 NPs)

An actual weighed of 0.03 mg of Fe_2O_3 or TiO_2 NPs was dissolved in 1000 ul concentrated H_2SO_4 and stirring the solution for 2 hrs to make the nanoparticles completely dissolved. Distilled 0.2 M aniline was prepared in 0.1 M H_2SO_4. After two hrs the solution of the nanoparticles and aniline were mixed together to form one solution under continuous stirrer at room temperature for overnight. The prepared solution was ultrasonicated for 30 minutes to remove the impurities, and deoxygenated under nitrogen bubbling for 15 minutes. The experimental measurements for the polymer nanocomposites were conducted at room temperature in solution of 1 M H_2SO_4 using three electrode cell in a BASi 100 system. The polymerization of PANI alone, PANI doped titanium dioxide (PANI/TiO_2) and PANI doped iron oxide nanoparticles (PANI/Fe_2O_3) was conducted on the cleaned GCE. The polymer nanocomposites were growth on a 0.0071 cm^2 electrode in an acidic medium (1 M H_2SO_4)

scanning anodically from -400 to + 1100 mV at 50 mV/s. The polymer growth of nanocomposites were obtained by CV applying 20 scans from the solution containing 0.2 M aniline doped metal oxide nanoparticles in 1 M H_2SO_4.

3.6. Characterization techniques

To determine the particle size, the morphology and particle distribution of the nanopowder, the sample was dispersed in ethanol and ultrasonicated for 3mins and then observed on Transmission Electron Microscope (TEM) TiO_2 and Fe_2O_3 nanopowder was suspended in ethanol under sonification for 15 minutes and then deposited on copper grids that were covered with a continuous film of carbon. The samples were dried using the oven at 35 °C for 15 minutes allowing the solvent to evaporate. UV/Vis spectra were collected with a Nicolette Evolution 100 spectrometer (Thermo Electron Co-operation, UK). UV-visible measurements were recorded over a range of 350 ï 700 nm using 3 cm^2 quartz cuvettes. Samples for UV/Vis were prepared by diluting the NP dispersion in ethanol. XRD analysis was used to determine the crystalline phase of the nanoparticles. SEM was used for the determination of morphology of the metal oxide nanoparticles. Teflon tape was used to attach the sample onto the vibration holder and followed by coating with carbon using a splutter coater.

Figure 3.11: Experimental design

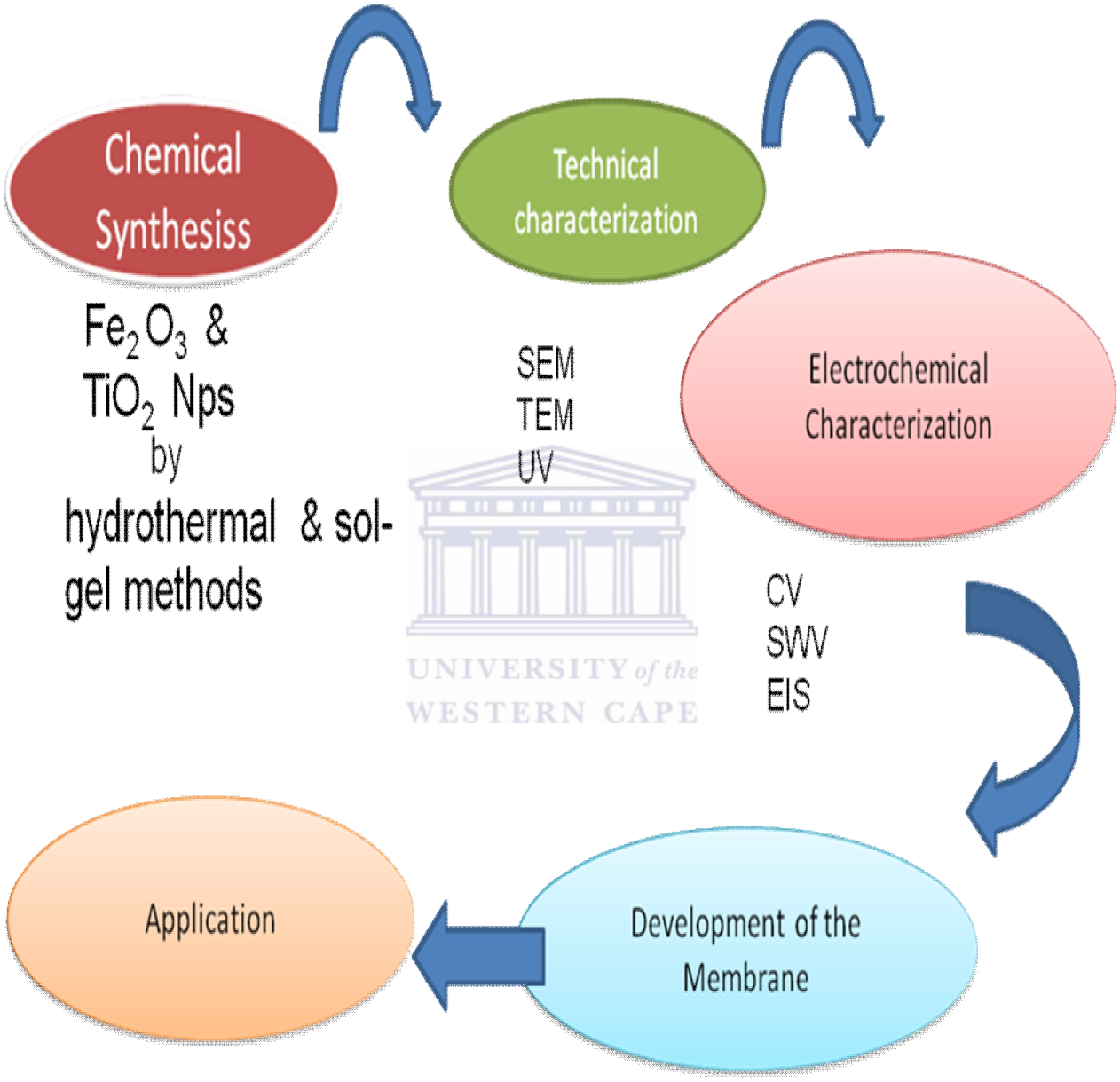

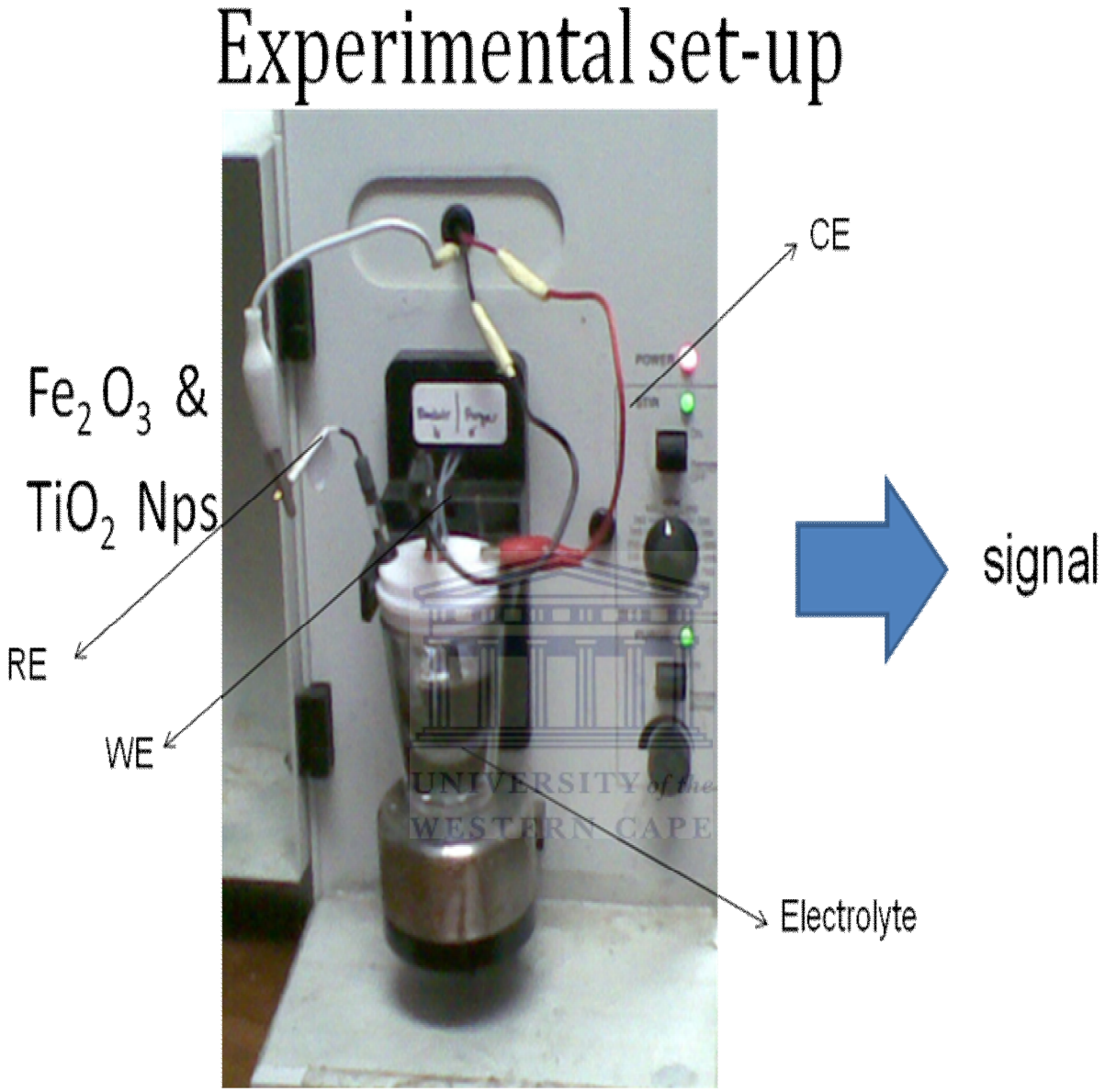

Figure 3.12: A diagram of an electrochemical cell

CHAPTER FOUR

RESULTS AND DISCUSSION

4. RESULTS AND DISCUSSION

4.1 Morphological study of Fe_2O_3 NPs and TiO_2 NPs

4.1.1 TEM analysis of Fe_2O_3 NPs and TiO_2 NPs

High resolution transmission electron microscopy (HRTEM) technique was used in the characterization of the metal oxide nano-powders to determine the size distribution, morphology and particle size and to study local microstructures (such as lattice vacancies and defects, lattice fringe and grid plan) (Haddad, Martins et al. 2008) and surface atomic arrangement of crystalline nanoparticles. Literature reported that the chemical synthesis of Fe_2O_3 and TiO_2 NPs can be divided into four steps (i) precursor formation, (ii) nucleation stage, (iii) growth and (iv) aging. Then after the formation of nucleation and growth stage the average size and size distribution that are observed from the HRTEM may change by aging. The rates of the four steps mentioned above are determined by the final particle size and size distribution. The free energy change due to nucleation, ΔG, can be described by: $\Delta G = n(\mu s - \mu L) + A\gamma$ *Equation (3)*

where n is the number of moles in the nucleus, μs and μL are the chemical potentials of the solid and the dissolved phase, A is the surface area, and γ is the surface energy of the solid – liquid interface. $(\mu s - \mu l) = -RT \ln \frac{cl}{cs} = -RT \ln S$ *Equation (4)* is used in determining the chemical potentials where cL and cs are the precursor concentration in the liquid and the solubility of the solid (assuming unity activity coefficients), respectively, R and T are the gas constant and temperature, and S is the super saturation, the combination of equation 1 and 2 leads to equation 3. $\Delta G^* = \frac{16\pi V 2m\gamma}{3(RT \ln S)2}$ *Equation (5)*

The nanoparticles obtained had a good uniform distribution of particle morphology with a size of 50 nm for a Fe_2O_3 nanoparticles as shown in figure 4.13 A & B while 20 nm was recorded for TiO_2 NP as shown in figure 4.14. Metal oxide nanoparticles revealed fine particle morphology with significantly low agglomeration and were round in shape. The titanium dioxide nanoparticles were prepared using sol-gel method and calcined at 550 °C while iron oxide nanoparticles were prepared on starch as a polysaccharide template using hydrothermal method. TEM results of the titanium dioxide nanoparticles revealed a highly aggregated nano-powder with globular structure in nature.

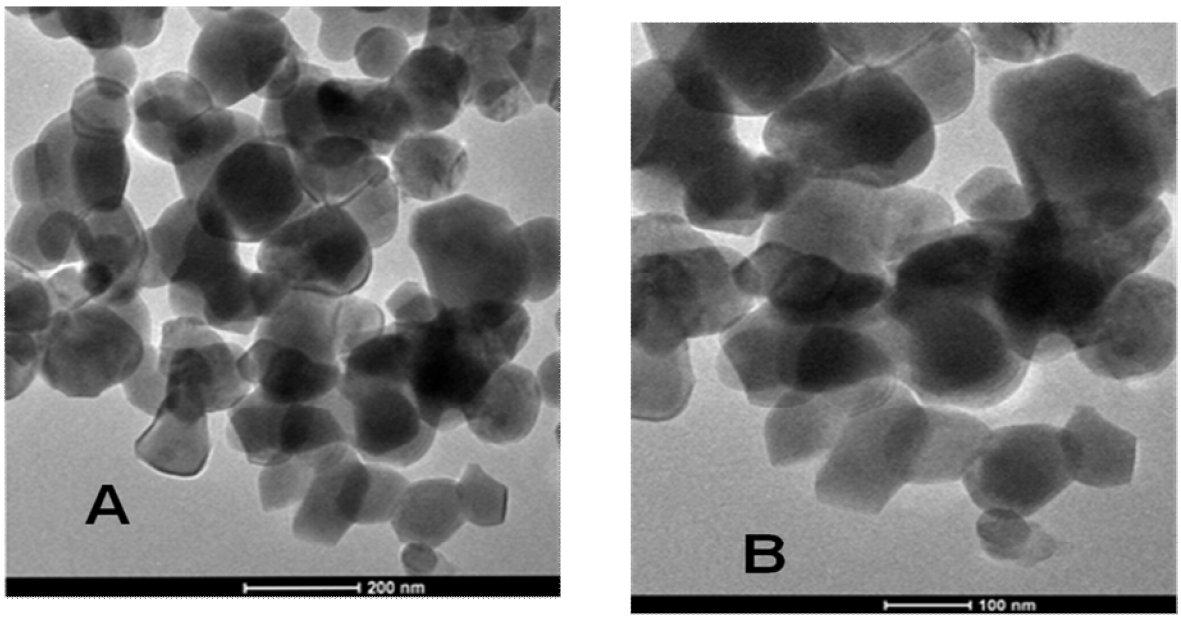

Figure 4.13: TEM images of the Fe_2O_3 NPs (50 nm), prepared by hydrothermal method, calcined at 800 °C for 3 hrs

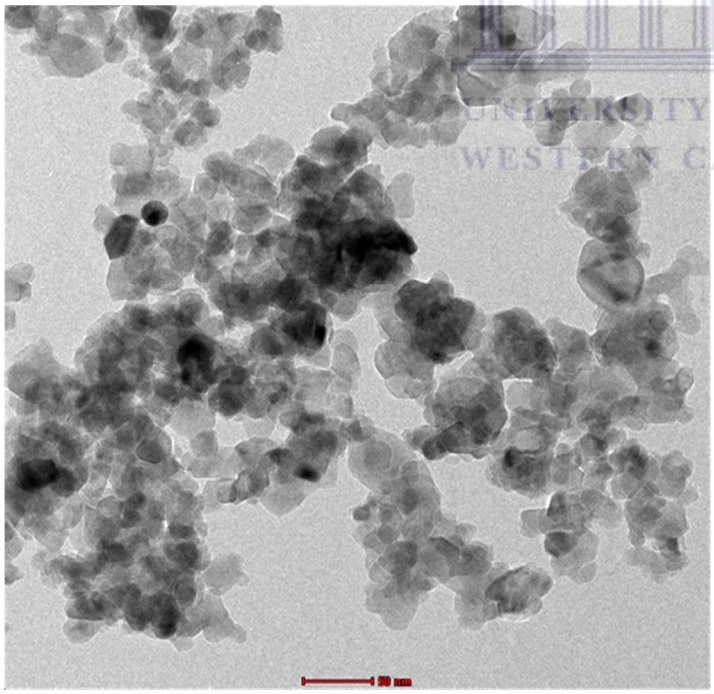

Figure 4.14: HRTEM images of the TiO_2 NPs (20 nm) prepared by sol-gel method, the sample was calcined for 2 hrs at 550 °C

4.1.2 SEM analysis of TiO_2 and Fe_2O_3 NPs

SEM was used to study the morphology of the metal oxide nanoparticles. The SEM pictures of TiO_2 and Fe_2O_3 NPs showed a high distribution and uniform pattern with an average of 20 nm 50 nm respectively. Typical SEM images at different magnification of the TiO_2 and Fe_2O_3 NPs are shown below in figure 4.15 & 4.16. The size and distribution of TiO_2 and Fe_2O_3 NPs in polyaniline matrix were also confirmed by SEM. SEM images of PANI, PANI/Fe_2O_3 NPs and PANI/TiO_2 nanocomposites are shown in figures 4.17, 18 and 19 respectively. PANI images revealed the porosity of cavity which may allow incorporation of doping nanoparticles to enhance its conductivity. The advantage of nanocomposite was to enhance the catalytic activity of the nanoparticles. The SEM images of PANI alone showed that the nanoparticles were cauliflower like whereas the structure changed when the metal oxides are introduced. It is clear that from the images, nanocrystalline TiO_2 and Fe_2O_3 NPs dispersed uniformly in the polyaniline matrix. The SEM images of PANI doped TiO_2 NPs showed that the small white particles were distributed in the polymer matrix. PANI/TiO_2 image showed decrease in the amount of globular structure observed in the morphology of PANI which revealed a compact appearance which may also be attributed to the charge transfer state. PANI/Fe_2O_3 NPs image showed an increased in surface porosity due to cavity as a results of incorporation of nanoparticles. It can be inferred from the morphology of the PANI doped nanoparticles will tend to allow electron flow easily more than PANI. The porous structure of PANI doped metal oxide nanoparticles were further confirmed by cyclic voltammetry.

A B

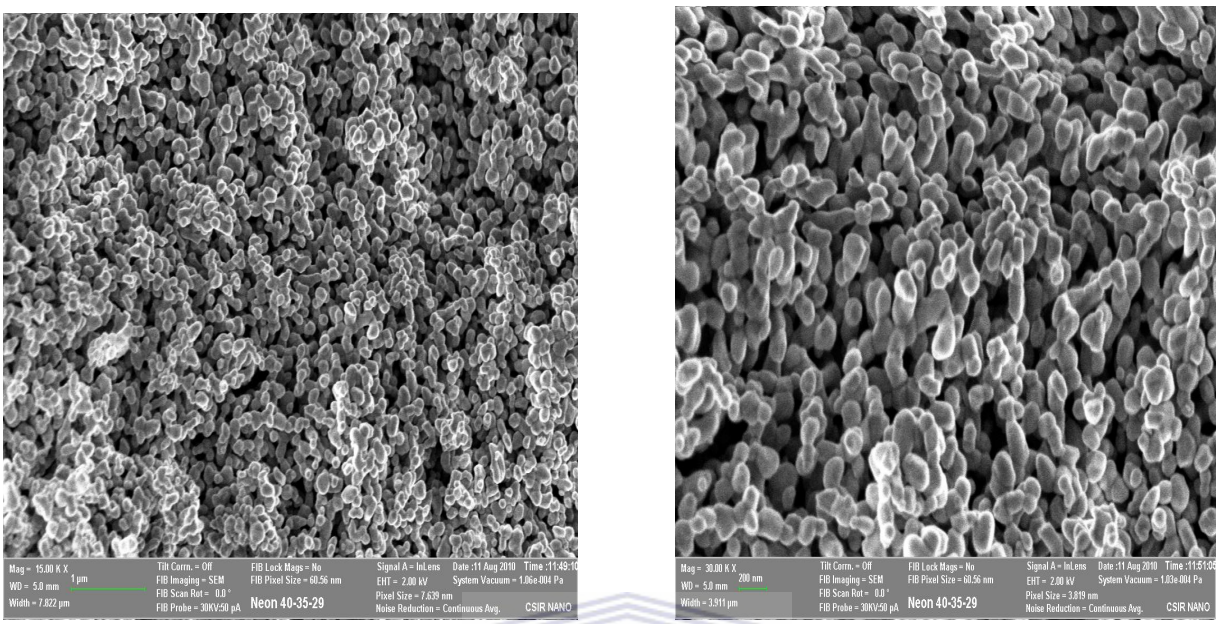

Figure 4.15: SEM images of Fe_2O_3 NPs at different magnification (a) at 1 εm (b) at 200 nm

A B

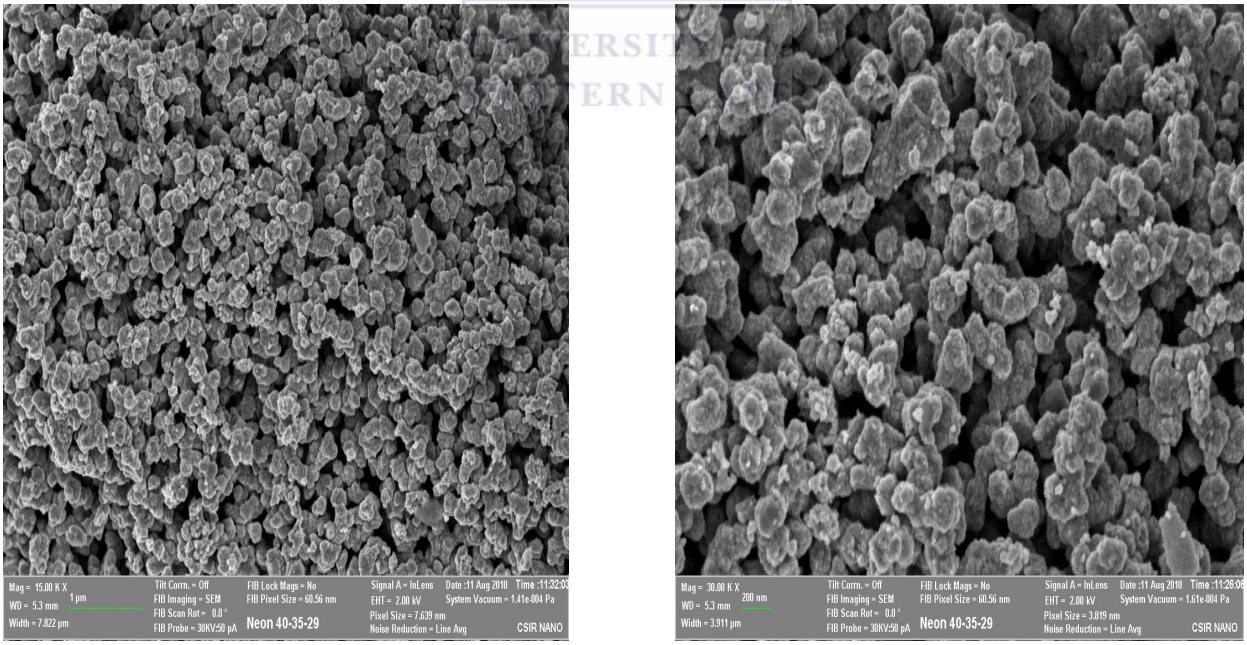

Figure 4.16: SEM images of TiO_2 NPs at different magnification (a) at 1 εm (b) at 200 nm

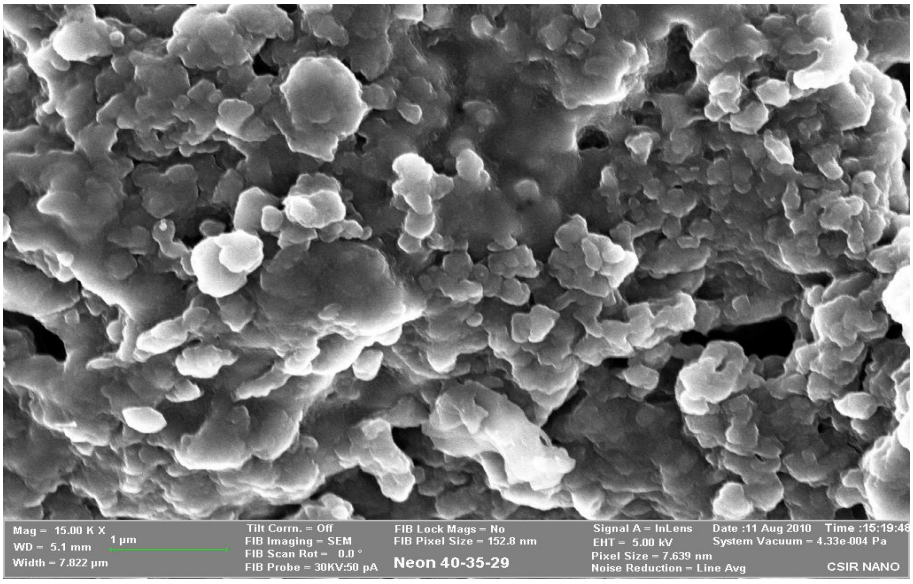

Figure 4.17: SEM image of PANI alone

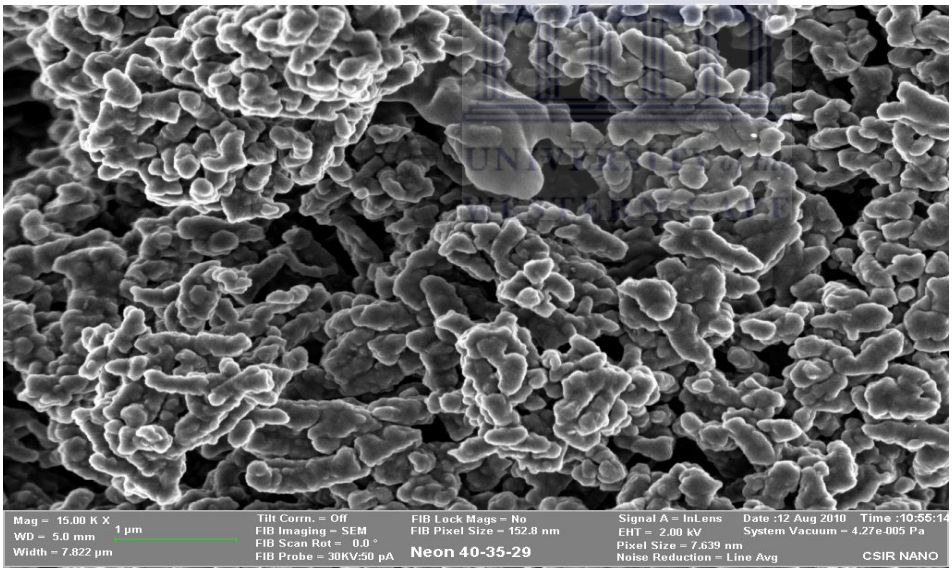

Figure 4.18: SEM image of PANI doped Fe_2O_3 NPs

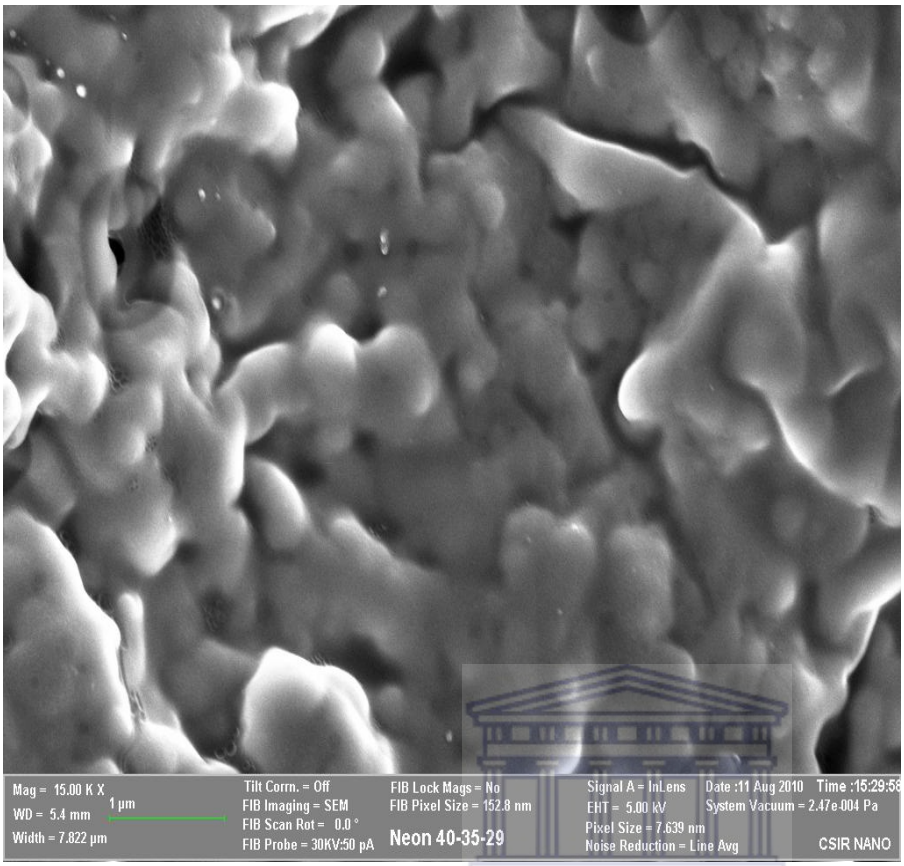

Figure 4.19: SEM image of PANI doped TiO_2 NPs

4.2 UV -vis analysis of Fe_2O_3 NPs and TiO_2 NPs

UV- vis was used for the quantitative determination of the sample at ultraviolet ï visible region. When the molecule absorbs UV -vis radiation, the absorbed energy excites an electron into an empty higher energy orbital (Singh, Ohlan et al. 2008)l. The wavelength and intensity of absorption spectra of samples depend on the size, crystalline type and morphology. UV-vis spectrometry measurement of Fe_2O_3 NPs showed the strongest peak at a wavelength of 574 nm, indicating that Fe_2O_3 NPs can absorb light in light visible region whereas TiO_2 can absorb light at a wavelength of 326 nm in ultraviolet region. Ultraviolet region has wavelength of 200 -400 nm and visible light has wavelength of 400 - 800 nm. The results of the UV ï vis spectroscopy are in agreement with the literature i.e. work of Guo Bin et.al showed the wavelength of TiO_2 NPs in ultraviolet region at the wavelength of 325 nm. The absorption band observed in the ultraviolet region at 325 nm was assigned to the electronic transition. Therefore the wavelength appearing 326 nm was related to O^{2-} Ÿ Ti^{4+} charge transfer transition (Kuiying Li a,b. et.al Ying Dinga, Jing Guo, et. al (2008)). Figures 4.20 and 4.21 showed the spectra of Fe_2O_3 and TiO_2 NPs respectively.

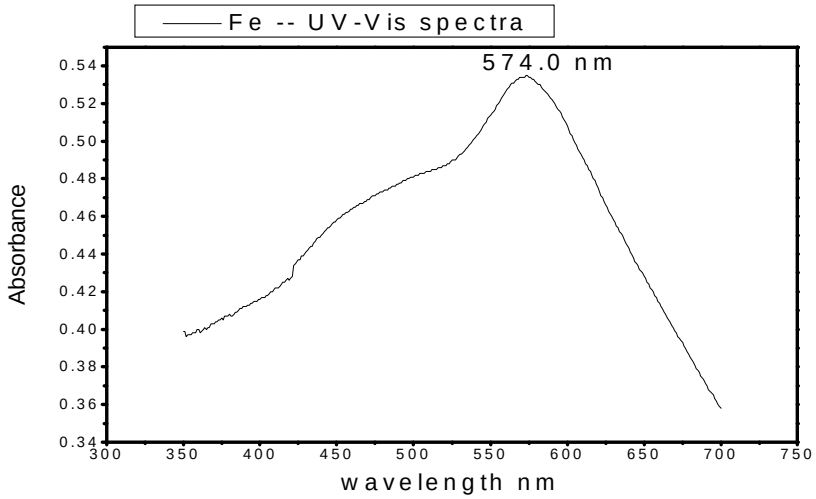

Figure 4.20: UV ï vis spectra of Fe_2O_3 NPs

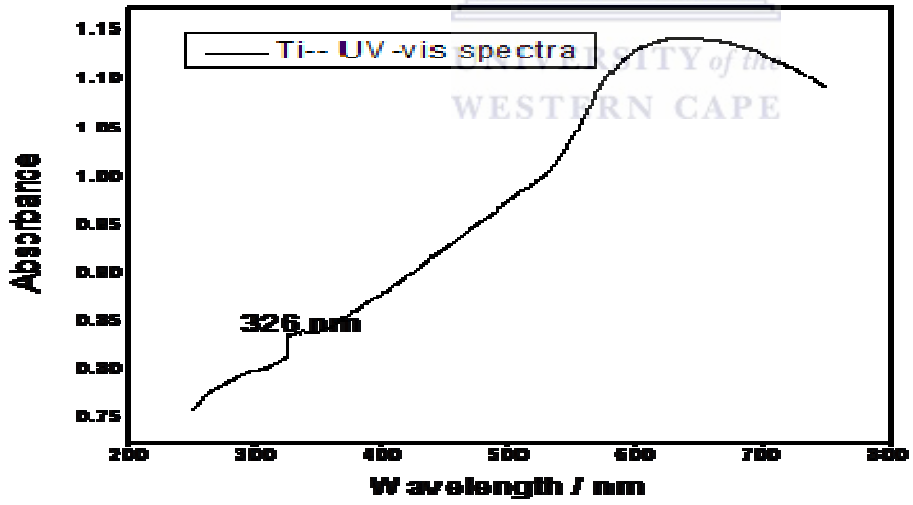

Figure 4.21: UV ï vis spectra of TiO_2 NPs

4.3 study of the crystalline nature of the metal oxide nanoparticles

XRD analysis was used to determine the crystalline phase and the purity of the nanoparticles (Nishio, Ikeda et al. 2007). The results revealed that the metal oxide nanoparticles were highly crystalline. All observed peaks diffraction indicated a high phase purity of metal oxide nanoparticles. In figure 4.22 XRD analysis of TiO_2 NPs calcined at 600 °C, the peaks appeared at 2 ɗ = 25.3° (101), 37.9°, and 48.1° were corresponding to anatase phase, whereas the peaks at 2 ɗ = 27.42° (110) 54.4° belongs to rutile. The XRD peaks of TiO_2 showed that TiO_2 NPs undergo two process of phase transition i.e. transformation of amorphous to rutile and rutile to anatase phase, which is most stable phase. The XRD pattern of Fe_2O_3 NPs showed the diffraction peaks ca 2 ɗ = 33.5°, 37.9°, 41. 2° and 48.1° indicated that the Fe_2O_3 NPs diffraction peaks are broadened owing to small particle size and the particle were highly crystalline. The Debye ï Scherer formula was used to calculate the crystal size of the nanoparticles from the broadening (101 and 311) of the reflection of the spinal structure (Fernandes, Hechenleitner et al. 2009).

Debye ï Scherer formula $D = \frac{0.9\lambda}{\beta Cos\theta}$ *Equation (6)* where D = particle size, ɔ = wavelength of the X-ray used ɓ and ɗ are half width of XRD lines and half diffraction angle of 2 ɗ (101 anatase and 311 for iron).The XRD pattern showed diffraction peaks with positions in excellent agreement with the literature values for Fe_2O_3 and TiO_2 NPs (Im, Lee et al. ; Wang, Gao et al. 2004; Bian and Xue 2007). Figure 4.22 and 4.23 show the XRD pattern of the synthesized TiO_2 and Fe_2O_3 NPs respectively.

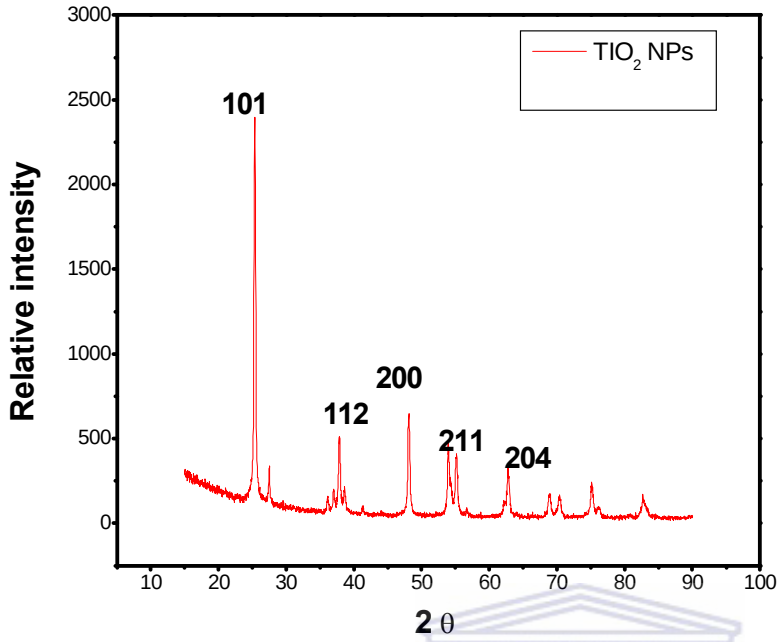

Figure 4.22: XRD pattern of the synthesized TiO_2 NPs, calcined at 550 °C

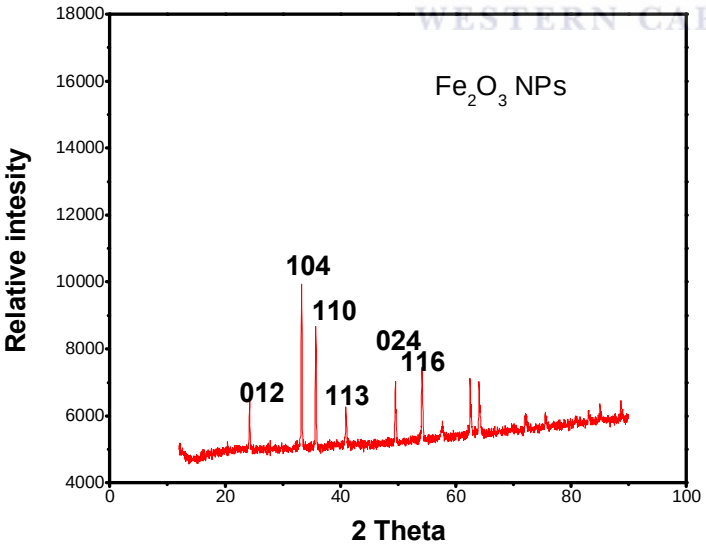

Figure 4.23: XRD pattern of the synthesized Fe_2O_3 NPs prepared by hydrothermal method using starch as a template

4.3 Voltammetric analysis

4.3.1 Electrochemical study of iron oxide nanoparticles by voltammeric technique

The characterization of the Fe_2O_3 NPs were carried out in two solutions (0.1 M PBS (pH 7.0) and 0.1 M $LiClO_4$ (pH 6.67)) at a room temperature. The electrochemical methods employed were CV and SWV at potential range of - 1350 to 500 mV at scan rates of 50 mV/s. According to the observed results both solutions showed the redox peaks of Fe_2O_3 NPs. Figure 4.24 showed the cyclic voltammogram (CV) of modified GCE with Fe_2O_3 NPs and unmodified in PBS whereas figure 4.25 was for the square wave voltammogram (SWV). The square wave voltammetry was used for the confirmation of the peaks that were observed on the cyclic voltammetry. The modified electrode was prepared by drop-coating the iron oxide nanoparticles on the surface of electrode. The solid line on the graph of cyclic and square wave voltammetry was for the results of the background in both solutions (0.1 M PBS & $LiClO_4$), whereas the dotted lines on cyclic and square wave voltammogram was the results of the modified glassy carbon electrode by immobilizing the iron oxide nanoparticles on the surface of a glassy carbon electrode. The results showed there was no electrochemistry observed on bare GCE, the electrochemistry occurred after the modification of the GCE with Fe_2O_3 NPs. Therefore the nanoparticles showed good electrochemical activity and catalytic effect. The cyclic and square wave voltammogram of the iron oxide nanoparticles immobilized on GCE at 50 mVs^{-1} showed reversible redox couple. The redox couple 1 in the graph of 0.1 M PBS occurred at E_{pa} = -600 mV; E_{pc} = -1200 mV; E^0 = -900 mV and æEp = - 600 mV, these peaks represents the reduction and oxidation of iron oxide nanoparticles. Our results indicated that at a formal potential (-900

mV) the nanoparticles Fe^{III} can be partially reduced into Fe^{II}. The results obtained were in agreement with earlier report that the nanoparticles are reduced to the metallic iron at highly negative potential of -1.5 to -1.8 V (Dubois* and J. Chevalet et.al. 2003). Figure 4.26 showed the cyclic voltammogram (CV) of Fe_2O_3 NPs in 0.1 M $LiClO_4$ (pH 6.7) as an electrolyte at a scan rates of 50 mV/s. The redox couple 1 occurred at E_{pa} = -503 mV; E_{pc} = -995 mV; E^o= -749 mV and æEp = -492 mV/s, these peaks stands for the REDOX of the iron oxide nanoparticles. At formal potential (-749 mV) show Fe^{III} can be partial reduced into Fe^{II} as the explanation given on the above statement for the redox couple of iron using 0.1 M PBS.

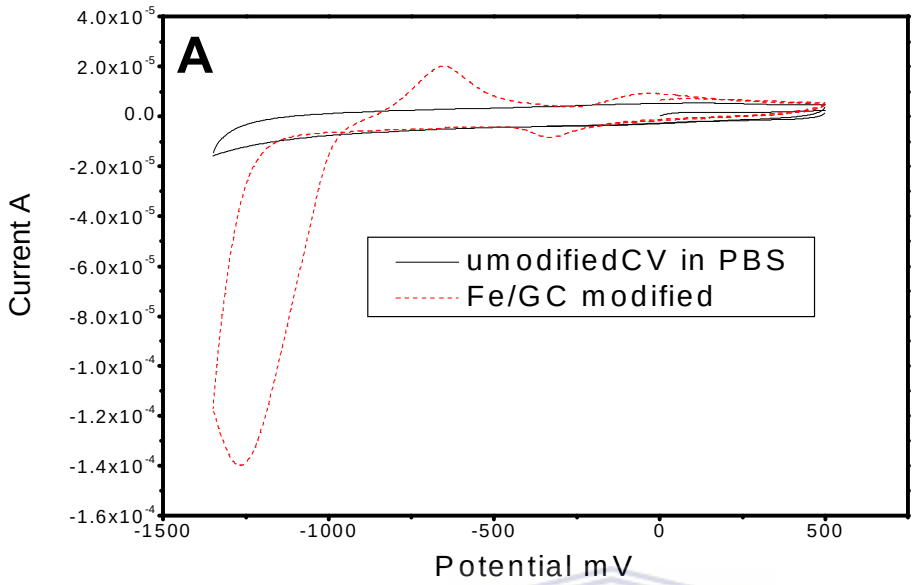

Figure 4.24 : CV of unmodified and modified GCE (Fe_2O_3 NPs) in 0.1 M PBS (pH 7.0).

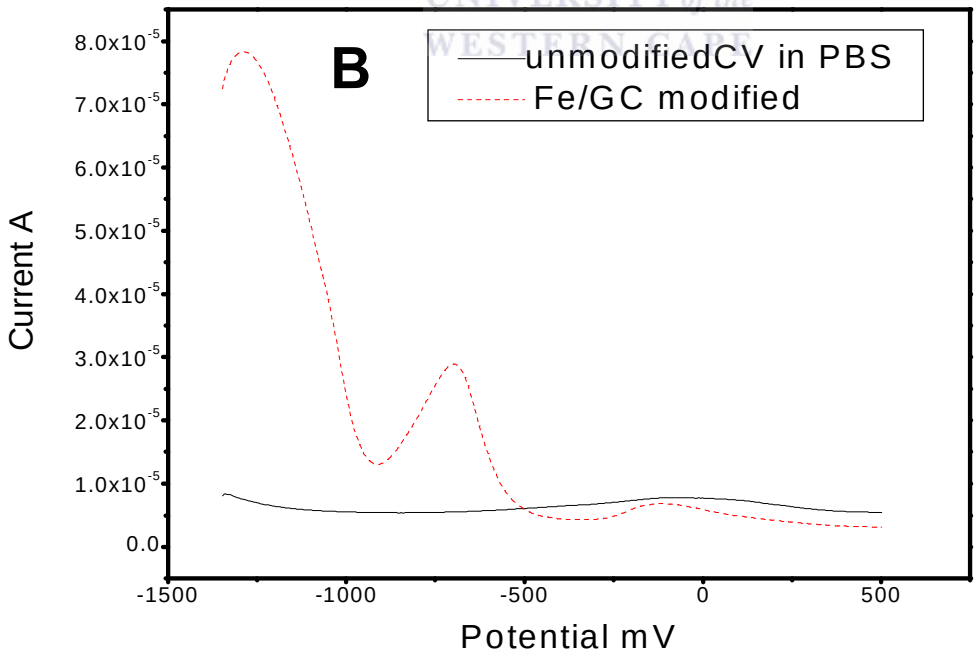

Figure 4.25: SWV of unmodified and modified GCE (Fe_2O_3 NPs) in 0.1 M PBS (pH 7.0)

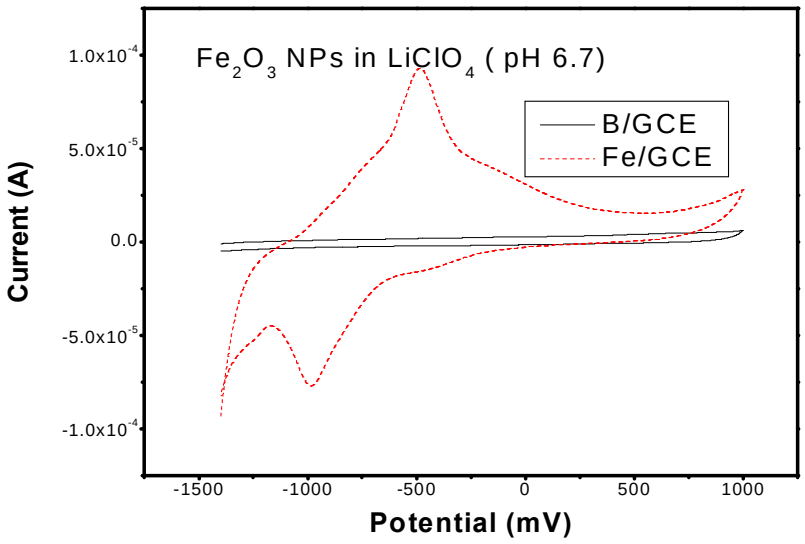

Figure 4.26: CV of unmodified and modified GCE (Fe_2O_3 NPs) in 0.1 M $LiClO_4$ (pH 6.7) at 50 mV/s

4.3.2 pH effects on modified electrode

This characterization effects of pHs was carried out in aqueous medium (0.1 M PBS) at a potential range of -1350 to 500 mV using the SWV techniques. The characterization was carried out on Fe_2O_3 NPs modified GCE in 0.1 M PBS at pH 7, pH 8 and pH 9 at a scan rate of 50 mV/s. The results illustrated that at pH 7 the peak current of the redox peaks had very high currents as compared to the peak currents of the other pHs (pH 8 & 9). Therefore the pH 7 was found to be a suitable pH for the characterization of iron oxide nanoparticles in 0.1 PBS (pH7) as shown in figure 4.27.The highest catalytic activity of the iron oxide nanoparticles was observed at pH 7. Beyond this pH, the catalytic activity decreased drastically as shown by decrease in peak current for pH 8 and 9. The decrease of the catalytic activity of iron can be caused by electrostatic stabilization attributed to the negative hydroxyl group (base) becoming predominant with the increase in pH (Li, Ding et al. 2008).

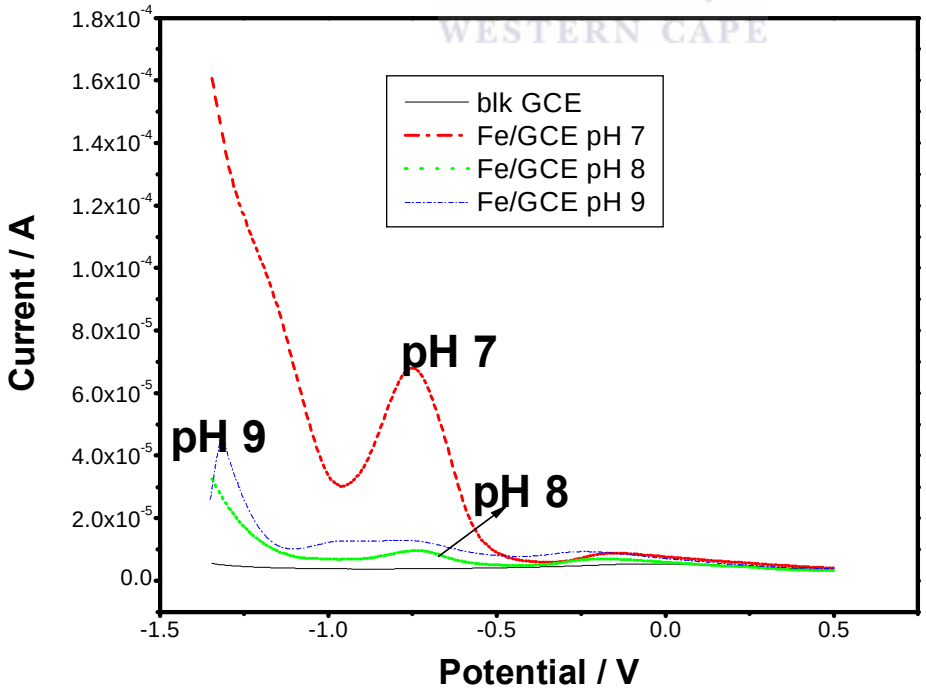

Figure 4.27: SWV of modified GCE with Fe_2O_3 NPs in 0.1 M PBS (pH 7, 8 & 9) 50 mV/s.

4.3.3 Electrochemical study of titanium dioxide nanoparticles by voltammetric technique

The characterization of the TiO_2 NPs was done in aqueous medium i.e. 0.1 M PBS (pH 7.0) and 0.1 M $LiClO_4$ (pH 6.67) at a scan rates of 5, 50 and 100 mV/s in which one redox peak was observed. This characterization was achieved using CV and SWV at potential range of - 1600 to 1000 mV. There was no electrochemistry observed on bare GCE, the electrochemistry occurred after the modification of the GCE with TiO_2 NPs in both solutions. Figure 4.28 showed the cyclic voltammogram (CV) of modified GCE with TiO_2 NPs and unmodified in 0.1 M $LiClO_4$ (pH 6.7) whereas figure 4.29 is for the square wave voltammogram (SWV). The square wave voltammetry was used for the confirmation of the peaks that were observed on the cyclic voltammetry. The modified electrode was prepared by drop-coating the TiO_2 NPs on the surface of GCE. The redox peak showed ca 1376 mV, this peak stands for the oxidation of titanium dioxide nanoparticles. The reduction peak was not shown from the graph but the square wave confirmed that the formal potential occurred at ca 1296 mV. Figure 4.30 showed the cyclic voltammogram (CV) of modified GCE with TiO_2 NPs and unmodified in 0.1 M PBS (pH 7.0) whereas figure 4.31 is for the square wave voltammogram (SWV). The redox couple show at Epa = - 10.10 mV, Epc = - 13.60 mV & E^0 = - 11.85 mV. The observed results were showed a good electro-activity of the nanoparticles and catalytic effects.

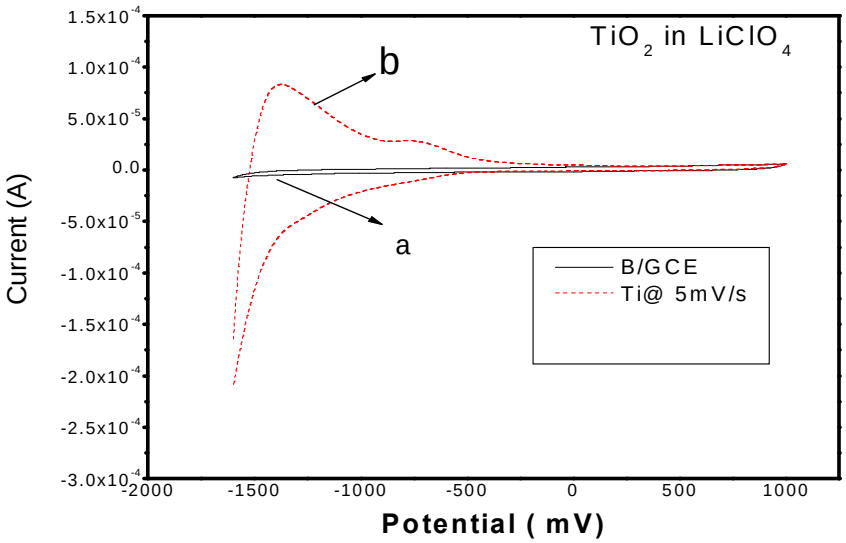

Figure 4.28: CV of unmodified and modified GCE (TiO_2 NPs) in 0.1 M $LiClO_4$ (pH 6.7) a) bare GCE, b) GCE/TiO_2 NPs at 50 mV/ s

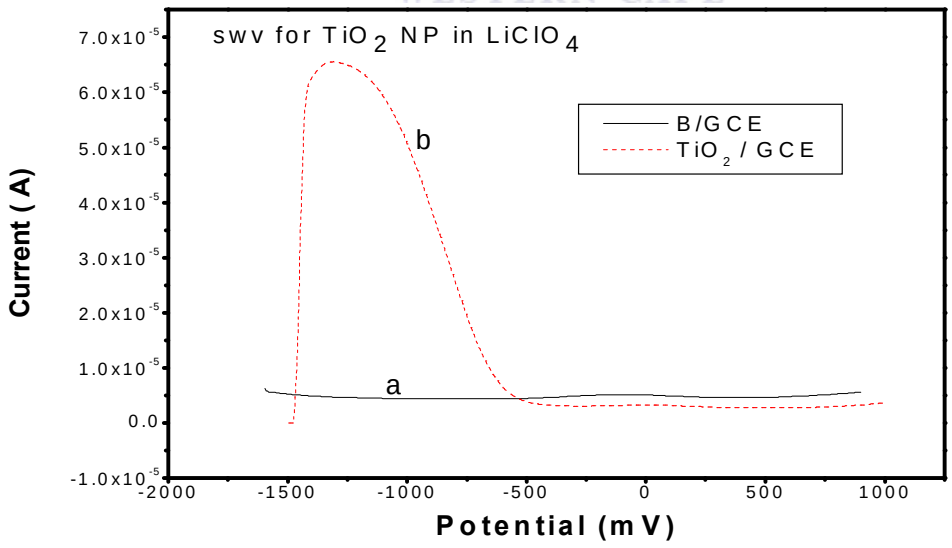

Figure 4.29: SWV of unmodified and modified GCE (TiO_2 NPs) in 0.1 M $LiClO_4$ (pH 6.7) a) bare GCE, b) GCE/TiO_2 NPs

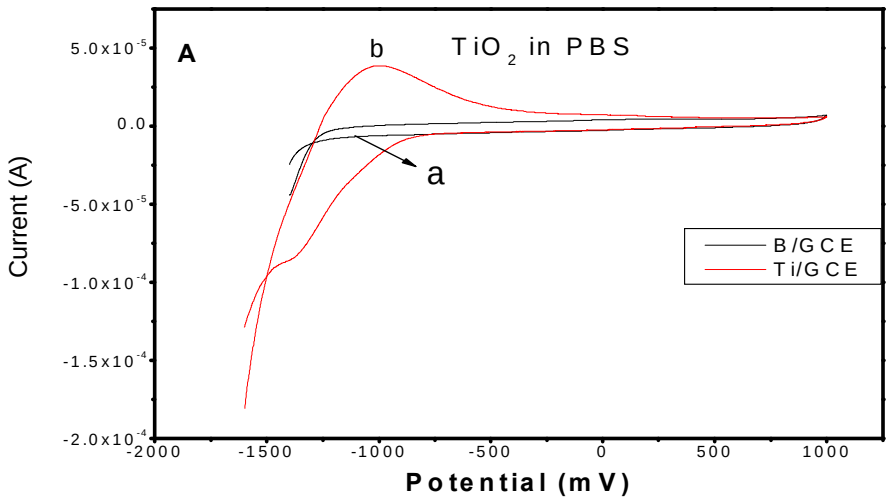

Figure 4.30: CV of unmodified and modified GCE (TiO_2 NPs) in 0.1 M PBS (pH 7.0) bare GCE, b) GCE/TiO_2 NPs at 50 mV/s

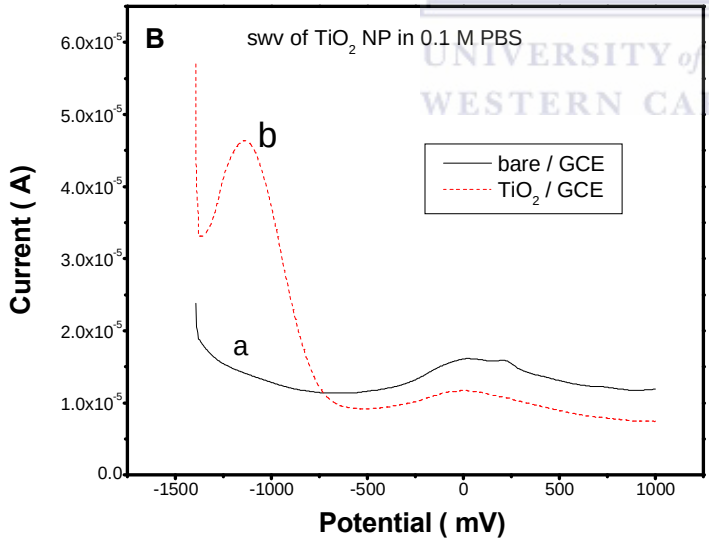

Figure 4.31: SWV of unmodified and modified GCE (TiO_2 NPs) in 0.1 M PBS (pH 7.0) bare GCE, b) GCE/TiO_2 NPs

4.4 Impedance analysis

4.4.1 Characterization of the Fe_2O_3 and TiO_2 nanoparticles by electrochemical impedance spectroscopy (EIS)

4.4.1. Nyquist plot analysis

Electrochemical impedance spectroscopy (EIS) has been an important tool in investigating the processes taking place on the surface of an electrode in the presence of a redox couple $Fe(CN)_6^{3/4-}$. EIS analysis was performed on the glassy carbon electrode to verify the different electron-transfer kinetics before and after binding of metal oxide nanoparticles. The result showed that the redox kinetics of $Fe(CN)_6^{3-/4-}$ were slow when GCE was modified with Fe_2O_3 and TiO_2 NPs compared to the unmodified GCE. The R_{ct} of modified electrode increased greatly compared to that of the bare GCE, due to electrostatic repulsion that existed between the metal oxide and the negative charge backbone of the redox probe thereby increasing the electron transfer tunnel which result in sluggish flow of electron from the solution interface into the surface of the electrode. The metal oxide insulated the flow of electron in between redox probe and the electrode surface and the due to increase in the electron transfer tunnelling. The increase in R_{ct} values reflected the diameter increase of the semicircle at high frequencies in the impedance graph due to the blocking behaviour of the electrode surface for the charge transfer to the redox probe. The metal oxide nanoparticles were less conducting and exhibited kinetically controlled electrochemistry at very low frequency compared to the bare electrode. To confirm the EIS data, the CV scans were used in the same solution. The results of CV revealed that metal oxides nanoparticles modification had less current than bare. The value of the exchange current obtained for the metal oxide modified electrode also corroborated the fact that the metal oxide

was less conducting when compared to bare electrode. It may also be attributed the blockage of the electrode by the metal oxide nanoparticles, which indicated that nanoparticles function as barriers that make interfacial charge transfer more difficult in the electrolytes solution [Tayo et al sensors paper,2008, Bard and Faulkner).

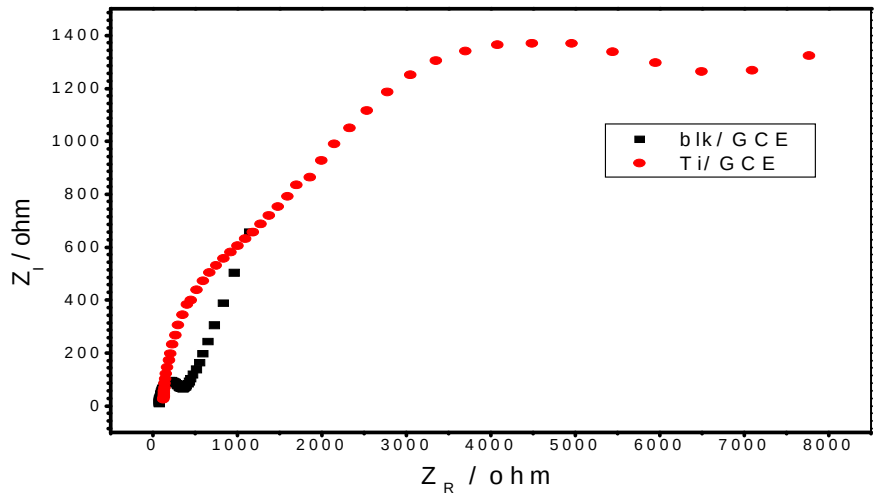

Figure 4.32: Nyquist plot of bare GCE and GCE/TiO_2 NPs in 5 mM $Fe(CN)_6^{3-/4-}$ redox probe.

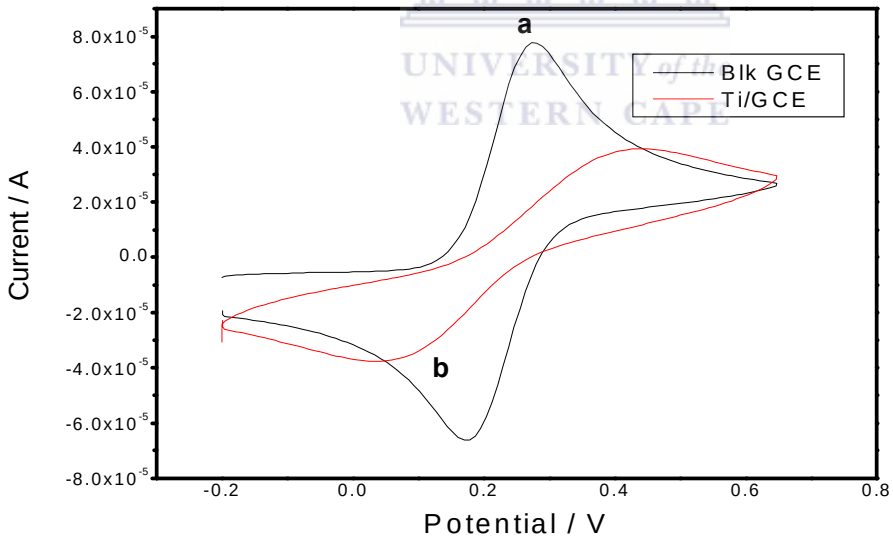

Figure 4.33: Cyclic voltammograms (CV for (a) bare glassy carbon electrode (GCE) and (b) modified GCE with TiO_2 NPs in 5 mM $Fe(CN)_6^{3-/4-}$ redox probe.

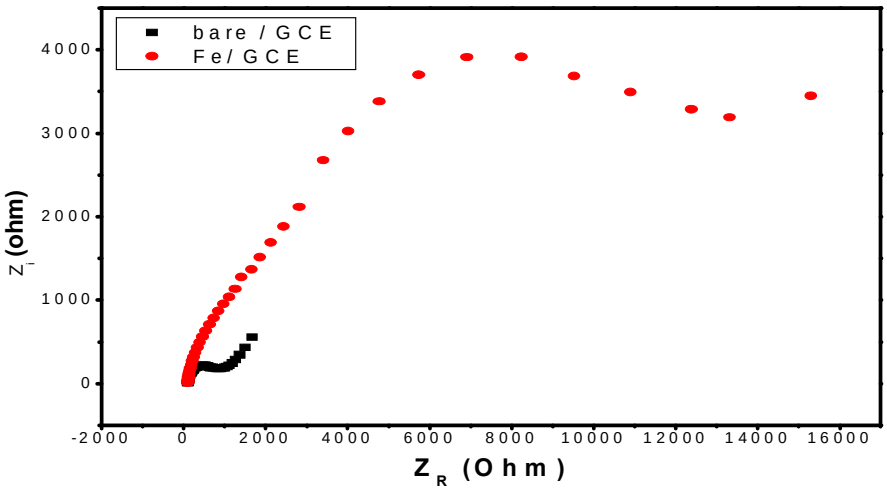

Figure 4.34: Nyquist plot of bare GCE and GCE/Fe_2O_3 NPs in 5 mM $Fe(CN)_6^{3-/4-}$ redox probe.

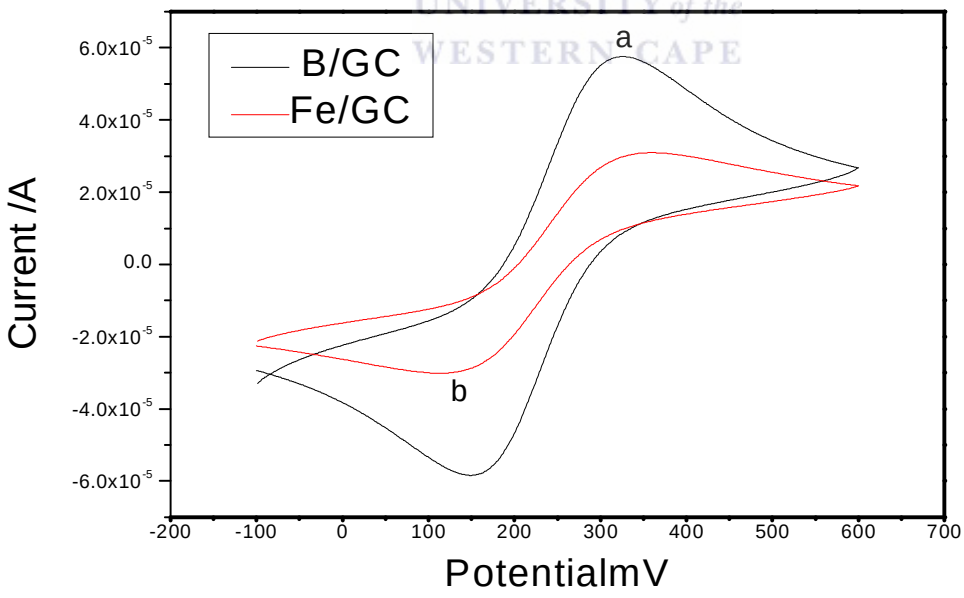

Figure 4.35: CV for (a) bare glassy carbon electrode (GCE) and (b) modified GCE with Fe_2O_3 NPs in 5 mM $Fe(CN)_6^{3-/4-}$ redox probe.

Table 4.1. The EIS parameters obtained from the circuit fitting of plots in figure 4.33 & 4.35 for bare and modified glassy carbon

	R_s	R_{ct}	Zw	CPE
GCE	88.28 q	224.2 q	859.4 DW	485.5 nF
Ti / GCE	153.5 q	1,779 K q	6.565 KDW	136 nF
Fe / GCE	124.7 q	1.646 K q	82.28 DW	499.27 nF

The parameters from table 4.1 were used to calculated the time constant use equation 5a & 5b and the exchange current by using equation 6 (Quintin, Devos et al. 2006)

Time constant = Ű

$$\omega_{max} = \frac{1}{R_{ct}C_{dl}} \qquad \textit{Equation (7a)}$$

$$\tau = R_{ct}C_{dl} \qquad \textit{Equation (7b)}$$

where C_{dl} = double layer capacitance; Ű= time constant; R_{ct} = charge transfer resistance

$\upsilon_{max} = 2\acute{}f$ *Equation (7c)*

$$i_o = \frac{RT}{nFR_{ct}} \qquad \textit{Equation (8)}$$

Where i_o = exchange current, R = gas constant, F = Faraday constant and n = number of electrons transferred.

Table 4.2 : calculated results for time constant and exchange current

Electrode	Ű(s rad^{-1})	a_o (A)
GCE / bare	116617.1	1.0697^{-4}
GCE / Fe_2O_3 NP	1601944	1.5597^{-6}
GCE / TiO_2	821798.42	1.4433^{-5}

4.4.2 Bode plot analysis of Fe_2O_3 NPs and TiO_2 NPs

The bare GCE electrode exhibited a high conductivity ability compared to modified GCE with iron and titanium nanoparticles with a lower charge transfer resistance thereby allowing free flow of electron from the solution electrolyte and the electrode. An increase in charge transfer resistance with a value of 1,779 kq and 1,646 kq were recorded for titanium and iron nanoparticles. These values revealed the insulating ability of the nanoparticles thereby hindering the free flow of electron from the redox probe to the surface of the electrode. Increases in the charge transfer resistance may be attributed to the electrostatic repulsion that existed between the nanoparticles and the negative charge redox probe. The value of the exchange current obtained for the bare electrode also showed that electron transfer was faster on the bare electrode compared to the modified electrode. The bode plot in fig 4.36 also corroborated this fact because a tremendous increase in impedance from 1.32 kÝ (bare) to 65.29 kÝ was observed after the electrode was modified with the nanoparticles with a corresponding shift in phase angle from 28.7 ° to 59.5° respectively for the bare and the nanoparticles modified electrode.

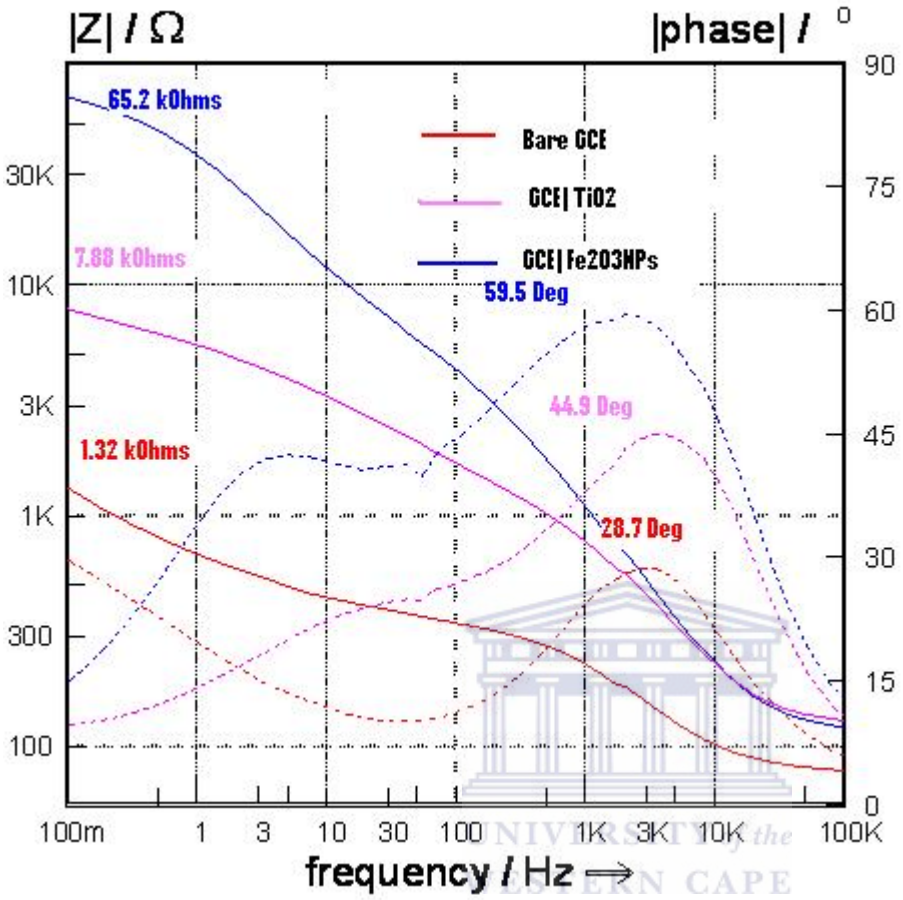

Figure 4.36 Bode plot of bare GCE, GCE/TiO_2 and GCE/Fe_2O_3 NPs in 5 mM $Fe(CN)_6^{3-/4-}$ redox probe

4.5.1. Electrochemical synthesis of PANI, PANI/TiO_2 and PANI/Fe_2O_3 NPs

The voltammogram of PANI alone and PANI doped metal oxide appears as three sets of redox peaks, namely A/B, C/D and E/F. The redox couple A/B is attributed to the transformation of PANI from the reduced leucoemeraldine (LE) state to the oxidized emeraldine (EM) state (Bian and Xue 2007; Singh, Ohlan et al. 2008). The redox couple C/D is attributed to the redox reaction of p-benzoquinone. The redox couple E/F is attributed to the transition of PANI from leucoemeraldine (LE) state to pernigraniline (PE) state and accompanied by the oxidation of aniline monomer. Figure 4.37 showed the polymerization of PANI, figure 4.38 showed the polymerization of PANI/TiO_2 NPs and figure 4.39 showed the polymerization of PANI/Fe_2O_3 NPs

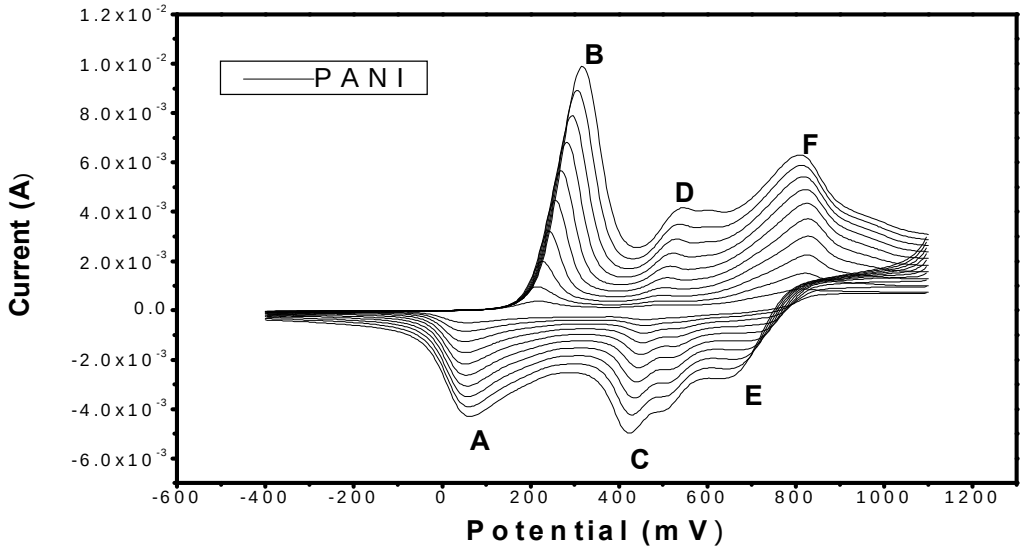

Figure 4.37: Polymerization of PANI in 1 M H_2SO_4 at a scan rate of 50 mV/s

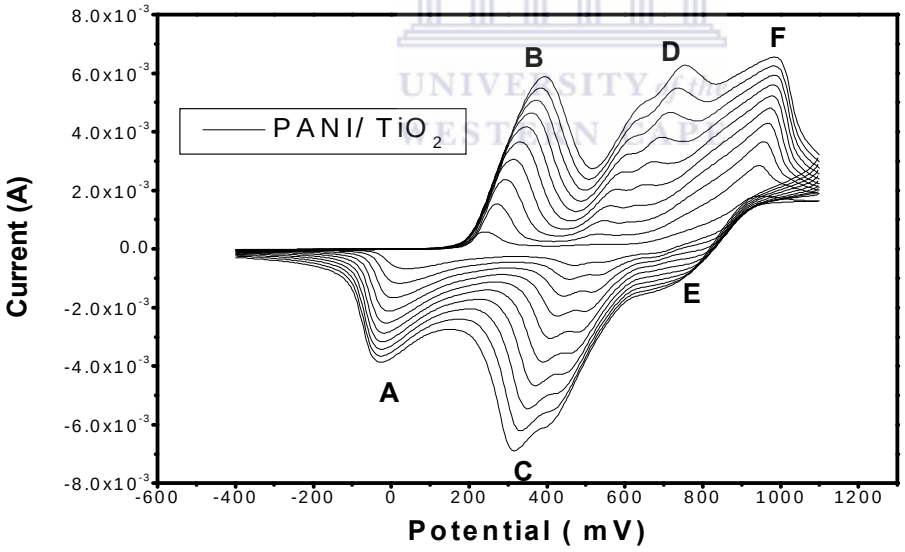

Figure 4.38: Polymerization of PANI doped TiO_2 NPs in 1 M H_2SO_4 at 50 mV/s

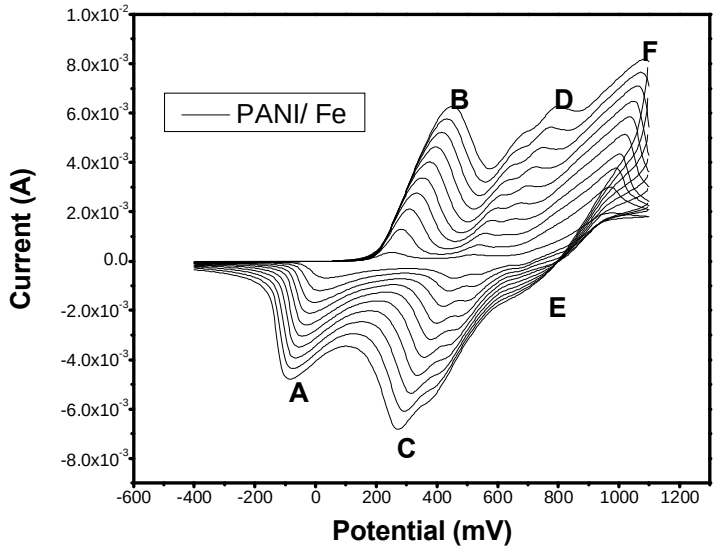

Figure 4.39: Polymerization of PANI doped Fe_2O_3 NPs in 1 M H_2SO_4 at 50 mV/s

The above figures showed the polymerization of PANI and PANI doped with the metal oxide nanoparticles that were conducted in acidic medium (1 M H_2SO_4) by applying 20 scans. The voltammograms appeared as three sets of redox peaks, namely A/B, C/D and E/F. The redox couple A/B was attributed to the transformation of PANI from the reduced leucoemeraldine (LE) state to the oxidized emeraldine (EM) state. The redox couple C/D was attributed to the redox reaction of p-benzoquinone. The redox couple E/F was attributed to the transition of PANI from leucoemeraldine (LE) state to pernigraniline (PE) state and accompanied by the oxidation of aniline monomer. The polymer growth on the glassy carbon electron was shown by the increase in the peak current as the number of scans increases. The shift in the peak potential was attributed to the conductivity of the polymer.

4.5.2 Characterization of PANI; PANI/TiO_2 and PANI/Fe_2O_3 NPs

The modified GC with PANI and PANI doped with the metal oxide nanoparticles were characterized in 0.1 M H_2SO_4. The voltammogram of PANI alone and PANI doped metal oxide appeared as three sets of redox peaks, namely A/B, C/D and E/F. The redox couple A/B was attributed to the transformation of PANI from the reduced leucoemeraldine (LE) state to the oxidized emeraldine (EM) state. The redox couple C/D was attributed to the redox reaction of p-benzoquinone. The redox couple E/F was attributed to the transition of PANI from leucoemeraldine (LE) state to pernigraniline (PE) state and accompanied by the oxidation of aniline monomer. On the effects of dopants, the cathodic peaks shifted to the lower potential values that might be an advantage of dopants compare to the PANI alone, whereas the anodic peaks shifted to the higher values. The E^0 values of PANI doped metal oxide nanoparticles are less than the PANI alone therefore these nanoparticles showed a good effect on the electron exchange (Bian and Xue 2007). The current amplitude on the electro-polymerization of PANI doped metal oxide nanoparticles was observed to be higher than that of PANI; this was an indication that the PANI/TiO_2 or Fe_2O_3 NPs were more conducting than PANI alone. The peak separation of PANI/TiO_2 and PANI/Fe_2O_3 NPs are higher compared to peak separation of the PANI alone. This was because of the presence of metal oxide nanoparticles on the PANI; it decreases the electrical conductivity of the film. The slight shift in both current and potential was illustrating the conductivity and electro activity of the polymer and also indicating fast charge transportation along the polymer chain. Figure 4.40 showed the characterization of PANI alone, PANI with TiO_2 and Fe_2O_3 NPs in 0.1 M H_2SO_4 at 20 mV/s. The effects of dopants on the polymerization of aniline are exhibited in table 3.

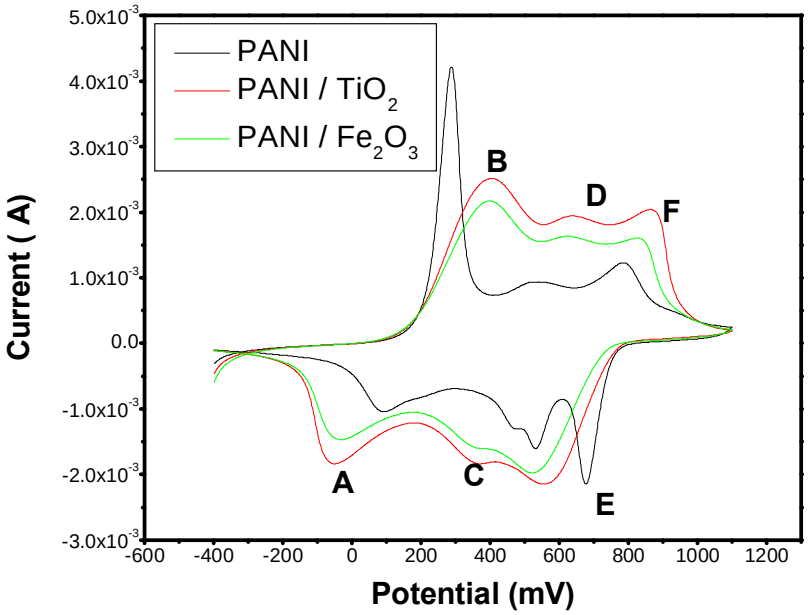

Figure 4.40: Characterization of PANI alone, PANI with TiO_2 and Fe_2O_3 NPs in 0.1 M H_2SO_4 at a scan rate of 20 mV/s.

Table 4. 3 :The potential parameters obtained from the CVs of PANI, PANI/TiO_2 and PANI/Fe_2O_3 NPs

Redox couples	Potentials	PANI	PANI/TiO_2 NPs	PANI/Fe_2O_3 NPs
A/B	Epa	283	402	402
	Epc	100	-123	434
	E^o	192	140	185
	æE	183	525	185
C/D	Epa	521	634	627
	Epc	528	297	339
	E^o	525	466	483
	æE	7	337	288
E/F	Epa	795	900	823
	Epc	676	479	515
	E^o	736	670	669
	æE	119	421	308

4.5.3 . The Characterization of PANI; PANI/TiO_2 and PANI/Fe_2O_3 NPs at a different scan rates.

The modified GC with PANI and metal oxide nanoparticles doped PANI were characterized in acidic medium at different scan rates of 5, 10, 15, 20 and 50 mV/s. The voltammogram of PANI alone and PANI doped metal oxide appeared as three sets of redox peaks, namely A/B, C/D and E/F. Figure 4.41 and 4.42 showed the CV voltammogram of the characterization of PANI/TiO_2 and PANI/Fe_2O_3 NPs at 5, 10, 15, 20 and 50 mV/s where three redox peaks couple were observed. As the scan rates increase, the amplitude of the redox peaks couple also increased confirming the growth of polymer on the electrode surface. A slight shift in potential was also observed confirming the conductivity and electro-activity of the polymer. The shift in potential was an indication of fast charge transportation along polymer chain.

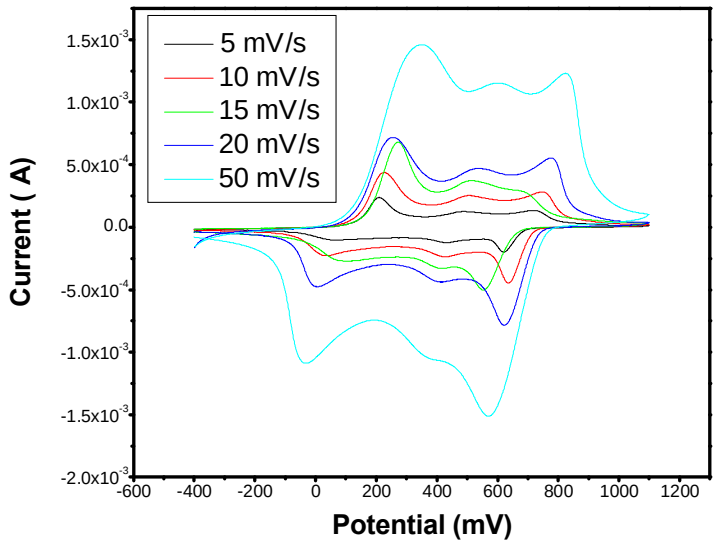

Figure 4. 41: Characterization of PANI doped TiO_2 NPs in 0.1 M H_2SO_4 at a different scan rates of 5, 10, 15, 20, 50 mV/s

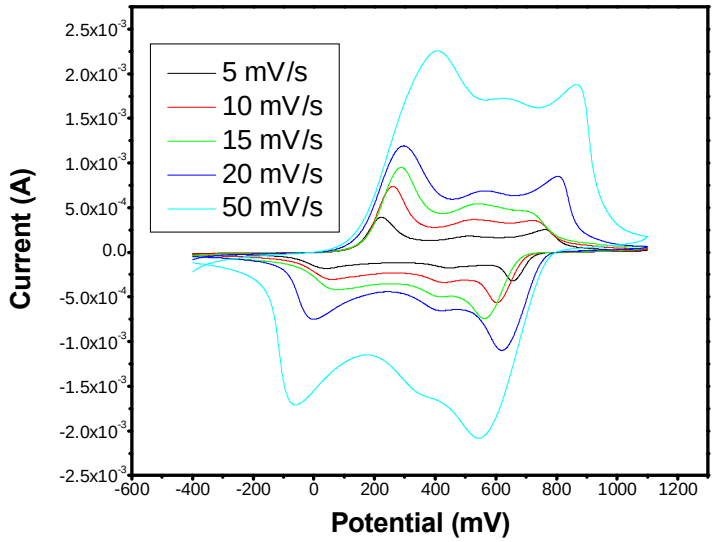

Figure 4. 42: Characterization of PANI doped Fe_2O_3 NPs in 0.1 M H_2SO_4 at a different scan rates of 5, 10, 15, 20, 50 mV/s

4.6 REFERENCES

- Bian C., Xue G. (2007) Nanocomposites based on rutile-TiO_2 and polyaniline. Materials Letters 61:1299-1302.
- E. Dubois* and J. ChevaletÀ(2003) Electrochemical Reduction of Iron Oxide Nanoparticles on mercury
- Fernandes D.M., Hechenleitner A.A.W., Silva M.F., Lima M.K., Bittencourt P.R.S., Silva R., Melo M.A.C., Pineda E.A.G. (2009) Preparation and characterization of NiO, Fe_2O_3, $Ni0.0_4Zn_{0.96}O$ and $Fe_{0.03}Zn_{0.97}O$ nanoparticles. Materials Chemistry and Physics 118:447-452.
- Nishio K., Ikeda M., Gokon N., Tsubouchi S., Narimatsu H., Mochizuki Y., Sakamoto S., Sandhu A., Abe M., Handa H. (2007) Preparation of size-controlled (30-100 nm) magnetite nanoparticles for biomedical applications. Journal of Magnetism and Magnetic Materials 310:2408-2410.

- Im J.S., Lee S.K., Lee Y.-S. Cocktail effect of Fe_2O_3 and TiO_2 semiconductors for a high performance dye-sensitized solar cell. Applied Surface Science In Press, Corrected Proof
- Singh K., Ohlan A., Kotnala R.K., Bakhshi A.K., Dhawan S.K. (2008) Dielectric and magnetic properties of conducting ferromagnetic composite of polyaniline with [gamma]-Fe_2O_3 nanoparticles. Materials Chemistry and Physics 112:651-658
- Kuiying Li a,b,, Ying Ying Dinga, Jing Guoa, DayangWangb, (2008) Surface electron structures and mechanism of nonradiative transitions on crystalline TiO_2 nanoparticles 112: 1001ï 1007

CHAPTER FIVE

APPLICATION

5. APPLICATION

5.1 Detection of phthalates using a sensor membrane (Fe_2O_3 and TiO_2 NPs)

The main challenge of the study was to develop the inexpensive and accurate method for the electrolytic determination of phthalates in waste water. The electrochemical sensor attracted the interest of clinical chemistry because they offer fast, reliable and inexpensive method. The detection was based on the redox behaviour of the Analyte. The sensor membrane prepared by modification of the GCE with Fe_2O_3 and TiO_2 NPs are the promising nano-materials for the determination of phthalates. The electrolytes used on this application were 0.1 M PBS (pH 7.0) and 0.1 M $LiClO_4$ (pH 6.7). Figure 5.43 and 5.44 showed the determination of dibutyl phthalates with modified GCE with TiO_2 NPs. The results showed that there was an oxidation peak at ca -1439 mV in $LiClO_4$ whereas the peak in PBS appeared at ca ï 852 mV. The results revealed that there was no reduction peak shown in both electrolytes which means the system was irreversible. The peak showed that the TiO_2 NPs was electro-active leading to the conclusion that the nanoparticles were effective for use in sensor membrane for the determination of phthalates. The oxidation peak current was shown a decrease after the introduction of phthalates. As the concentration of phthalates increased the peak current decreases which means there was an interaction between the phthalates analyte and nanoparticles leading to the blockage of an electron transfer to the system. The structure of different types of phthalates are shown in the literature, it has a COOR (R ï alkyl group) substituent to the phenol ring that makes the structure of phthalates to be negative charged. Titanium dioxide nanoparticles have also a negative charge backbone from oxides. The decrease in the peak current after the introduction of phthalates revealed the electrostatic repulsion of charges that existed between the negative charge from the metal oxide and the negative charge of COOR (R ï alkyl group) from the phthalates structure.

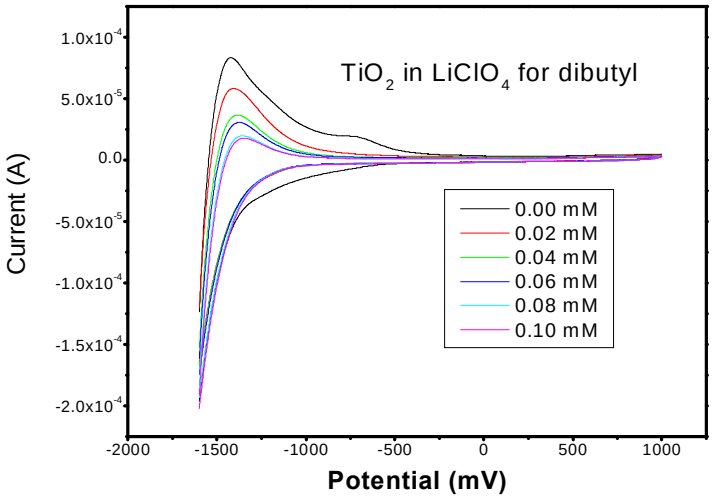

Figure 5.43: CV response of GCE modified with TiO_2 NPs on the determination of different concentration of DBP in 0.1 M $LiClO_4$ (pH 6.8) at a scan rate of 20 mV/s

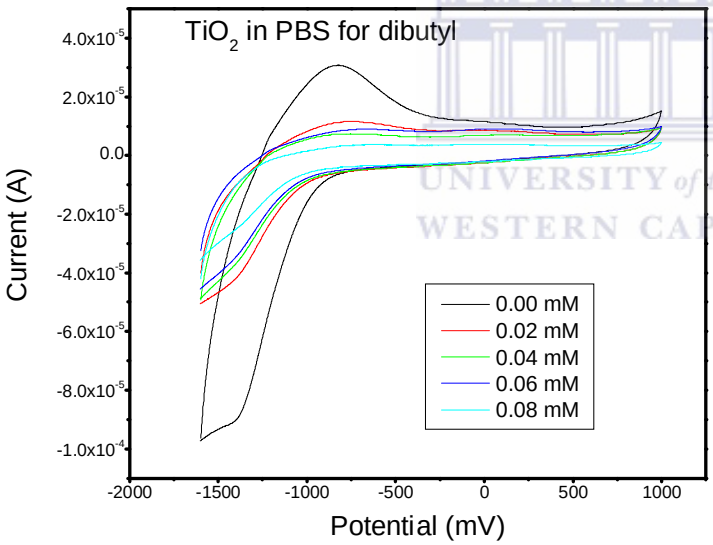

Figure 5.44: CV response of GCE modified with TiO_2 NPs on the determination of different concentration of DBP in 0.1 M PBS (pH 7.0) at a scan rate of 20 mV/s

5.2 Detection of phthalates using polymer nanocomposites

5.2.1 Detection of phthalates using PANI/TiO_2 NPs

The polyaniline nanocomposites were developed to enhance the catalytic activity of the nanoparticles for the detection of phthalates. The effects of doping with metal oxide nanoparticles on PANI play an important role in an electron conductivity tunnel, making electron transfer easier to the system. In the polymerization process , the voltammograms of PANI doped metal oxide appears as three sets of redox peaks, namely A/B , C/D and E/F in 0.1 M H_2SO_4 as an electrolyte as reported on the literature. The redox couple A/B is attributed to the transformation of PANI from the reduced leucoemeraldine (LE) state to the oxidized emeraldine (EM) state. The redox couple C/D is attributed to the redox reaction of p-benzoquinone. The redox couple E/F is attributed to the transition of PANI from leucoemeraldine (LE) state to pernigraniline (PE) state and accompanied by the oxidation of aniline monomer. The PANI/TiO_2 NPs modified electrode was then used on the electro-determination of different types of phthalates in 0.1 M H_2SO_4. The CV response at a different concentration of phthalates show a decrease on the redox peak currents and slight shift observed on peak potentials. The peak current decreases was caused by the negative charge backbone of PANI/TiO_2 NPs and the negative charge of COOR (R ï alkyl group) from the phthalates structure due to electrostatic repulsion. The peak potential A which was attributed to the reduced leucoemeraldine recorded a slight shift to more anodic potential; meaning that in the presence of phthalates the leucoemeraldine state was easily reduced.

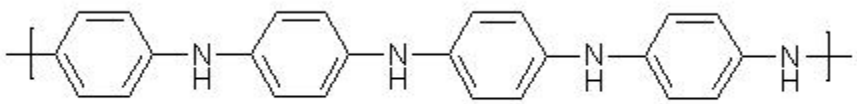

leucoemeraldine structure

The peak potential E which was the reduced pernigraniline (PE) state exhibited a slight shift to less cathodic potential. However in the presence of phthalates the pernigraniline (PE) required more potential to get reduced.

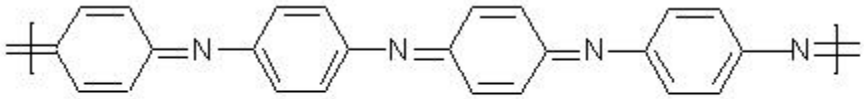

Pernigraniline (PE)

The CV response in the determination of phthalates showed differences between the peak of leucoemeraldine and of pernigraniline. The response to leucoemeraldine state revealed that the peak shifted to more anodic potential whereas the pernigraniline state shifted to less cathodic. The leucoemeraldine state was easily reduced whereas the pernigraniline state needs more potential to be reduced due to more negative charge existing in the structure of pernigraniline state from double bonds N between the rings which was absent in leucoemeraldine structure with only NH bonds between the rings. The graphs from figure 5.45 to figure 5.49 are the CV and SWV results of the determination of different types of phthalates such as dibutyl, dioctyl and diethylhexyl phthalates using PANI/TiO_2 NPs modified electrode in 0.1 M H_2SO_4 as an electrolyte at a 20 mV/s.

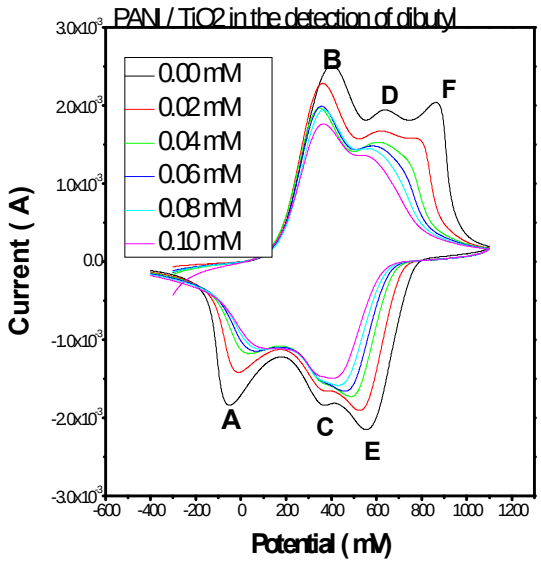

Figure 5.45: CV response of GCE modified with PANI/TiO_2 NPs on the determination of different concentration of DBP in 0.1 M H_2SO_4 at a scan rate of 20 mV/s

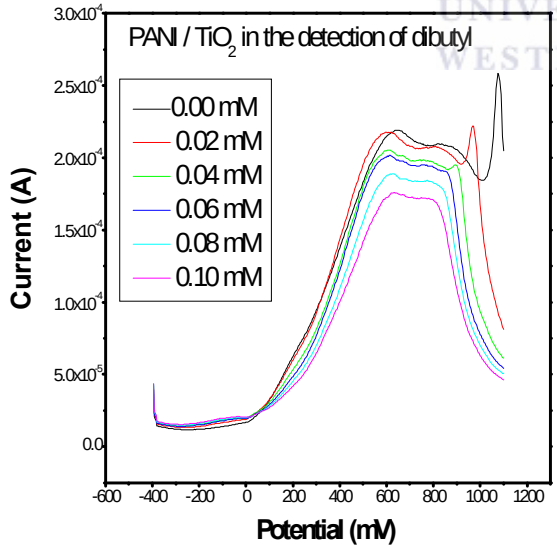

Figure 5.46: SWV response of GCE modified with PANI/TiO_2 NPs on the determination of different concentration of DBP in 0.1 M H_2SO_4

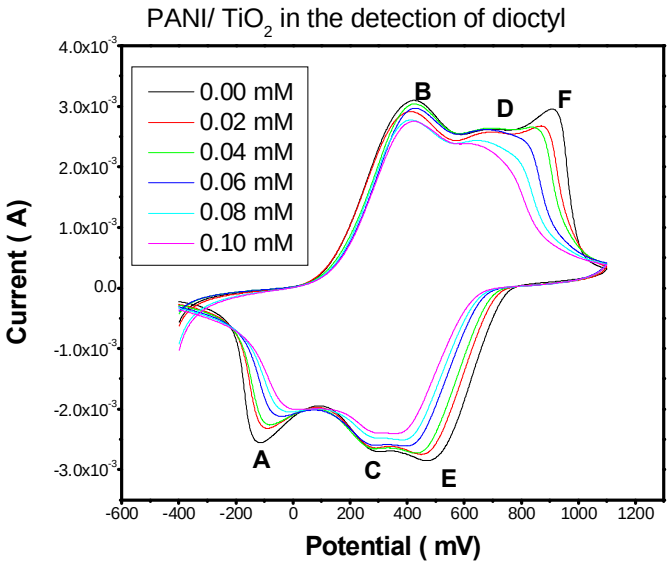

Figure 5.47: CV response of GCE modified with PANI/TiO_2 NPs on the determination of different concentration of DOP in 0.1 M H_2SO_4 at a scan rate of 20 mV/s

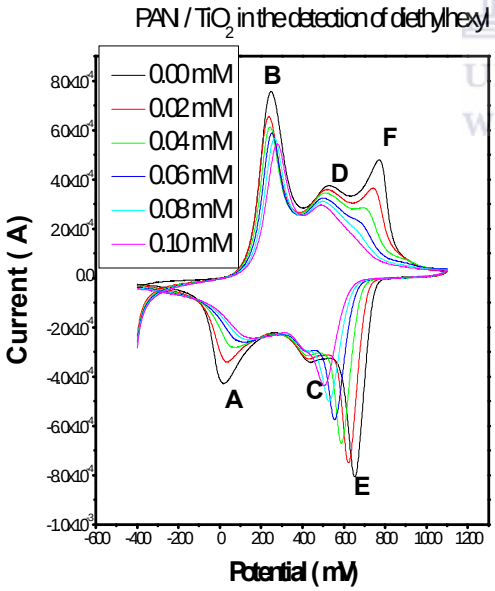

Figure 5.48: CV response of GCE modified with PANI/TiO_2 NPs on the determination of different concentration of DEHP in 0.1 M H_2SO_4 at a scan rate of 20 mV/s

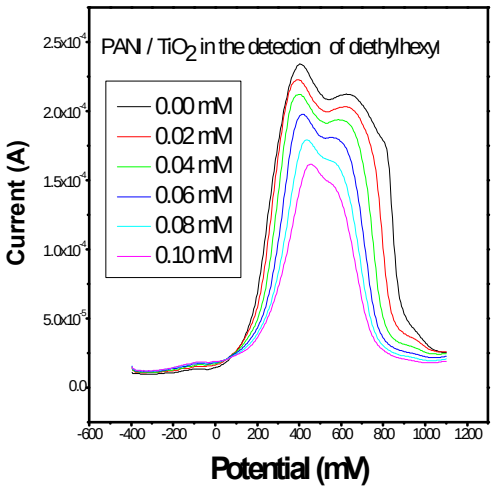

Figure 5.49: SWV response of GCE modified with PANI/TiO_2 NPs on the determination of different concentration of DEHP in 0.1 M H_2SO_4

5.2.2. Calibration curves of CV at GCE/PANI/TiO_2 NPs

The linearity of the method was tested with calibration curves at five different concentrations of phthalates studied (dibutyl, dioctyl and diethylhexyl) and were measured on the peak of leucoemeraldine (peak A) and pernigraniline state (peak E) at GCE/PANI/TiO_2 NPs. Calibration curves were constructed using analyte (phthalates) peak ratio versus concentration of analyte. A linear fit of the ratios was obtained with high correlation coefficients. The detection limits were calculated from the standard deviation of six replicates of the blank solution. Calibration curves showed a positive slope on the peak potential of leucoemeraldine state whereas negative slope showed on the peak potential of pernigraniline state due to a slight shift in leucoemeraldine peak potential to more anodic of which the shift in pernigraniline peak potential to less cathodic potential. The potential peak decrease was caused by the explanation given from the CV results on the above. Calibration curves obtained for each compound are summarized on table 5.1

Table 5.1 : The parameters of linear curve from CV of GCE/PANI/TiO_2 NPs

Phthalates	Peaks	Graph	Slope (mV/mM)	R	Detection limit
Dibutyl	Leucoemeraldine	E vs conc.	1312.98571	0.9794	0.77 µmol L^{-1}
	Pernigraniline	E vs conc.	-1383.04286	-0.9876	0.98 µmol L^{-1}
Dioctyl	Leucoemeraldine	E vs conc.	10189	0.9911	0.09 µmol L^{-1}
	Pernigraniline	E vs conc.	-962.64286	-0.9989	1.40 µmol L^{-1}
Diethylhexyl	Leucoemeraldine	E vs conc.	1557.88286	0.9902	0.65 µmol L^{-1}
	Pernigraniline	E vs conc.	-1479.5	-0.9970	0.92 µmol L^{-1}

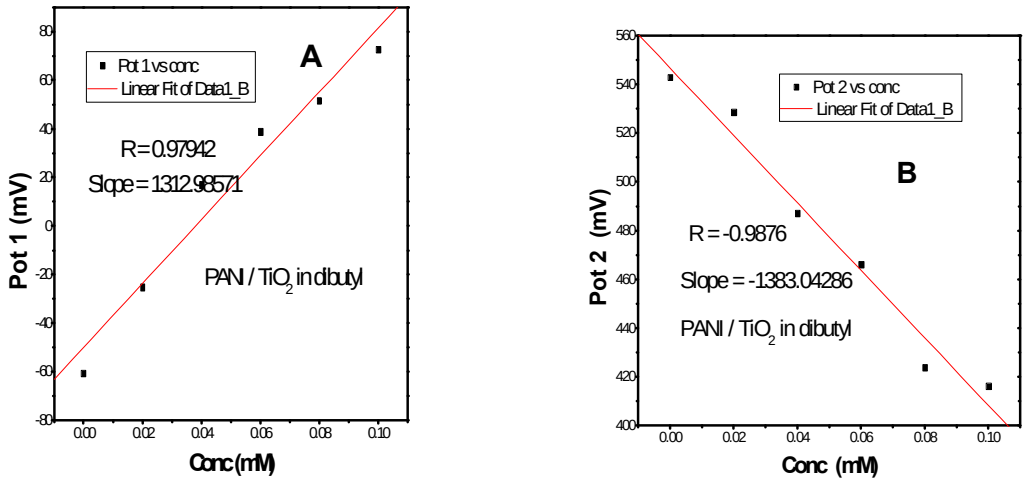

Figure 5.50: Calibration curve of leucoemeraldine peak (A) and pernigraniline peak (B) on the determination of DBP illustrating linear of PANI/TiO_2 NPs sensor, potential vs concentration

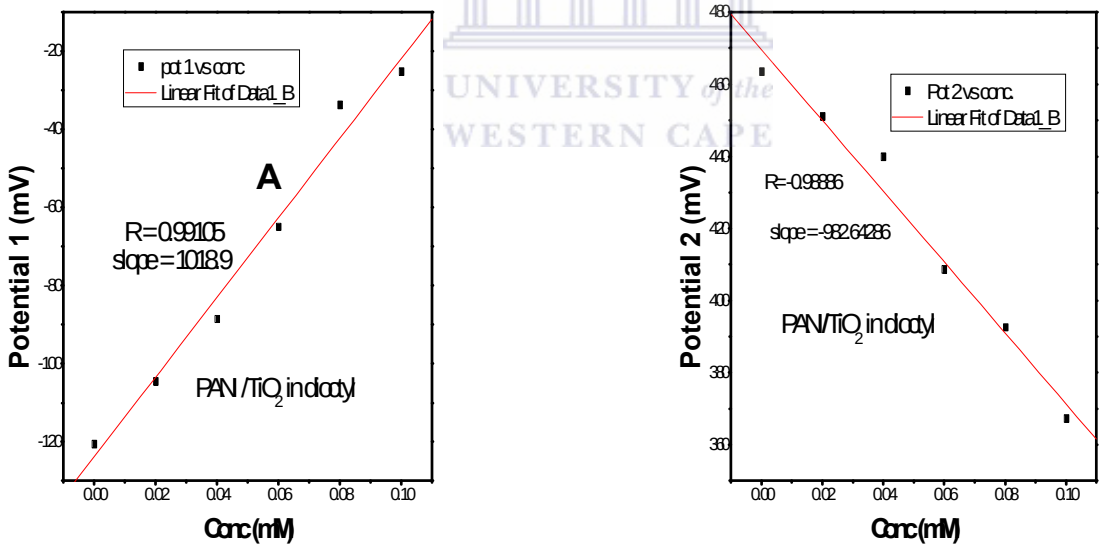

Figure 5.51: Calibration curve of leucoemeraldine peak (A) and pernigraniline peak (B) on the determination of DOP illustrating linear of PANI/TiO_2 NPs sensor, potential vs current

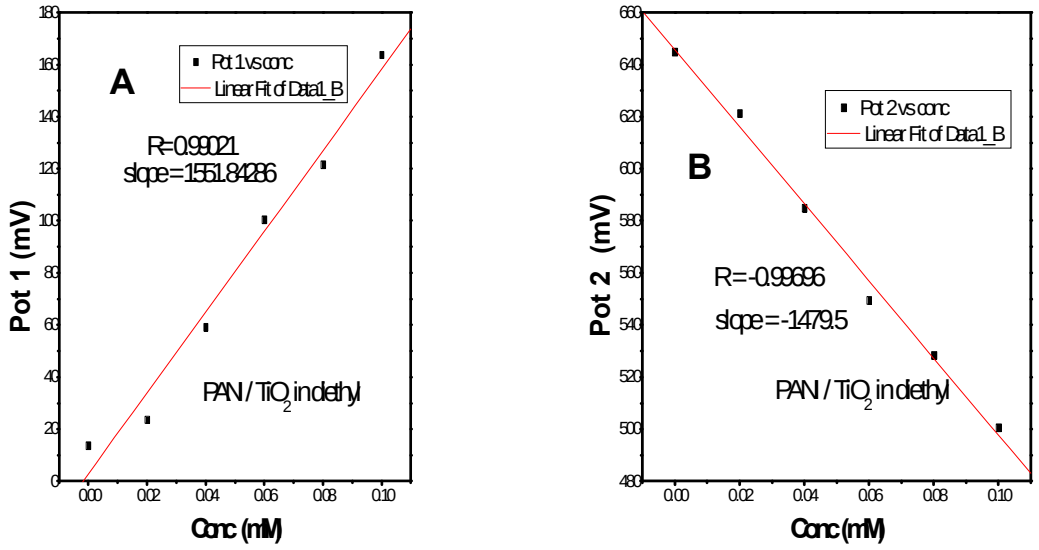

Figure 5.52: Calibration curve of leucoemeraldine peak (A) and pernigraniline peak (B) on the determination of DEHP illustrating linear of PANI/TiO_2 NPs sensor, potential vs concentration

5.2.2. Detection of phthalates using PANI/Fe_2O_3 NPs

The determination of phthalates was done in 0.1 M H_2SO_4 at 20 mV/s scan rate and a potential range of -400 to 1100 mV using PANI/Fe_2O_3 NPs modified GCE. The electrolytic determination was performed in the presence of different types of phthalates such as dioctyl and diethylhexyl phthalates. The CV response in the presence of different concentration of phthalates showed decrease in currents of the three redox peak couple that were observed on characterization of modified electrode after the polymerization of PANI/Fe_2O_3 NPs and slight shift observed in peak potentials. The results observed were similar to the above results obtained when the electrode was modified with PANI/TiO_2 NPs. The peaks of interest are leucoemeraldine and pernigraniline state. The currents of leucoemeraldine and pernigraniline state decreased as the concentration of dioctyl of diethylhexyl phthalates increased due to negative charge backbone of PANI/Fe_2O_3

NPs and the negative charge of COOR (R ï alkyl group) from the phthalates structure. The negative charge backbone caused an electrostatic repulsion leading to the decrease in current. The peak potential of leucoemeraldine recorded a slight shift to more anodic potential, meaning that in the presence of phthalates the leucoemeraldine state is easily reduced.

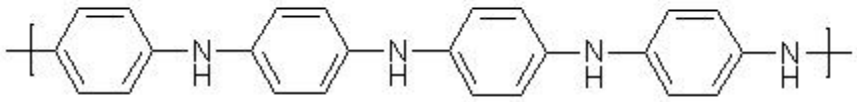

leucoemeraldine structure

The peak potential pernigraniline (PE) state showed a slight shift to less cathodic potential, meaning that in the presence of phthalates the pernigraniline (PE) required more potential to get reduced.

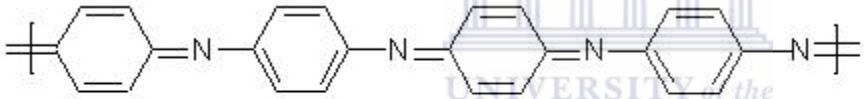

Pernigraniline (PE)

The following CV and SWV graphs with figure numbers refer to the results obtained for the determination of different types of phthalates such as dibutyl, dioctyl and diethylhexyl phthalates using PANI/TiO_2 or Fe_2O_3 NPs modified electrode in 0.1 M H_2SO_4 as an electrolyte at 20 mV/s. The calibration dependence of all studies of phthalates for CV at GCE/PANI/TiO_2 or Fe_2O_3 NPs were measured in concentration range in the peak of leucoemeraldine (peak A) and pernigraniline state (peak E) potential vs concentration

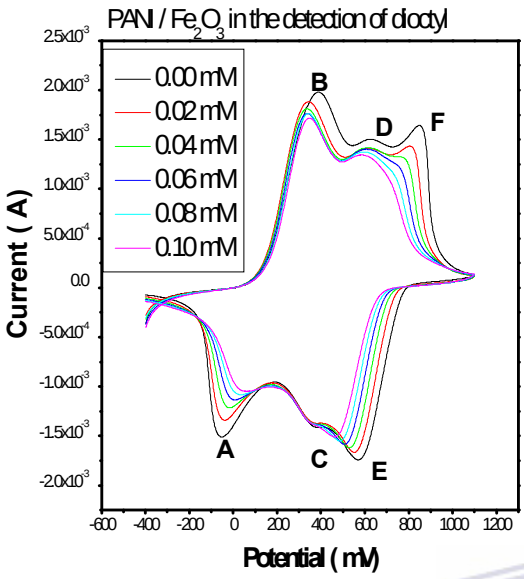

Figure 5.53: CV response of GCE modified with PANI/Fe_2O_3 NPs on the determination of different concentration of DOP in 0.1 M H_2SO_4 at a scan rate of 20 mV/s

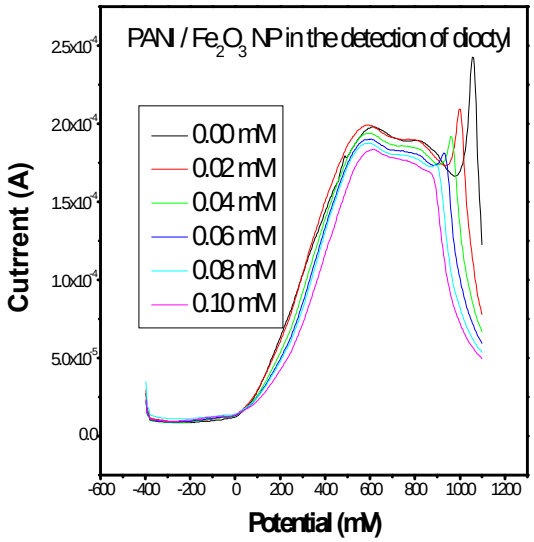

Figure 5.54: SWV response of GCE modified with PANI/Fe_2O_3 NPs on the determination of different concentration of DOP in 0.1 M H_2SO_4

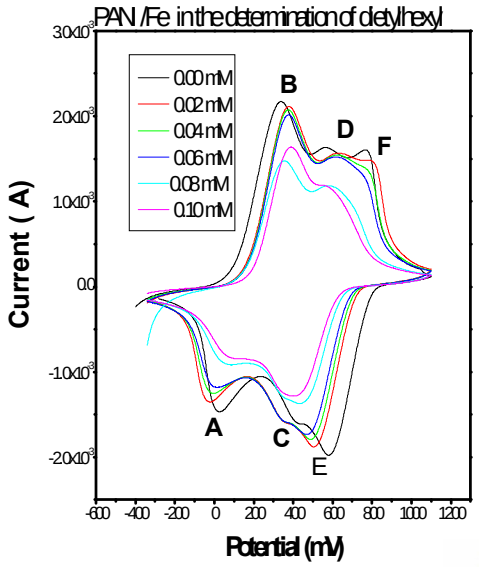

Figure 5.55: CV response of GCE modified with PANI/Fe_2O_3 NPs on the determination of different concentration of DEHP in 0.1 M H_2SO_4 at a scan rate of 20 mV/s

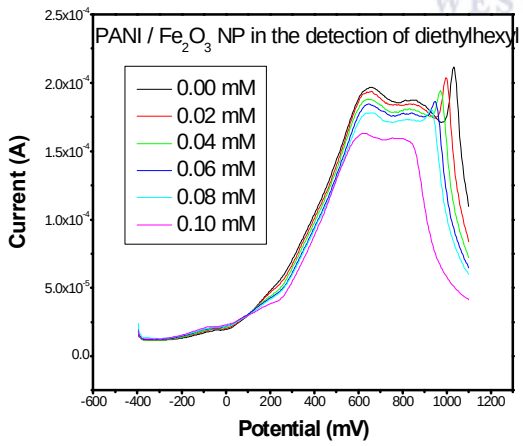

Figure 5.56: SWV response of GCE modified with PANI/Fe_2O_3 NPs on the determination of different concentration of DEHP in 0.1 M H_2SO_4

5.2.3. Calibration curves of GCE/PANI/Fe_2O_3 NPs

The calibration response of phthalate studies (refer to figures 5.53 and 5.55) were measured in concentration range on the peak of leucoemeraldine (peak A) and pernigraniline state (peak E). The linear graph was performed at potential vs. concentration. The calibration curves showed a positive slope on the peak potential of leucoemeraldine state whereas a negative slope was observed on the peak potential of pernigraniline state due to slight shift in leucoemeraldine peak potential to more anodic of which the shift in pernigraniline peak potential to less cathodic potential. The parameters of the obtained linear calibration curve from CVs of GCE/PANI/Fe_2O_3 NPs are summarized in table 5.2

Table 5.2: Results of calibration curve from CVs of GCE/PANI/Fe_2O_3 NPs

Phthalates	Peaks	Graph	Slope (mV/mM)	R	Detection limit
Dioctyl	Leucoemeraldine	E vs conc.	1035.75714	0.9961	0.98 µmol L^{-1}
	Pernigraniline	E vs conc.	-1032.18571	-0.9957	1.31 µmol L^{-1}
Diethylhexyl	Leucoemeraldine	E vs conc.	1065.9	0.9871	0.95 µmol L^{-1}
	Pernigraniline	E vs conc.	-1128.61429	-0.9970	1.20 µmol L^{-1}

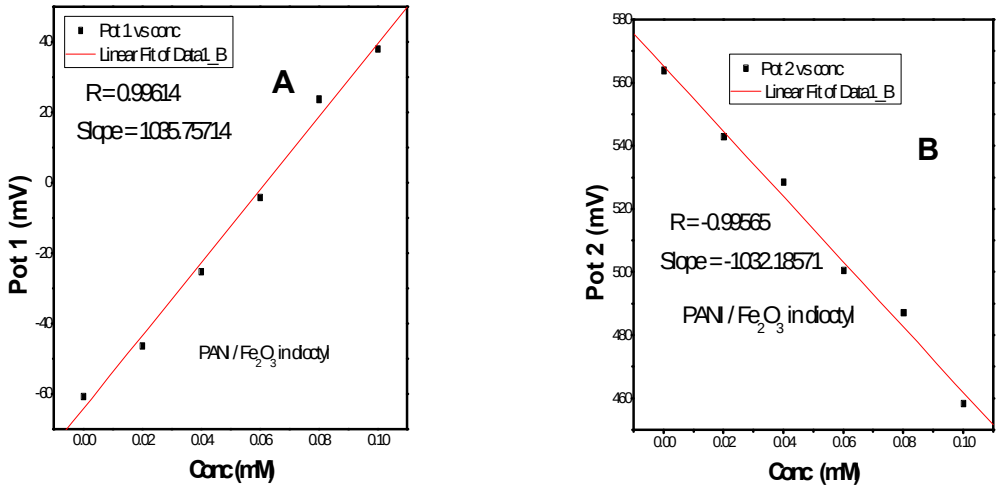

Figure 5.57: Calibration curve of leucoemeraldine peak (A) and pernigraniline peak (B) on the determination of DOP illustrating linear of PANI/Fe_2O_3 NPs sensor, potential vs concentration

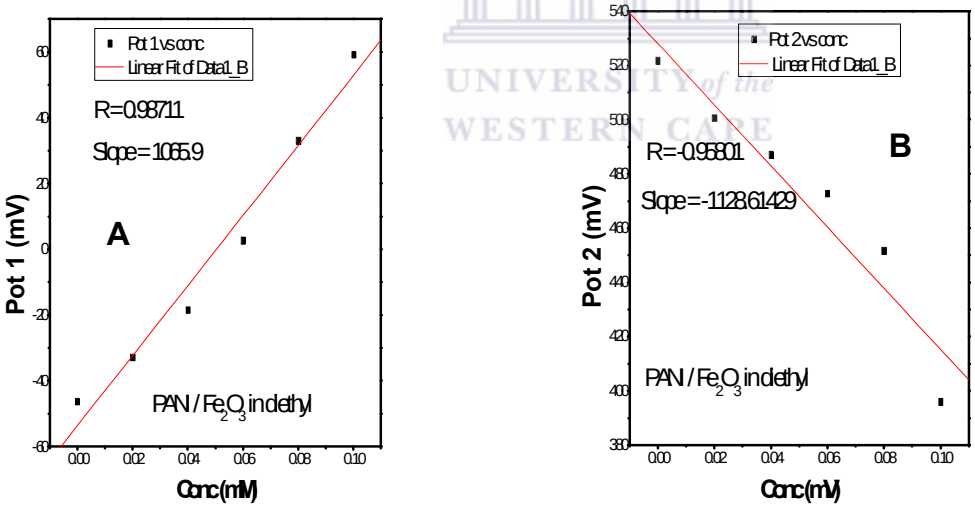

Figure 5.58: Calibration curve of leucoemeraldine peak (A) and pernigraniline peak (B)on the determination of DEHP illustrating linear of PANI/Fe_2O_3NPs sensor, potential vs concentration

The linearity of the method was tested with calibration curves obtained on table 5.1 and 5.2. The detection limits were calculated by $3 \times s \div m$ *Equation (9)* where s is the relative standard deviation of the intercept and m is the slope of the linear curve. Classical methods (gas chromatography, HPLC, mass spectroscopy, etc) have been reported in literature for the detection of poly aromatic hydrocarbon and were found to exhibit good detection limit. However due to expensive nature of these methods and longer time employed on the processing the sample for analysis it is paramount to make use of a simpler, more sensitive ,user friendly and low cost method due to the high risk of pollution posed by the pollutant (phthalates). The most important method that fit into this is the electrochemical sensing technique. The sensor fabricated in this work for the detection of phthalates (dibutyl, dioctyl and diethylhexyl) was found to exhibit higher detection limits as compared to what was obtained when gas chromatography was employed by Ivan Ostrovsky and his co workers. Detection limit of 0.02 µM was reported by (D.C. Mita, A.; Altanasio et. al.2007) which was also found to be lower than the one obtained in this work.

For the first time, this study illustrates the successful use of metal oxide nanoparticles and conducing polymers for the electrolytic detection of phthalates. Literature only suggests the use of bare electrodes for the electrolytic detection of phthalates such as; the work carried out by Gonzalez and co-workers where a Hanging Drop Mercury (HDM) was employed for the detection of dimethyl phthalates (A. Gonzalez Corters; J.M. Pingarron Carrazonand et.al.1991). In another study done by Munawer, phthalates (dibutyl,dietyl didecyl and diallyl) were detected using Hanging Drop Mercury (HDM) electrode (M. S. Qureshi; J.F. Fisher; et.al.2010). The disadvantage associated with these methods is that phthalates are dissolved in organic solvents

and detections are carried out at very high potentials. There is a high probability that what were observed at these potentials are the organic solvents and not the phthalates as these are the potential ranges where their activities are seen.

This study demonstrates the ability of the constructed sensor to function both at low potentials and low scan rates. This is beneficial since the rate of the reaction can be monitored effectively as these parameters are controlled and properly calibrated.

CHAPTER SIX

CONCLUSSION

6.1. CONCLUSSION

The prepared nanoparticles resulted in uniform and homologous particles with the particle sizes of 20 nm (TiO_2 NPs) and 50 nm (Fe_2O_3 NPs) were estimated from transmission electron microscopy by sol-gel and hydrothermal method respectively. The morphology, size particles, size distribution, crystalline structure, wavelength and intensity of the nanoparticles were estimated from SEM, XRD and UV- visible spectroscopy techniques. The XRD pattern showed the peaks with position in excellent agreement with literature values for TiO_2 and Fe_2O_3 NPs. The metal oxide nanoparticles were electrochemical active from aqueous media; the responses were amperometrically monitored by cyclic and square wave voltammetry. The results from electrochemical characterization of nanoparticles showed that nanoparticles can be reduced into metallic iron, the reduction always occur at a higher negative potential ca.-1.5 V. The nanoparticles showing the semi-conductivity in ferricynade solution obtained from EIS characterization. The PANI doped nanoparticles showed a catalytic effect and highly conductivity due to the shifting of peak potential. PANI doped nanoparticles were suitable sensor for the determination of different phthalates in acidic media making the electrode suitable for application in environmental analysis with low detection limits.